THE EARLY ANTHROPOGENIC HYPOTHESIS: CHALLENGES AND RESPONSES

William F. Ruddiman

Received 22 June 2006; revised 15 January 2007; accepted 26 March 2007; published 31 October 2007.

[1] Ruddiman (2003) proposed that late Holocene anthropogenic intervention caused CH_4 and CO_2 increases that kept climate from cooling and that preindustrial pandemics caused CO_2 decreases and a small cooling. Every aspect of this early anthropogenic hypothesis has been challenged: the timescale, the issue of stage 11 as a better analog, the ability of human activities to account for the gas anomalies, and the impact of the pandemics. This review finds that the late Holocene gas trends are anomalous in all ice timescales; greenhouse gases decreased during the closest stage 11 insolation analog; disproportionate biomass burning and rice irrigation can explain the methane anomaly; and pandemics explain half of the CO_2 decrease since 1000 years ago. Only ~25% of the CO_2 anomaly can, however, be explained by carbon from early deforestation. The remainder must have come from climate system feedbacks, including a Holocene ocean that remained anomalously warm because of anthropogenic intervention.

Citation: Ruddiman, W. F. (2007), The early anthropogenic hypothesis: Challenges and responses, *Rev. Geophys.*, *45*, RG4001, doi:10.1029/2006RG000207.

1. INTRODUCTION

[2] For decades most climate scientists have accepted four views of Holocene climatic change: (1) Rising greenhouse gas concentrations in the atmosphere during the 1800s mark the first major anthropogenic effects on global climate. (2) After the last remnants of the Laurentide ice sheet disappeared near 7000 years ago, orbital-scale temperature has remained nearly stable for natural reasons. (3) A small cooling gradually occurred at north polar latitudes in recent millennia, but it has fallen short of the threshold needed to initiate glaciations. (4) Small suborbital climate oscillations during recent millennia have been driven by variations in solar output and volcanic eruptions and by natural multicentury variability.

[3] These four views can be condensed into a single statement: We live in a naturally warm and stable interglacial climate. Recently, however, *Ruddiman* [2003] put forward a very different view of the Holocene in the "early anthropogenic hypothesis": (1) Anthropogenic effects on greenhouse gases and global climate began thousands of years ago and slowly increased in amplitude until the start of the rapid increases of the industrial era. (2) Global climate would have cooled substantially during recent millennia, but anthropogenic greenhouse gas increases countered much of the natural cooling. (3) Had it not been for human interference in the operation of the climate system, ice caps and small sheets would have begun forming in north polar regions. (4) Shorter-term climatic oscillations during the last 2000 years resulted in part from pandemics that caused massive mortality, reforestation, and sequestration of carbon.

[4] This revised view can be summarized in this way: We live in a world in which peak interglacial warmth has persisted only because of the inadvertent impact of early farming.

[5] Several challenges to the early anthropogenic hypothesis have been published. The purpose of this review is to examine these challenges, summarize the arguments for and against the original hypothesis, update its current status, and suggest future research that could further clarify key issues. Section 2 of this paper briefly reviews the original hypothesis. Sections 3 through 10 address the published challenges. Section 11 summarizes the implications of the hypothesis for past, present, and future climate.

2. EARLY ANTHROPOGENIC HYPOTHESIS

[6] The early anthropogenic hypothesis consists of four parts, three of which pertain to gradual orbital-scale changes during the middle and late Holocene, while the fourth focuses on shorter-term changes within the last 2000 years.

2.1. Anomalous Methane Trend

[7] The CH_4 increase during the last 5000 years is not natural (Figure 1a). Changes in solar radiation have driven

[1]Department of Environmental Sciences, University of Virginia, Charlottesville, Virginia, USA.

8755-1209/07/2006RG000207$15.00
Paper number 2006RG000207

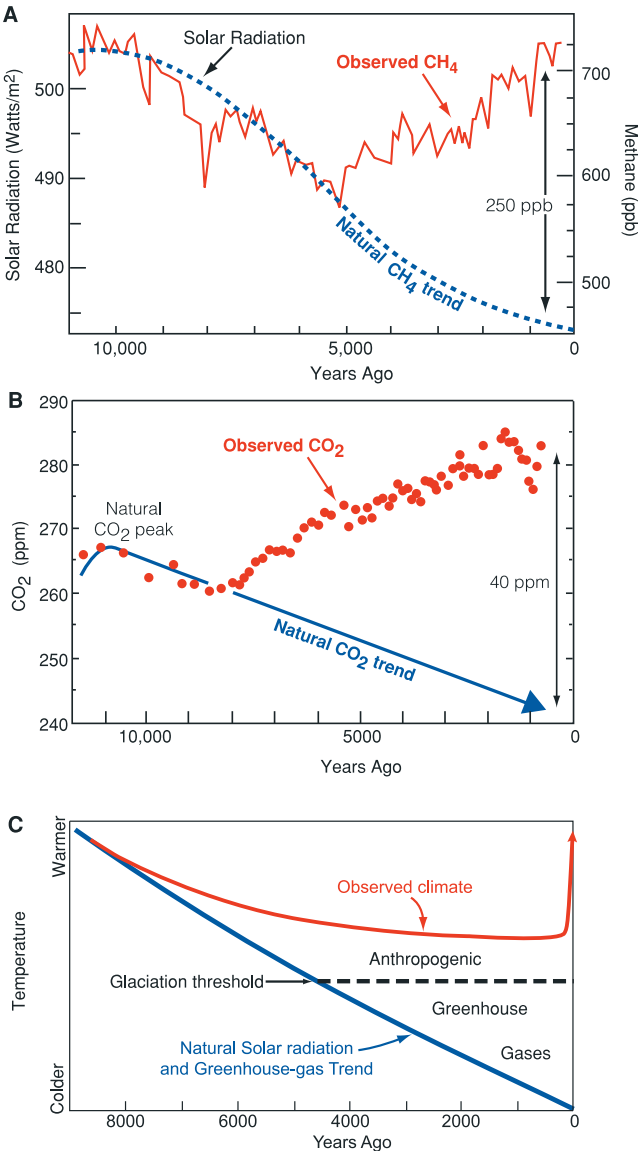

Figure 1. Early anthropogenic hypothesis. Human activities during the late Holocene causing increases in (a) CH_4 and (b) CO_2 in contrast to the downward trends during previous interglaciations. (c) Late Holocene greenhouse gas increases preventing much of the natural cooling that occurred in previous interglaciations.

natural changes in methane emissions from tropical and boreal wetlands at the 23,000-year precession cycle by variable heating of the Asian interior [*Chappellaz et al.*, 1990]. Because summer insolation has been steadily decreasing since 11,000 years ago, the methane concentration should have been dropping continuously throughout the Holocene. The CH_4 concentration did decrease until 5000 years ago, but then it began an anomalous rise to a value of ~700 ppb in the preindustrial Holocene. Had the CH_4 level followed the trends observed during the three prior interglaciations, it would by now have fallen to a value of ~450 ppb. The 250-ppb difference between the observed value and the estimated natural value is the Holocene methane anomaly, and the anomaly is the result of early farming. The onset of the CH_4 anomaly matches the time that people in southern Asia first began to irrigate for rice, and its slow growth in amplitude occurred during subsequent millennia in which irrigation expanded across the river valleys of Southeast Asia and up steeper hillsides in terraced rice paddies.

2.2. Anomalous CO_2 Trend

[8] The CO_2 increase during the last 8000 years is anomalous in a similar way (Figure 1b). Although the mechanisms of orbital-scale CO_2 changes are not yet certain, the natural course of CO_2 changes in the Holocene can be predicted from trends during previous interglaciations when major climatic parameters (insolation trends and ice volume) were similar to those today. At those times, CO_2 values fell to an average of 240–245 ppm, whereas during the Holocene they rose to 280–285 ppm prior to the start of the industrial era. The difference between the observed and predicted values is the Holocene CO_2 anomaly. The anomaly first became evident just as European farmers began to clear forests in southeastern Europe to grow crops previously domesticated in the Middle East [*Zohary and Hopf*, 1993]. The anomaly grew in size throughout millennia in which farmers were deforesting major portions of southern Asia, including China, India, and southern and western Europe [*Williams*, 2003]. On the basis of persistent increases in frequency of charcoal occurrence observed on several continents, *Carcaillet et al.* [2002] had previously concluded that biomass burning played a role in the Holocene CO_2 increase.

2.3. Overdue Glacial Inception

[9] Holocene climate would have naturally cooled by a substantial amount during recent millennia, but the anthropogenic greenhouse gas emissions reduced the cooling (Figure 1c). For a doubled-CO_2 sensitivity of 2.5°C the 40-ppm CO_2 anomaly and the 250-ppb CH_4 anomaly translate into a mean annual global warming anomaly of ~0.75°C. At polar latitudes, albedo-temperature feedback from the increased extent of snow, sea ice, and tundra, along with other factors, would have amplified this value to ~2°C. This anthropogenic warming effect at north polar latitudes offset much of an insolation-driven cooling that would otherwise have initiated ice sheet growth in locations such as Baffin Island and the Canadian Arctic [*Andrews and Mahaffy*, 1976; *Williams*, 1978]. Greenhouse gas emissions from early farming are the reason that Holocene climate remained relatively stable and that new ice sheets failed to appear.

2.4. Pandemic-Driven CO_2 Drop

[10] Short-term CO_2 decreases of 4–10 ppm during the last 2000 years are difficult to explain entirely by natural solar-volcanic forcing, and humans may also have played an inadvertent role through the effect of major pandemics (Figure 2). The pandemics killed tens of millions of people, who left hundreds of millions of acres of farmed land abandoned. Reforestation of this abandoned land sequestered carbon from the atmosphere and caused CO_2 concentrations to fall. Within the limits of ice core dating, intervals

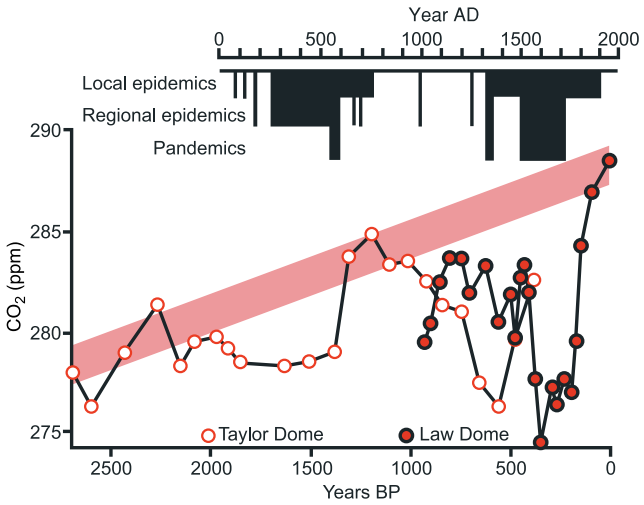

Figure 2. Rising CO_2 trend during the Holocene (light red) interrupted by decreases during the last 2000 years. Several of the CO_2 drops may have been caused by reforestation resulting from massive mortality during pandemics.

of major plagues in Europe (the late Roman Era and the medieval Black Death) correlate with decreases in CO_2 levels. The largest CO_2 drop, which began in the 1500s, occurred at a time of mass mortality caused by early contact of indigenous Americans with Europeans. By affecting atmospheric CO_2 concentrations, pandemics played a role in the century-scale temperature oscillations of the last 2000 years.

3. IS THE HYPOTHESIS BASED ON A VALID TIMESCALE?

[11] One potential criticism of the early anthropogenic hypothesis is that the timescale used to define the greenhouse gas trends during the three previous interglaciations may not have been accurate. In this section the greenhouse gas trends in Vostok ice from the timescale of *Ruddiman and Raymo* [2003], the one on which the hypothesis was based, are compared to those from the timescales of *Petit et al.* [1999] and *Shackleton* [2000].

[12] The three timescales were based on tuning fluctuations in various gases to different target signals. The landmark paper of *Petit et al.* [1999] presented the full Vostok record and the first timescale (called GT4). The part of the timescale younger than 110,000 years ago came from *Jouzel et al.* [1990]. The timescale for the part of the record older than 110,000 years ago was based on a single control point at 390,000 years ago derived from correlating to a feature in the marine isotopic record. Depths between those two levels were dated using an ice flow model. *Petit et al.* [1999] noted a close correlation between $\delta^{18}O_{atm}$ and Northern Hemisphere insolation in the record above 110,000 years ago, but they noted large offsets below that level and summarized these offsets in their Table 1. Subsequent modeling has confirmed that these offsets are the result of anomalous ice flow near Vostok [*Parrenin et al.*, 2004]. The version of the GT4 timescale in this paper uses Table 1 from *Petit et al.* [1999], with the adjustment for the offsets.

[13] *Shackleton* [2000] created a timescale that tuned the $\delta^{18}O_{atm}$ record to orbital precession. The $\delta^{18}O_{atm}$ signal reflects changes in both global ice volume and in biogenic exchanges [*Bender et al.*, 1994]. The ice volume component of the $\delta^{18}O_{atm}$ signal is controlled by the mean $\delta^{18}O$ ratio in ocean water, which, in turn, is controlled by storage of ^{16}O-rich water in ice sheets. The ice volume component accounts for the major part (~1.1 out of 1.5‰) of the glacial-interglacial range of $\delta^{18}O_{atm}$ changes. The biogenic part of the $\delta^{18}O_{atm}$ signal superimposes large 23,000-year variations tied to monsoonal and other controls of global photosynthesis on the ice volume part of the signal. Shackleton based his tuning procedure on the assumption that the prominent 23,000-year component of the $\delta^{18}O_{atm}$ signal has an early September phase that lags ~3500 years behind midsummer (July) insolation.

[14] *Ruddiman and Raymo* [2003] devised a CH_4 timescale by tuning the methane record to mid-July Northern Hemisphere insolation. They based this choice on the orbital monsoon hypothesis of *Kutzbach* [1981], who proposed that midsummer (July) insolation drives tropical monsoons. *Chappellaz et al.* [1990, 1997] linked this hypothesis to CH_4 emissions by assuming that monsoonal rains flood wetlands and create standing water from which plants emit methane. Because the 23,000-year cycle of orbital precession dominates insolation changes at tropical-subtropical latitudes, methane emissions generated by tropical monsoon should occur in phase with the 23,000-year (July) insolation cycle. This link is supported by the close match between the most recent insolation maximum calculated from orbital variations and the methane maximum in Greenland Ice Core Project ice dated by counting annual layers [*Blunier et al.*, 1995]. Both maxima occurred 11,000–10,500 years ago.

[15] The three timescales for Vostok ice yield similar average phases for greenhouse gas changes at the orbital periods of 23,000, 41,000, and ~100,000 years, although they differ by thousands of years at specific levels. The timescales are also very similar to one derived independently by correlating N_2/O_2 ratios to Southern Hemisphere insolation [*Bender*, 2002]. Given this general similarity, the first question asked here is this: Do these timescales support or oppose the hypothesis that the late Holocene greenhouse gas trends are anomalous?

[16] Late in the last three deglaciations, CO_2 and CH_4 concentrations rose rapidly to maximum values (Figures 3–5). The estimated ages of the greenhouse gas peaks indicated by the three timescales agree to within 1000–2000 years. Similar rises in CO_2 and CH_4 occurred during the most recent deglaciation (Figures 1a and 1b).

[17] All three timescales then show persistent CO_2 and CH_4 decreases early in each of the three previous interglaciations (Figures 3–5), with at most brief reversals. These downward trends differ markedly from the persistent gas increases during the Holocene (Figure 1). All three time-

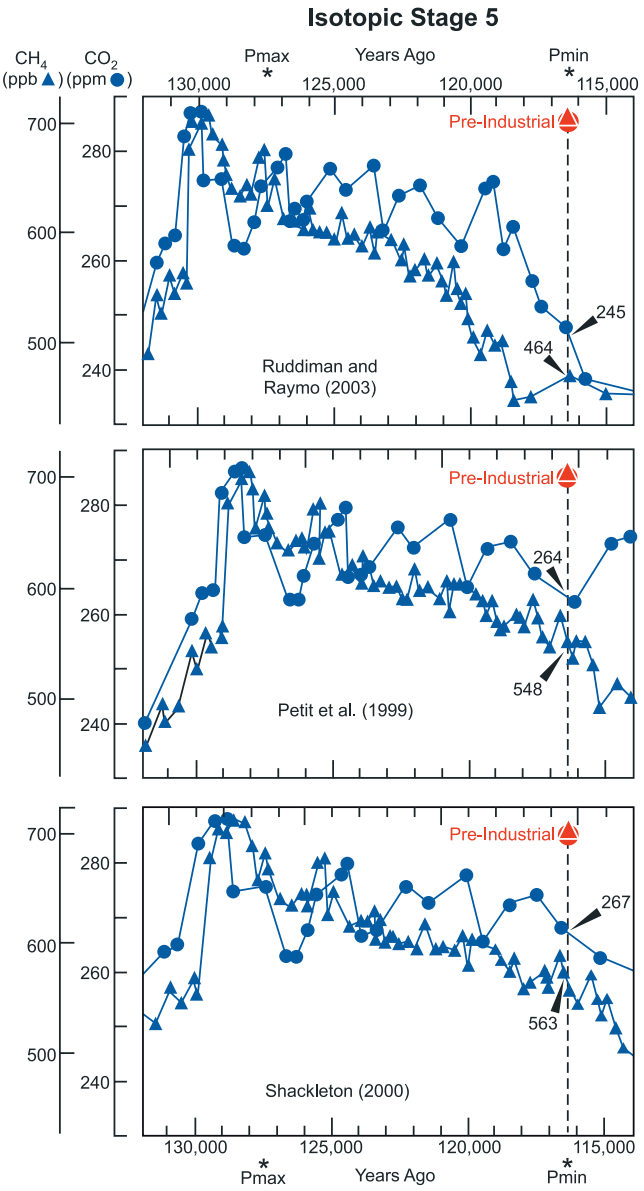

Figure 3. Three independent gas timescales for Vostok ice [*Petit et al.*, 1999; *Shackleton*, 2000; *Ruddiman and Raymo*, 2003] showing methane and CO_2 concentrations reaching maximum values near the start of interglacial stage 5 and then declining to concentrations well below peak preindustrial Holocene values (red) by the time of the first precession minimum.

scales thus clearly support the centerpiece of the early anthropogenic hypothesis: Natural forcing early in the three previous interglaciations caused gas concentrations to fall, and the rising gas trends in the Holocene are anomalous by comparison.

[18] The second question addressed in this section (and revisited in sections 4 through 6) is whether or not the anomalies are as large as those claimed in the early anthropogenic hypothesis: 40 ppm for CO_2 and 250 ppb for methane. Calculating the size of the Holocene greenhouse gas anomalies first requires choosing a preindustrial Holocene value. The peak Holocene CO_2 value of 284 ppm chosen here is from Law Dome [*Etheridge et al.*, 1996] and Taylor Dome [*Indermuhle et al.*, 1999]. The choice of a peak CH_4 value is potentially complicated by the interhemispheric methane gradient between Antarctica and Greenland. Because all comparisons made here are based on analyses of Antarctic (Vostok) ice, the peak Holocene CH_4 value used (704 ppb) is taken from Law Dome [*Etheridge et al.*, 1998].

[19] The next step is to choose those times during previous interglaciations that were most similar to the preindustrial Holocene and to the present day. *Ruddiman*

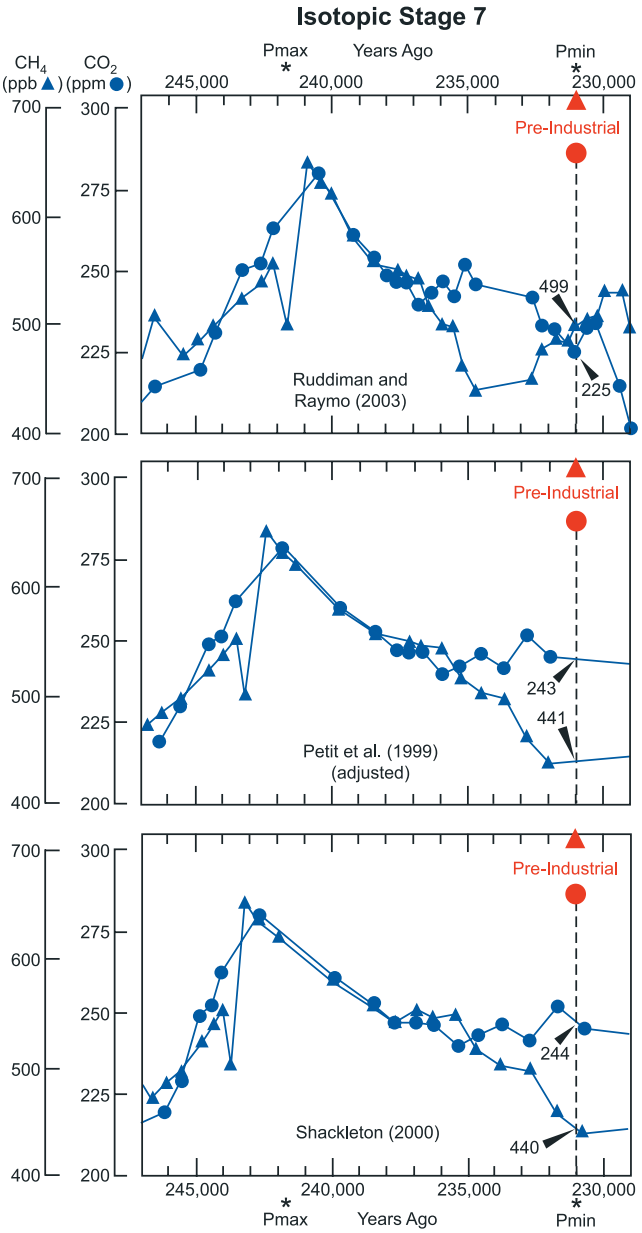

Figure 4. Three independent gas timescales for Vostok ice [*Petit et al.*, 1999; *Shackleton*, 2000; *Ruddiman and Raymo*, 2003] showing methane and CO_2 concentrations reaching maximum values near the start of interglacial stage 7 and then declining to concentrations well below peak preindustrial Holocene values (red) by the time of the first precession minimum.

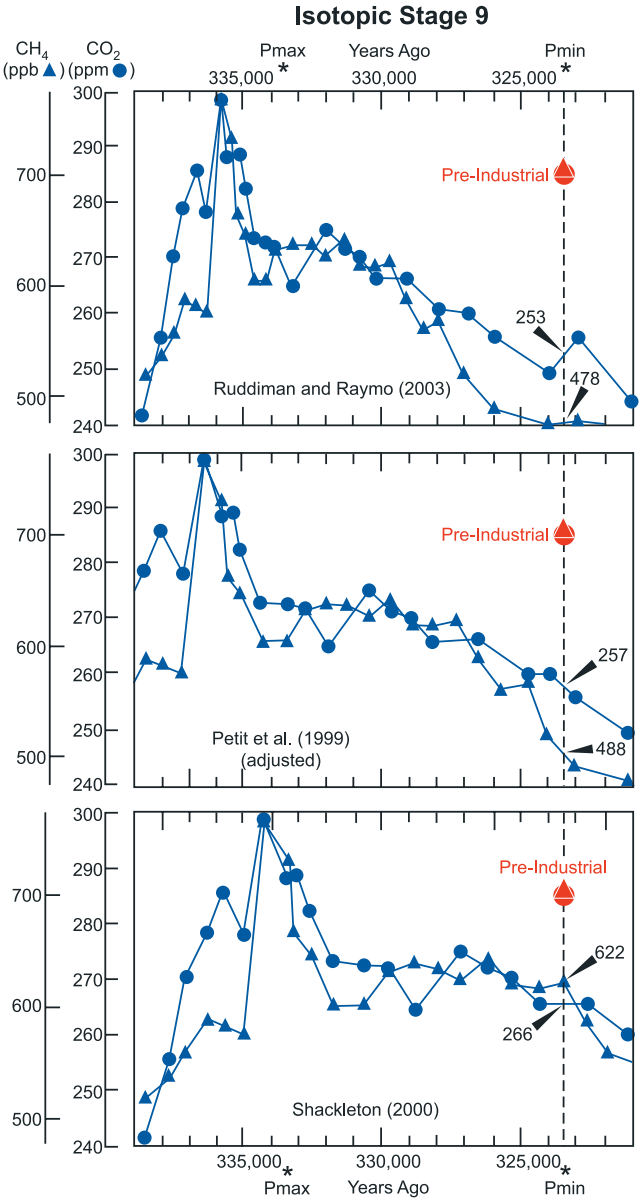

Figure 5. Three independent gas timescales for Vostok ice [*Petit et al.*, 1999; *Shackleton*, 2000; *Ruddiman and Raymo*, 2003] showing methane and CO_2 concentrations reaching maximum values near the start of interglacial stage 9 and then declining to concentrations well below peak preindustrial Holocene values (red) by the time of the first precession minimum.

[2003] chose as a reference level the first precession minimum after complete deglaciation. Because precession dominates monthly summer insolation changes at northern latitudes during interglacial isotopic stages, it is the main driver both of tropical monsoons [*Kutzbach*, 1981; *Yuan et al.*, 2004] and the CH_4 fluxes they generate [*Chappellaz et al.*, 1990, 1997]. Changes in precession during interglacial isotopic substages are also an important cause of Northern Hemisphere summer cooling and ice growth.

[20] Astronomical variations place precession minima during previous interglaciations at ~323,500 years ago for isotopic stage 9, ~231,000 years ago for stage 7, and ~116,500 years ago for stage 5. Summer half-year insolation minima at 65°N calculated from the combined effects of tilt and precession fall within ~1500 years of these levels [*Berger*, 1978]. Tables 1 and 2 compare the greenhouse gas concentrations at these precession minima during previous interglaciations against peak preindustrial values. Because the peak amplitudes of the gas concentrations vary considerably among these interglaciations, the anomalies are also calculated relative to the late deglacial gas concentration peaks within each interglaciation.

[21] For all three timescales and for all three previous interglaciations both the CO_2 and methane concentrations at the time of the closest modern analog (the first precession minimum) were substantially lower than the preindustrial concentrations (Tables 1 and 2). Individual anomalies range from 82 to 295 ppb for methane and from 17 to 54 ppm for CO_2. The *Petit et al.* [1999] timescale yields average anomalies of 199–206 ppm for methane and 30–34 ppm for CO_2, while the *Shackleton* [2000] timescale gives average anomalies ranging from 25 to 29 ppm for CO_2, and from 162 to 169 ppb for methane. In summary, regardless of which timescale is chosen, the Holocene trends are anomalous by large amounts relative to the three previous interglaciations.

4. TESTING THE TIMESCALES

[22] Disagreements among the three timescales over the size of the CH_4 and CO_2 anomalies in Tables 1 and 2 follow a similar pattern. The average anomalies calculated from the timescale of *Ruddiman and Raymo* [2003] are largest; those based on the timescale of *Shackleton* [2000] are smallest; and those from the (adjusted) GT4 timescale of *Petit et al.* [1999] are intermediate in size. These differences presumably result from the differing assumptions used in creating each timescale. The following discussion primarily focuses on differences between the two most discrepant timescales, those of *Shackleton* [2000] and *Ruddiman and Raymo* [2003].

[23] *Shackleton* [2000] tuned $\delta^{18}O_{atm}$ variations to the precession signal. He assumed an early September phase for the tuning target as an average response of the combined ice volume and biomass contributions to $\delta^{18}O_{atm}$ changes. Questions have been raised, however, about whether the phase of the $\delta^{18}O_{atm}$ response to insolation remained constant through time, given changes in the relative contributions from ice volume and biomass [*Sowers et al.*, 1993; *Bender et al.*, 1994].

[24] *Ruddiman and Raymo* [2003] tuned methane variations to the midsummer phase of the 23,000-year precession signal, which dominates forcing of tropical-subtropical monsoons. This choice assumes a fast methane response to midsummer insolation forcing, but it ignores the possibility that methane concentrations might also have been affected by processes linked to slow increases in ice volume early in each interglaciation. Sections 4.1–4.3 summarize three independent assessments of the validity of these timescales.

TABLE 1. CH_4 Anomalies (in ppb) During Stages 5, 7, and 9

	CH_4 at Precession Minimum	Anomaly Versus Preindustrial, 704 ppb	Anomaly Versus Previous CH_4 Maximum
Stage 5 (710 ppb maximum)			
Ruddiman and Raymo [2003]	464	240	246
Petit et al. [1999]	548	156	162
Shackleton [2000]	563	141	147
Stage 7 (650 ppb maximum)			
Ruddiman and Raymo [2003]	499	205	151
Petit et al. [1999]	441	263	209
Shackleton [2000]	440	264	210
Stage 9 (773 ppb maximum)			
Ruddiman and Raymo [2003]	478	226	295
Petit et al. [1999]	488	216	285
Shackleton [2000]	622	82	151
Averages			
Ruddiman and Raymo [2003]	480	224	231
Petit et al. [1999]	492	212	219
Shackleton [2000]	542	162	169
All timescales	505	199	206

4.1. Speleothem Evidence of Monsoon Timing

[25] Analyses of the $\delta^{18}O$ composition of speleothem calcite in southern Asia provide one way to test the validity of these timescales. *Yuan et al.* [2004] found orbital-scale $\delta^{18}O$ changes of such large amplitude that they can only have been produced by air mass variations linked to summer monsoons. Because these $\delta^{18}O$ changes in southern China have the phase of July insolation forcing, they must be the product of July monsoon forcing (consistent with *Kutzbach* [1981]). The Holocene $\delta^{18}O$ increase in southern Oman speleothems suggests that midsummer insolation also drives the strength of the Asian monsoon in the Indian sector [*Fleitmann et al.*, 2003]. Because 60% or more of orbital-scale variations in methane may have originated from wetland emissions in summer monsoon regions [*Chappellaz et al.*, 1990], the timing of methane variations early in prior interglacial stages should reflect a strong monsoonal imprint.

[26] Wetlands in northern Asia are the second important source of methane. Emissions from these regions are likely to have responded to the same heating of central Asia that drove enhanced south Asian monsoons. *Karabanov et al.* [1998] found a strong response to 23,000-year forcing by summer insolation at the 23,000-year precession cycle in late Pleistocene climatic fluctuations in Lake Baikal in Siberia. With south Asian and, apparently, boreal CH_4 emissions, both apparently driven by the same 23,000-year insolation forcing, atmospheric CH_4 concentrations should have covaried with south Asian monsoonal $\delta^{18}O$ fluctuations.

[27] Current studies of U series–dated speleothems only permit a test of the early part of interglacial stage 5 at this time. Speleothem $\delta^{18}O$ values had reached an orbital-scale maximum that indicates a full reduction in the strength of the summer monsoon by 115,500 years ago [*Yuan et al.*, 2004]. This age closely matches the first methane minimum near 116,000 years ago in the timescale of *Ruddiman and Raymo* [2003]. In contrast, the timescales of *Petit et al.* [1999] and *Shackleton* [2000] predict much later methane minima near 109,000 and 107,000 years ago (Figure 3 and Table 3a). In summary, this test favors the early stage 5 methane drop in the *Ruddiman and Raymo* [2003] timescale rather than the later decrease of the other timescales.

4.2. Rates of Ice "Accumulation"

[28] A second way to assess the validity of each timescale is to see if the age/depth relationships at Vostok are consistent with the expected patterns of initial ice accumulation and subsequent ice flow. At Vostok, long-term ice flow and thinning has gradually reduced the thickness of ice preserved per unit time from more than 20 m/1000 years in the early Holocene to ~3 m/1000 years in stage 9 [*Petit et al.*, 1999].

[29] Deuterium (δD) trends at Vostok indicate that the early interglacial intervals under consideration here were the warmest times in Antarctica within the last 400,000 years. On the basis of regional δD trends in present-day Antarctica [*Jouzel et al.*, 1990], warmer temperatures during these peak interglacial intervals should have produced greater fluxes of water vapor and higher rates of initial ice accumulation. As a result these warm early interglacial intervals should have recorded high ice accumulation rates (ice thickness per unit time) compared to the immediately overlying and underlying levels in the ice.

[30] Table 3b compares the ice thickness per unit time in each early interglacial interval with the values for the immediately preceding and succeeding intervals. Each "early interglacial" interval is defined as the length of ice core between the age equivalent to the late deglacial precession maximum and the early interglacial precession minimum, based on the ages estimated by each timescale. Accumulation rates during these intervals are compared to

TABLE 2. CO_2 Anomalies (in ppm) During Stages 5, 7, and 9

	CO_2 at Precession Minimum	Anomaly Versus Preindustrial, 284 ppm	Anomaly Versus Previous CO_2 Maximum
Stage 5 (287 ppm maximum)			
Ruddiman and Raymo [2003]	245	39	42
Petit et al. [1999]	264	20	23
Shackleton [2000]	267	17	20
Stage 7 (279 ppm maximum)			
Ruddiman and Raymo [2003]	225	59	54
Petit et al. [1999]	243	41	36
Shackleton [2000]	244	40	35
Stage 9 (299 ppm maximum)			
Ruddiman and Raymo [2003]	253	31	46
Petit et al. [1999]	257	27	42
Shackleton [2000]	266	18	33
Averages			
Ruddiman and Raymo [2003]	241	43	47
Petit et al. [1999]	254	30	34
Shackleton [2000]	259	25	29
All timescales	251	32	37

TABLE 3A. Predicted Age of the First Methane Minimum Early in Interglacial Stage 5 for Three Timescales Compared to Age of 115,000 Years Based on Speleothem $\delta^{18}O$ Trends FromSouth China[a]

	Age of Methane Mimimum, years
Speleothems	115,500
Ruddiman and Raymo [2003]	116,200
Petit et al. [1999]	109,000
Shackleton	107,200

[a]See *Yuan et al.* [2004].

those during the 20,000 years preceding the late deglacial precession maxima and the 20,000 years following the early interglacial precession minima, again using age estimates based on each timescale.

[31] The analysis shows five departures (keyed with footnotes) from the expected pattern of highest ice accumulation rates during the warmest peak interglacial intervals. The longer-term down-core thinning trend of Vostok ice (ignoring shorter-term climate-related changes in accumulation) averages ~5% per 10,000 years. For the 15,000-year span between the middle of the peak interglacial intervals and the middle of the overlying intervals this rate would imply a reduction of 7–8% in initial ice accumulation. All of the footnoted intervals have accumulation rates at least 7.5% higher than those during the peak interglacial intervals, and these higher rates cannot be ascribed to ice flow and gradual down-core thinning.

[32] The three intervals footnoted during stages 7 and 9 in the timescale of *Shackleton* [2000] have much higher accumulation rates during colder climates and fail this test. The two intervals footnoted in stages 7 and stage 9 in the timescale of *Petit et al.* [1999] have accumulation rates that are anomalous by lesser amounts but also fail this test. None of the intervals in the timescale of *Ruddiman and Raymo* [2003] are anomalous. In summary, the timescale of *Shackleton* [2000] fails the accumulation rate tests in stages 7 and 9, while that of *Ruddiman and Raymo* [2003] passes all the tests.

4.3. Comparing Atmospheric and Marine $\delta^{18}O$ Trends

[33] A third way to test the relative validity of the ice core timescales is to compare the timing of changes in the marine $\delta^{18}O$ carbonate signal ($\delta^{18}O_c$) against the timing of the Vostok atmospheric signal ($\delta^{18}O_{atm}$) predicted by each timescale. Because the mean value of seawater $\delta^{18}O$ ($\delta^{18}O_{sw}$) accounts for a large fraction of the $\delta^{18}O_c$ signal and is also the major control on the $\delta^{18}O_{atm}$ signal, trends of these two indices should be closely linked in time after allowing for various overprints.

[34] The Spectral Analysis: Mapping and Prediction (SPECMAP) project [*Imbrie et al.*, 1984] devised an age scale for the marine $\delta^{18}O_c$ record by treating it as an ice volume signal and lagging it behind the insolation forcing at the periods of precession and tilt. Subsequent U series dates on coral reefs [*Edwards et al.*, 1987; *Bard et al.*, 1990] led to a substantial reduction in the estimated response time of ice sheets at these two periods [*Imbrie et al.*, 1992]. Independent analyses have suggested that the original timescale of SPECMAP needs to be shifted 1500 to 2000 years earlier in time to reflect this faster ice response [*Pisias et al.*, 1990; *Shackleton*, 2000]. For the comparisons shown in Figure 6, the ages of all SPECMAP substage boundaries have been shifted by 2000 years.

[35] Midpoint positions of the early interglacial marine $\delta^{18}O_c$ transitions (5.5/5.4, 7.5/7.4, and 9.3/9.2) are marked in Figure 6 by red asterisks, and midpoint positions of the $\delta^{18}O_{atm}$ transitions for each gas timescale for Vostok are indicated by black arrows. If ice volume were the only factor controlling both the marine and ice core $\delta^{18}O$ signals, the $\delta^{18}O_{atm}$ transitions should lag the $\delta^{18}O_c$ signal by 1000–2000 years, the time required for the $\delta^{18}O_{sw}$ signal to mix through the large O_2 reservoir in the atmosphere [*Bender et al.*, 1994]. Both signals, however, contain overprints that could also affect the timing of major $\delta^{18}O$ transitions.

[36] Marine $\delta^{18}O_c$ signals have temperature overprints that may account for as much as half of the $\delta^{18}O$ increases following peak interglacial conditions [*Labeyrie et al.*, 1987; *Lea et al.*, 2001]. If this temperature overprint has the "late" phase of ice volume ($\delta^{18}O_{sw}$), it would cause no shift in the timing of the $\delta^{18}O_c$ signal. However, if the temperature overprint has the "early" phase of the insolation forcing, it could shift the marine $\delta^{18}O_c$ signal earlier in time by several thousand years.

[37] Similarly, $\delta^{18}O_{atm}$ signals are overprinted by a secondary biomass ("Dole effect") component. Tropical monsoons play a large role in the Dole effect [*Bender et al.*, 1994], and monsoonal changes at the precession signal have the "early" phase of July insolation [*Yuan et al.*, 2004]. Because this biomass overprint is phased some 5000 years ahead of the ice volume ($\delta^{18}O_{sw}$) response, it should shift the observed $\delta^{18}O_{atm}$ signal to a substantially earlier phase.

TABLE 3B. Ice Accumulation/Preservation Rates for Interglacial Isotopic Stages 5, 7, and 9[a]

Interglacial Stage	Ice Thickness per Unit Time, m/1000 years		
	Peak Interglaciation	Preceding 20,000 Years	Subsequent 20,000 Years
Stage 5			
Ruddiman and Raymo [2003]	21	15	10
Petit et al. [1999]	16	13	13
Shackleton [2000]	15	10	13
Stage 7			
Ruddiman and Raymo [2003]	7.0	3.6	6.5
Petit et al. [1999]	6.6	4.5	6.9[b]
Shackleton [2000]	3.2	4.3[b]	6.6[b]
Stage 9			
Ruddiman and Raymo [2003]	4.2	4.1	3.0
Petit et al. [1999]	3.3	1.9	3.7[b]
Shackleton [2000]	3.3	3.1	4.0[b]

[a]Thickness is given per unit time.
[b]Values higher than peak interglacial value (suspect) are indicated.

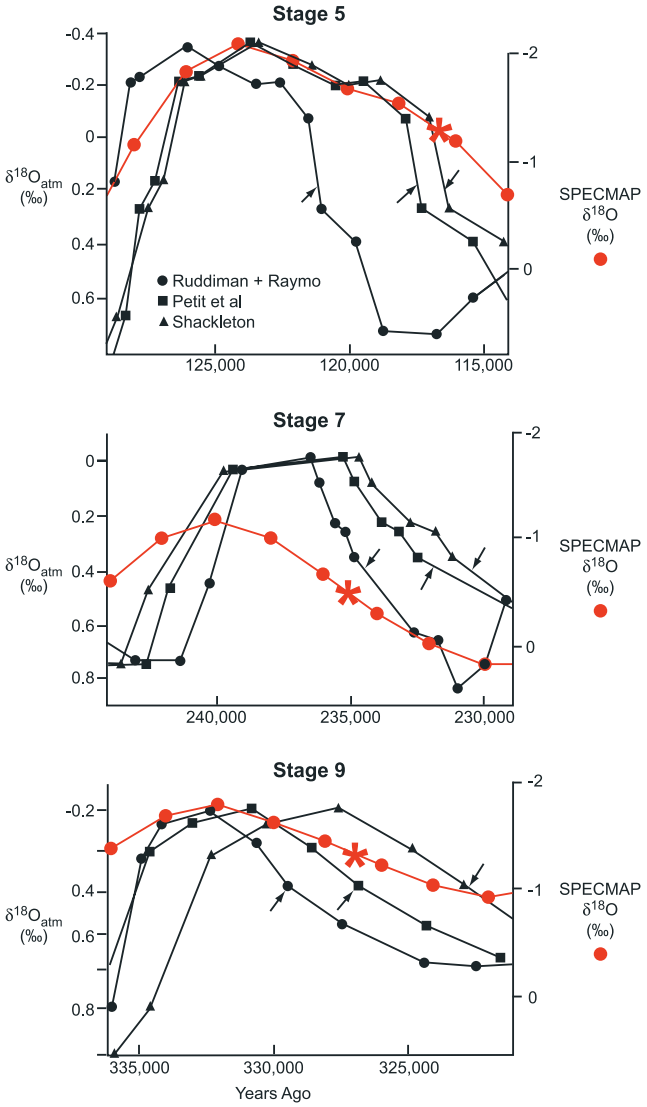

Figure 6. Comparison of marine and ice core $\delta^{18}O$ records. The normalized marine $\delta^{18}O$ signal from SPECMAP [*Imbrie et al.*, 1984] is shown in red, with asterisks marking the midpoints of the early interglacial $\delta^{18}O$ increases. The $\delta^{18}O_{air}$ records for the three Vostok gas timescales [*Petit et al.*, 1999; *Shackleton*, 2000; *Ruddiman and Raymo*, 2003] are shown in black, with arrows marking the midpoints of the $\delta^{18}O_{air}$ increases.

[38] The combined effect of these overprinting factors on the relative $\delta^{18}O$ phasing between the marine cores and the ice cores is difficult to predict. In view of the large uncertainties the ice core $\delta^{18}O_{atm}$ and marine $\delta^{18}O_c$ increases that followed peak interglacial conditions could have led or lagged each other by a few thousand years. In the analysis summarized in Table 3c, only leads or lags larger than 2000 years (an arbitrary choice) are tagged as suspect.

[39] In interglacial stage 5 the $\delta^{18}O_{atm}$ signal of *Ruddiman and Raymo* [2003] leads the marine $\delta^{18}O$ signal by ~4400 years, while the $\delta^{18}O_{atm}$ signals from the other two timescales are in phase to within 1000 years. The large lead from the *Ruddiman and Raymo* [2003] timescale is thus suspect, but this conclusion is contradicted by the close match between the CH_4 decrease and the change in speleothem $\delta^{18}O$ values for this timescale (Table 3a).

[40] In interglacial stage 7 the $\delta^{18}O_{atm}$ signals for all three timescales lag the marine $\delta^{18}O$ signal: by ~700 years for *Ruddiman and Raymo* [2003], by ~3300 years for *Petit et al.* [1999], and by ~4800 years for *Shackleton* [2000]. The lags of the *Petit et al.* [1999] and *Shackleton* [2000] timescales are both consistent with the anomalous ice accumulation rates in Table 3b.

[41] For interglacial stage 9 the $\delta^{18}O_{atm}$ signal from *Ruddiman and Raymo* [2003] has a marginally suspect lead of ~2600 years relative to the marine $\delta^{18}O$ signal. The $\delta^{18}O$ transitions are closely positioned in the *Petit et al.* [1999] timescale. The large lag (4100 years) of the $\delta^{18}O_{atm}$ signal from *Shackleton* [2000] behind the marine $\delta^{18}O$ timescale (Table 3c) matches the anomaly in accumulation rates in Table 3b.

[42] In summary, three independent tests (Table 3) identify instances in which the timescales shown in Figures 3–5 could be in error. One test in stage 5 (Table 3c) identifies the timescale of *Ruddiman and Raymo* [2003] as suspect, but another test (Table 3a) identifies it as the best of the timescales. Analysis of accumulation rate and $\delta^{18}O$ trends suggests that the timescale of *Shackleton* [2000] is considerably in error during stages 7 and 9. The *Petit et al.* [1999] timescale also fails some tests in stage 7 and 9 but by more marginal amounts.

[43] In general, these tests suggest that the timescale of *Shackleton* [2000] should be rejected along with the smaller CO_2 and CH_4 anomalies it predicts. Because the timescale of *Ruddiman and Raymo* [2003] passes more tests than that of *Petit et al.* [1999], the larger gas anomalies it predicts (Tables 1 and 2) are more likely to be valid. New methods for improving the ice core timescales in early interglacial intervals are obviously critical for resolving remaining uncertainties.

5. IS ISOTOPIC STAGE 11 A BETTER ANALOG FOR THE HOLOCENE?

[44] Another challenge to the early anthropogenic hypothesis is that the wrong interglaciations were used as analogs for the Holocene. *Ruddiman* [2003] compared

TABLE 3C. Age Offsets in Years Between the Midpoints of Early Interglacial $\delta^{18}O_{atm}$ Transitions as Predicted by the Three Timescales Shown and the Midpoints of Marine $\delta^{18}O$ Transitions Based on *Imbrie et al.* [1984][a]

	Stage 5	Stage 7	Stage 9
Ruddiman and Raymo [2003]	+4400[b]	−700	+2600[b]
Petit et al. [1999]	+1000	−3300[b]	−100
Shackleton [2000]	−200	−4800[b]	−4100[b]

[a]Timescales are shifted older in age by 2000 years as explained in text.
[b]Suspect lead or lag values are indicated.

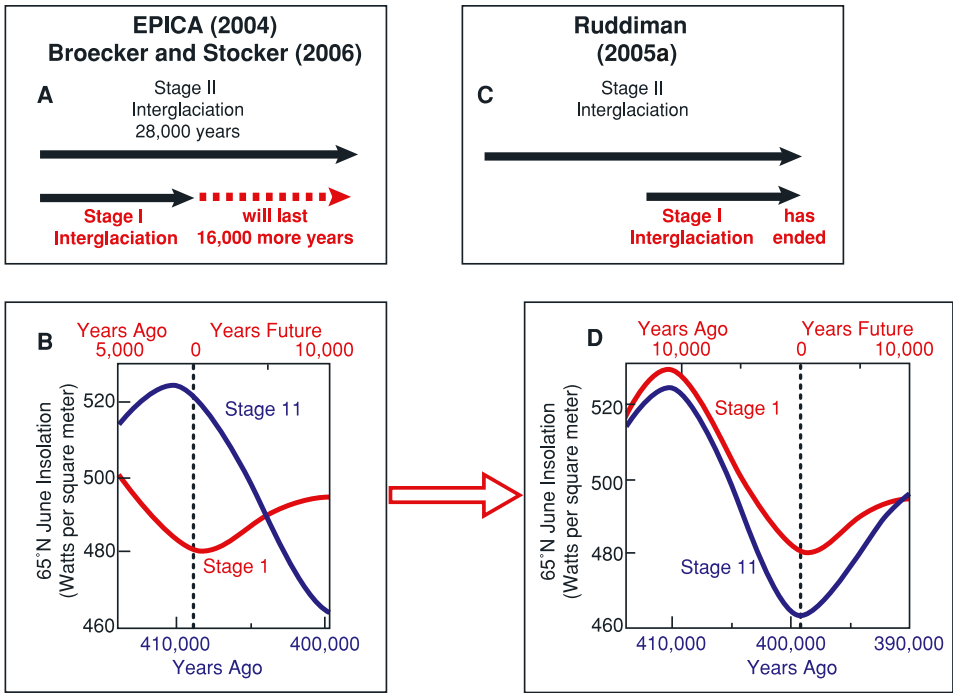

Figure 7. (a) Alignment of interglacial warmth during stages 1 and 11 proposed by *EPICA Community Members* [2004] and by *Broecker and Stocker* [2006] resulting in (b) an inverted alignment of 65°N summer insolation trends for the two interglaciations. (d) The closest 65°N insolation analog within stage 11 indicating that (c) the current (Holocene) interglaciation should have ended by now.

trends in the Holocene to those in the last three interglaciations, but insolation changes at the 23,000-year precession cycle were larger in amplitude during those interglaciations than during the Holocene because of stronger modulation by eccentricity variations at the 413,000-year cycle. Because the isotopic stage 11 interglaciation ~400,000 years ago was the last time that eccentricity was as low as it is now, stage 11 has been proposed as the best analog for Holocene climate.

[45] Several studies tied to stage 11 have come to the conclusion that the current interglaciation may last thousands of years into the future. First, analysis of changes in the δD ratio in the EPICA (European Programme for Ice Coring in Antarctica) Dome Concordia (EDC) ice core from Antarctica indicated that the interglacial warmth of isotopic stage 11 lasted 28,000 years, whereas the warmth of the current interglaciation has only lasted 12,000 years [*EPICA Community Members*, 2004]. These results implied that the current interglaciation could last another 16,000 years. Similarly, analysis of marine sediment cores in the North Atlantic showed that warm stage 11 sea surface temperatures persisted for ~28,000 years [*McManus et al.*, 2003], whereas full interglacial warmth in stage 1 in that region has only lasted 11,500 years. Third, energy balance model simulations suggested that future orbital insolation changes in the Northern Hemisphere will not produce ice growth for at least another 40,000 years [*Loutre and Berger*, 2000].

[46] This convergence of evidence appeared to refute the claims by *Ruddiman* [2003] that climate should have cooled by now and that the start of the "next" glaciation is actually overdue. A close examination of the evidence on which those conclusions were based, however, has revealed flaws that refute this conclusion.

[47] *Ruddiman* [2005a] concluded that the method used by *EPICA Community Members* [2004] to align stage 11 with the Holocene was flawed. They chose to align deglacial terminations V and I and to count forward in "elapsed time" in order to determine the relative lengths of the two intervals of interglacial warmth (Figure 7a). Comparison of the δD records showed that the relative warmth in Antarctica lasted much longer for stage 11 than it has for the Holocene.

[48] This method, however, ended up aligning the present-day Northern Hemisphere summer insolation minimum with a stage 11 insolation maximum (Figure 7b). Such an alignment would only make sense if insolation changes have had no impact on Earth's climate. Yet both the Ice Age hypothesis of *Milankovitch* [1941] and the orbital monsoon hypothesis of *Kutzbach* [1981] are rooted in the premise of insolation forcing, specifically insolation variations during Northern Hemisphere summer. From the vantage point of these two hypotheses, which are arguably the two greatest advances in our current understanding of orbital-scale climate, the insolation "misalignment" shown in Figure 7b makes no sense.

[49] The cause of this misalignment is the result of two factors. The first problem is the use of δD data by the EPICA group to define the length of the two "interglaciations." The problem is that the interval during which the Antarctic region remained at or near maximum warmth (as indicated by the δD data) is not equivalent to ice-free conditions in the Northern Hemisphere. The onset of warm

temperatures in the circum-Antarctic began early in terminations I and V, long before Northern Hemisphere ice sheets melted.

[50] The second problem is the unusual length of termination V compared to termination I. Termination V lasted nearly 20,000 years (from ~428,000 to ~408,000 years ago) in the timescales of both SPECMAP [*Imbrie et al.*, 1984] and *Lisiecki and Raymo* [2005]. In contrast, termination I only lasted ~10,000 years (from ~17,000 to ~7000 years ago).

[51] As a result of these two factors the Antarctic was in a warm "interglacial" state for the full 20,000-year length of termination V (from ~428,000 to ~408,000 years ago) before the Northern Hemisphere finally became ice-free. During the most recent deglaciation the Antarctic region was in a similarly warm state for the final 5000 years of termination I (from ~12,000 to ~7,000 years ago) before the last northern ice melted. Consequently, by the time the northern continents reached true interglacial (ice free) conditions, the EPICA "interglacial clock" had already been running for 20,000 years on termination V but only for 5000 years on termination I. As a result the EPICA estimates of the lengths of the two interglacials were already offset by ~15,000 years before the actual interglaciations even began. This offset accounts for the misalignment shown in Figure 7b.

[52] The obvious insolation analog is the alignment that juxtaposes the present-day insolation minimum against the first insolation minimum in the ice-free part of stage 11 (Figure 7d). The alignment selected by *Berger and Loutre* [2003] is the insolation minimum just after 400,000 years ago. As discussed in section 5.1, this insolation minimum coincided with a time when greenhouse gas levels were falling and climate was cooling, consistent with the early anthropogenic hypothesis. In short, a long interval of relative warmth did exist in Antarctica during much of termination V and in the early part of stage 11, but it had come to an end by just after 400,000 years ago, the time of the best insolation analog to the Holocene (Figure 7c).

[53] A similar conclusion holds for the long interval of warm sea surface temperatures in the North Atlantic during stage 11 noted by *McManus et al.* [2003]: Times of warmth in the North Atlantic cannot be equated with ice-free conditions on nearby continents. For example, during marine isotopic substage 5a, North Atlantic temperatures were at or near peak interglacial values [*Sancetta et al.*, 1973], yet the ice sheets at that time were large enough to account for the sea level drop of 15–20 m below the modern position [*Chappell and Shackleton*, 1986; *Bard et al.*, 1990]. In addition, *Ruddiman and McIntyre* [1979] showed that Atlantic surface waters south of Iceland can remain at interglacial warmth early in episodes of ice growth on land.

[54] Finally, the same model that simulated 40,000 future years with no new ice growth also simulated a very long ice-free interval during stage 11 [*Loutre and Berger*, 2000]. Yet when CO_2 forcing for stage 11 based on the Vostok ice core record was added to the insolation forcing, the model simulated ice growth by ~400,000 years ago, shortening the ice-free interval in stage 11 by ~40,000 years [*Berger and Loutre*, 2003]. According to this simulation, stage 11 was not ice-free for many tens of thousands of years but was so for probably less than 10,000 years.

[55] In summary, arguments that use stage 11 as a basis for concluding that natural climate will not cool and that northern ice sheets will not form until far in the future are flawed. Instead, major cooling had begun by the time of the closest stage 11 analog to modern insolation.

5.1. Greenhouse Gas Changes During the Closest Insolation Analog in Stage 11

[56] The stage 11 interval with 65°N insolation values most similar to those in the late Holocene dates to just after 400,000 years ago (Figure 7d). Three independent timescales identified the same interval of Vostok ice as containing this closest modern analog: the GT4 timescale of *Petit et al.* [1999], the $\delta^{18}O_{atm}$ timescale of *Shackleton* [2000], and a timescale based on correlating O_2/N_2 variations in Vostok ice to summer solstice (December 21) insolation at 78°S [*Bender*, 2002].

[57] The GT4 timescale of *Petit et al.* [1999] showed that CO_2 and CH_4 concentrations had decreased by the time of the closest stage insolation analog to today (Figure 8), although the estimated anomalies relative to the peak concentrations in the late Holocene were smaller than those derived from the stages 5, 7, and 9 interglaciations (Table 4). Trends from *Shackleton* [2000] are omitted because of the many tests failed in interglacial stages 5, 7, and 9 (Tables 3a–3c).

[58] *Ruddiman* [2005a] proposed a different timescale for this interval (Figure 8a). The methane minimum in the Vostok record was placed at the first July insolation minimum (here dated to 398,500 years ago). This choice followed the strategy of *Ruddiman and Raymo* [2003] of tuning methane concentrations to midsummer insolation. The second control level used was the first stage 11 $\delta^{18}O_{atm}$ maximum in the Vostok record. *Bassinot et al.* [1994] named this feature substage 11.24 and assigned it an age of 390,000 years ago by correlation to the SPECMAP timescale of *Imbrie et al.* [1984]. Because ice volume changes dominate the $\delta^{18}O_{atm}$ signal, *Petit et al.* [1999] subsequently used this level and age estimate as their lowermost tie point for the Vostok G4 timescale. The age choice used by *Ruddiman* [2005a] for this feature, 392,000 years, adds the 2000-year age adjustment to the SPECMAP timescale discussed in section 4.3.

[59] The resulting timescale (Figure 8a) indicates that full interglacial conditions early in stage 11 had come to an end by the time (~398,500 years ago) when the July insolation configuration was most similar to the late Holocene. Methane concentrations had fallen to 448 ppb, nearly identical to the 450-ppb estimate in the early anthropogenic hypothesis. The anomaly calculated relative to both the preindustrial Holocene methane maximum and the peak interglacial value in stage 11 (both of which were ~704 ppb) is ~256 ppb, near the 250-ppb estimate from the early anthropogenic hypothesis. The CO_2 concentration at this

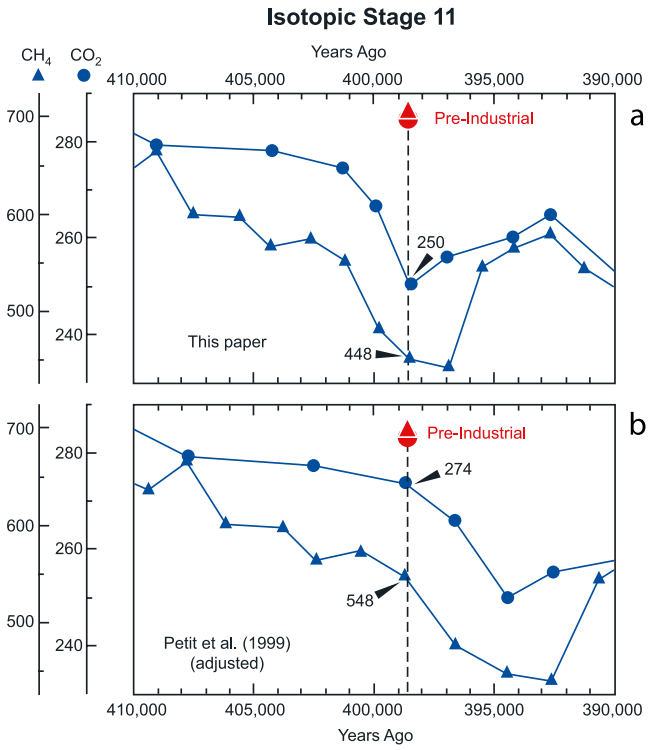

Figure 8. Gas timescales for Vostok ice from (a) this paper and (b) *Petit et al.* [1999] showing methane and CO_2 concentrations reaching maximum values near the start of interglacial stage 11 (~408,000 years ago) and then declining to concentrations below peak preindustrial Holocene values by the time of the first stage 11 precession minimum.

level in the Vostok record had fallen to ~250 ppb (Figure 8a), indicating a late Holocene CO_2 anomaly of 34 ppm (Table 4). Although the timescale for the EDC record has not yet been refined by tuning, the correlative part of the EDC record shows a slightly larger CO_2 drop to 248 ppm [*Siegenthaler et al.*, 2005a].

[60] As was the case for interglacial stages 5, 7, and 9, the critical question is which timescale for stage 11 is the most plausible. This choice effectively comes down to whether the prominent methane minimum correlates with maximum forcing of monsoons by low-latitude insolation (as in Figure 8a) or with the later substage 11.24 $\delta^{18}O$ (ice volume) maximum (as in Figure 8b).

[61] For stage 11 a strong case can be made that the best choice is to tune the methane signal to low-latitude insolation. No one has at this point suggested that large ice sheets were growing this early in stage 11. In fact, as discussed in section 5.2, the current debate centers on whether or not any ice had accumulated by this time. With minimal ice growth any effect of northern ice sheets in delaying the CH_4 response to midsummer (July) insolation forcing should have been negligible. As a result the rapid response of Asian monsoons to July insolation forcing found by *Yuan et al.* [2004] should have controlled the timing of the methane response, consistent with the timescale in Figure 8a. If so, the gas anomalies at Vostok during the closest stage 11 insolation analog to the present were very near those estimated in the early anthropogenic hypothesis. This conclusion should now be tested by tuning the full stage 11 record available in the EDC and Dome Fuji cores using a range of tuning assumptions.

5.2. Cold Climate During the Closest Insolation Analog in Stage 11

[62] By the time of the insolation minimum 398,500 years ago (Figure 7c), the δD trend in Vostok ice had fallen well toward the full glacial extreme of its range, based on the methane timescale (Figure 8a). The large δD change by this time indicates that air temperatures in the Antarctic region had already cooled well toward "glacial" levels, consistent with the early anthropogenic hypothesis (Figure 1c).

[63] A more difficult question is whether northern ice sheets had begun to grow in stage 11 by 398,500 years ago, the closest insolation analog to the late Holocene. Benthic $\delta^{18}O$ trends in many marine cores begin to increase between 402,000 and 400,000 years ago. These increases permit the growth of new ice, but they could also be an artifact of colder temperatures.

[64] The time by which new ice must have been growing in stage 11 can be estimated from benthic $\delta^{18}O$ trends in the eastern Pacific Ocean, where temperature overprints are relatively small. Large increases in benthic foraminiferal $\delta^{18}O$ values occurred between 400,000 and 390,000 years ago in cores from this region [*Mix et al.*, 1995a, 1995b]. In the same cores the total marine $\delta^{18}O$ change across termination I was 1.61‰, and the ice volume component is estimated at 1.05–1.1‰ [*Duplessy et al.*, 2002; *Schrag et al.*, 1996]. The difference between the two values, 0.51–0.56‰, can be ascribed to temperature change.

[65] This amount of temperature effect (warming) on terminations can be assumed to define the maximum size of the temperature effect (cooling) that occurred during the $\delta^{18}O$ increase early in stage 11. If so, then the time by which the total $\delta^{18}O$ increase early in stage 11 exceeded this 0.51–0.56‰ value should be the time when new ice must have existed. In Ocean Drilling Program sites 846 and 849 [*Mix et al.*, 1995a, 1995b], that time is ~395,000 years ago.

TABLE 4. Stage 11 Anomalies of CO_2 and CH_4 Relative to Late Holocene Value

	CO_2 Value at Insolation Minimum, ppm	Anomaly Versus Preindustrial Value, 284 ppm
Ruddiman [2005a]	250	34
Petit et al. [1999]	274	10
	CH_4 Value at Precession Minimum, ppb	Anomaly Versus Preindustrial Value, 704 ppb
Ruddiman [2005a]	448	256
Petit et al. [1999]	548	156

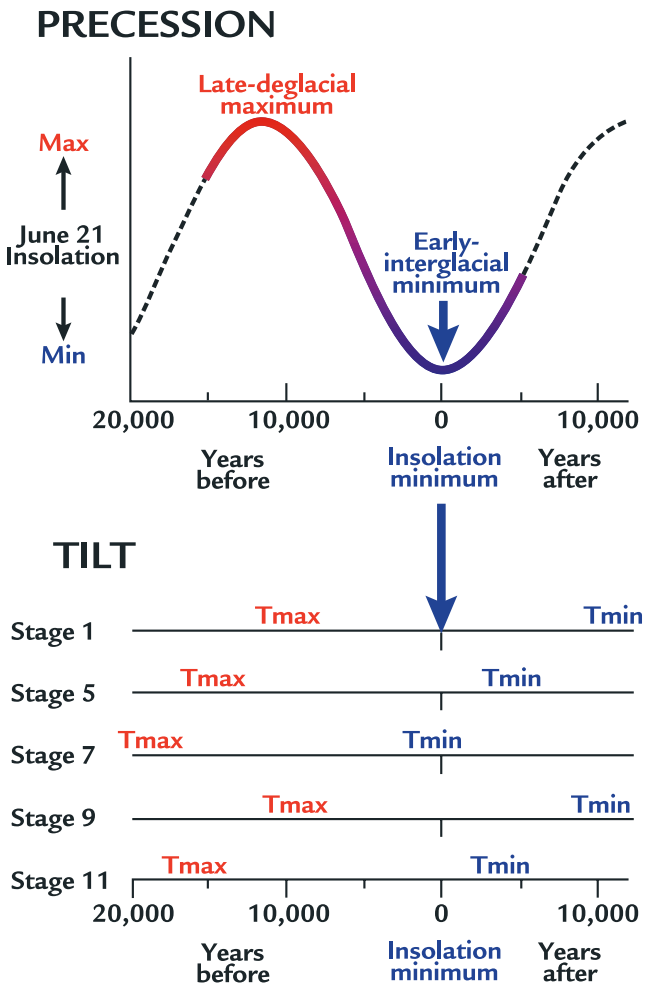

Figure 9. (top) Late deglacial and early interglacial insolation change caused by precession shown schematically. (bottom) Relative positions of insolation maxima and minima caused by changes in tilt. The most similar alignment of tilt and precession trends to those in the Holocene occurs in stage 9.

[66] In summary, benthic $\delta^{18}O$ data permit new ice sheets by 402,000–400,000 years ago, a few thousand years before the closest stage 11 insolation analog to the present day, and they require new ice by 395,000 years ago, a few thousand years after the closest modern analog. This evidence is consistent with the overdue glaciation concept, but it does not constitute unambiguous proof. The issue of whether or not a glaciation is overdue today will be revisited in section 9.

[67] Finally, what is the length of the ice-free interval during interglacial stage 11? The marine $\delta^{18}O$ timescales of SPECMAP [*Imbrie et al.*, 1984] and *Lisiecki and Raymo* [2005] both place the end of the $\delta^{18}O$ decrease in termination V near 408,000 years ago. The first increase in $\delta^{18}O$ values in deep Pacific Ocean cores (with small temperature overprints) occurred near 402,000 years ago [*Mix et al.*, 1995a, 1995b]. The evidence summarized above indicates that new ice is required by 395,000 years ago. Consequently, the ice-free part of stage 11 lasted no longer than 13,000 years and may have been as short as 6000 years.

6. WHAT IS THE OPTIMAL HOLOCENE INSOLATION ANALOG?

[68] Challenges to the early anthropogenic hypothesis [e.g., *Masson-Delmotte et al.*, 2006] have pointed out two additional problems with the search for Holocene insolation analogs. First, the 65°N insolation alignment shown in Figure 7c is not a perfect analog to the late Holocene because the stage 11 insolation minimum is deeper than the one today. Second, the choice of a monthly 65°N insolation metric places too much emphasis on insolation changes caused by precession and gives too little emphasis to tilt [see also *Huybers*, 2006]. These criticisms point to the need for a wider perspective on the issue of insolation forcing.

6.1. Does Stage 11 Provide the Best Insolation Analog to the Present?

[69] Although stage 11 would seem to be the best analog for stage 1 because it was a time of comparably low eccentricity, tilt and precession were phased very differently during these two interglaciations (Figure 9). Northern Hemisphere insolation at the precession cycle is near a minimum today, but the minimum at the tilt cycle will not occur until more than 10,000 years from now. In contrast, during stage 11 the tilt and precession minima were more nearly aligned. Because of these differing offsets, stage 11 is not a perfect insolation analog for the Holocene or for the present day [*Masson-Delmotte et al.*, 2006].

[70] On the basis of the sole criterion of the relative alignment of tilt and precession the closest analog to the Holocene is actually stage 9, with the tilt minimum falling ~10,000 years after the precession minimum (Figure 9). Of course, this assessment ignores the other major factor in the search for an analog: the amplitude of the precession minima (larger in stages 5, 7, and 9 and smaller in stages 1 and 11). The problem in finding the closest modern analog is to weigh these two competing factors.

[71] During the 1980s through the early 2000s most studies focused on insolation changes during specific summer months: either June (perihelion in the Northern Hemisphere) or July (the month of maximum midsummer heating response to seasonal Northern Hemisphere insolation). Because the slow precession of the equinoxes offers climate scientists a year-round array of extra "boosts" to each month of orbital forcing at the 23,000-year cycle, the choice of any one particular month as "critical" is arbitrary.

[72] *Milankovitch* [1941] used a different (and arguably more robust) metric, the "summer caloric half-year," defined as those 182 days of the year for which insolation is higher than the other 182 days of the year. *Berger* [1978] chose this metric in an influential early paper on insolation trends, as have some more recent studies [e.g., *Vettoretti and Peltier*, 2004]. Milankovitch's caloric summer half-year metric has the advantage of not requiring the choice of a

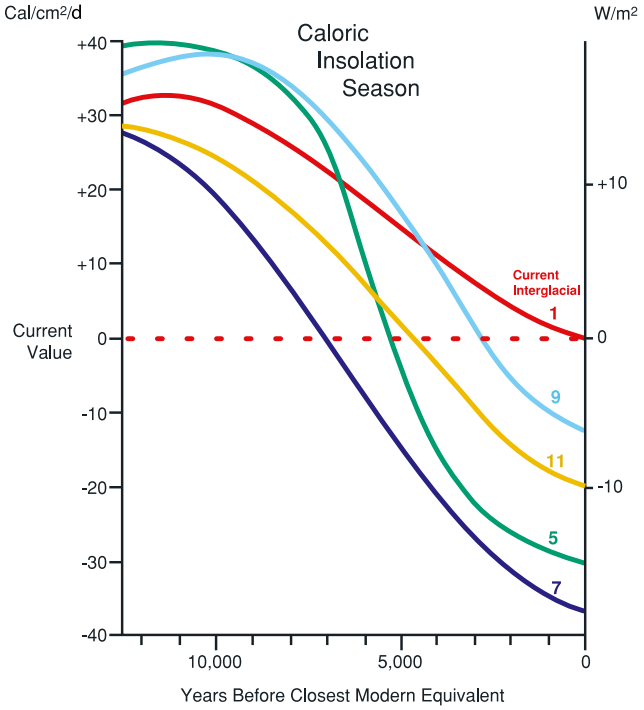

Figure 10. Caloric summer half-year insolation trends during the early parts of the last five interglaciations [from *Berger*, 1978]. The timescales are aligned on the first precession insolation minimum in each interglaciation. At and near the point of alignment the insolation values most similar to modern levels occur in stage 9.

particular month of insolation forcing. Rather, it integrates insolation surpluses and deficits throughout the entire year into a single number.

[73] This approach has a benefit somewhat analogous to that of glaciologists who use "degree days" to assess the integrated impact of all parts of the warm season on ice sheet mass balance. In their calculations, 10 days of April temperatures at 1° above freezing have the same net effect on ice mass balance as one day of July temperatures at 10° above freezing. In a similar way, Milankovitch's choice of the insolation half year integrates the forcing across the bulk of the ablation season rather than focusing only on peak summer ablation.

[74] One result of this approach is that insolation changes at the 41,000-year tilt cycle are boosted in importance relative to those at the 23,000-year precession cycle. Caloric half-year insolation surpluses and deficits for the early parts of the last five interglacial stages are compared in Figure 10. By Milankovitch's index, stage 11 is not the closest analog to the present day; instead, stage 9 is. Because Milankovitch's half-year index gives greater emphasis to tilt, the tilt minimum in stage 11 adds to the size of the (nearly coincident) precession minimum, while the much later tilt minimum in stage 9 does not do so. Consequently, the combined minima in stage 9 shown in Figure 10 remains the best analog to the Holocene. If an index were devised that gave even more importance to tilt (while not ignoring precession), stage 9 would remain the closest insolation analog to the Holocene, while the other three interglaciations would become progressively worse analogs. In summary, stage 9 is the closest insolation analog to the late Holocene based on a "robust" index that more evenly weights tilt and precession.

6.2. How Large Are the Holocene Greenhouse Gas Anomalies?

[75] Gas trends for all five interglaciations based on the timescale of *Ruddiman and Raymo* [2003] are shown in Figure 11. In comparison to the Holocene CH_4 peak of

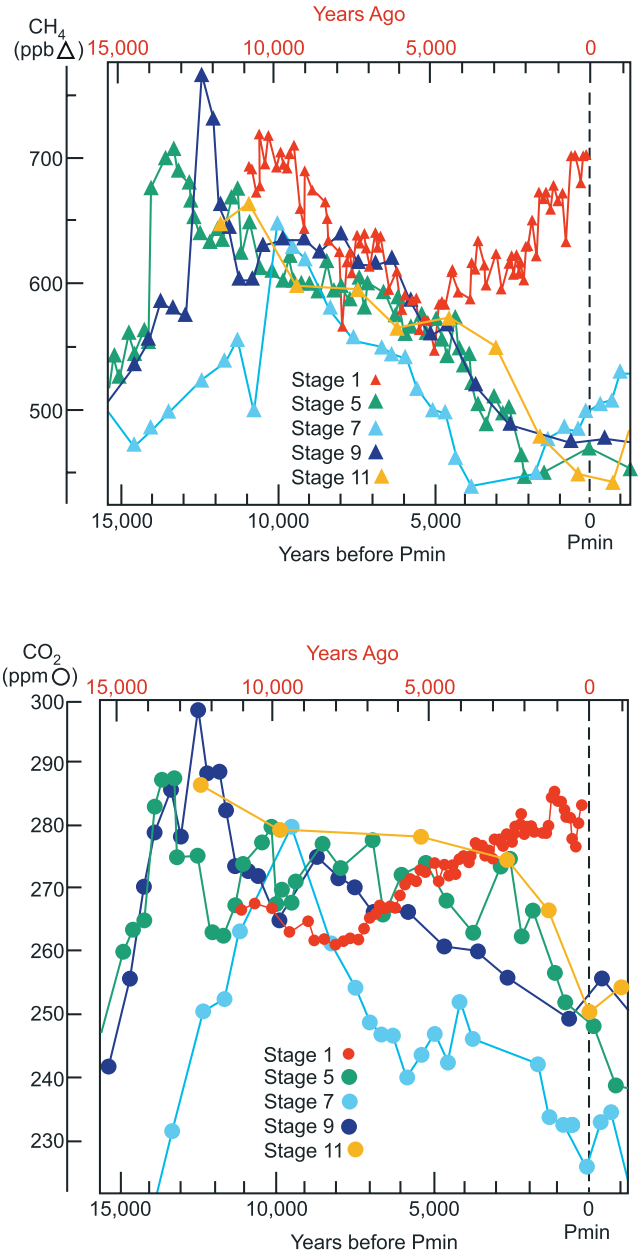

Figure 11. Comparison of trends of (top) methane and (bottom) CO_2 during the last five interglaciations based on the Vostok gas timescale of *Ruddiman and Raymo* [2003] and *Ruddiman* [2005a]. Only the Holocene shows an increase in gas concentrations.

704 ppb, methane values during precession minima cluster near 450–500 ppb for all four previous interglaciations. In comparison to the Holocene CO_2 peak of ~284 ppm, values from the previous interglaciations range from 225 to 252 ppm.

[76] The CO_2 trends in stage 7 are anomalous compared to those in stages 5, 9, and 11, with a smaller late deglacial peak and considerably lower values early in the interglaciation. Marine $\delta^{18}O$ signals indicate that termination III was not a complete deglaciation and that some ice remained during the peak of the substage 7.5 interglaciation. This lingering ice presumably kept climate colder and hastened the growth of new ice early in the interglaciation. Because of this complication the trends in stage 7 are not used here as an analog to the late Holocene.

[77] On the basis of the trends in stages 5, 9, and 11, CH_4 values should have fallen by now to ~475 ppb, and CO_2 values should have fallen to ~250 ppm. Compared to the late Holocene gas maxima, the anomalies are 230 ppb for CH_4 and 35 ppm for CO_2. Both estimates are ~10% smaller than those posed in the initial early anthropogenic hypothesis.

[78] Two additional challenges to the early anthropogenic hypothesis remain to be considered. Because the insolation decrease in stage 1 is smaller than those the four previous interglacial stages (Figure 10), the claim might be made that the greenhouse gas anomalies in the Holocene should be weaker than those in the other interglaciations. Yet no obvious trend toward weaker gas anomalies during weaker insolation anomalies is obvious in the previous interglaciations (Figures 10 and 11). Stage 9 has the weakest insolation anomaly (except for the Holocene), yet the CO_2 and CH_4 anomalies fall within the cluster of the other interglaciations. Why would a modest additional reduction of insolation values during the late Holocene cause the complete reversal of greenhouse gas trends observed (Figure 11)?

[79] A second challenge is that the closest analog to the present-day insolation minimum should be picked at the time when insolation values fell through the precise modern value on their way to the lower levels reached at each precession minimum rather than at the time of the subsequent precession minima. This approach would place the closest insolation analog earlier in time during all of the previous interglaciations (Figure 10).

[80] Choosing (earlier) times of precisely equivalent insolation levels would produce shifts ranging from ~2500 years for stage 9 to ~7000 years for stage 7 and would also yield higher CO_2 and CH_4 values as closest modern analogs. On the other hand, stage 9 is the closest summer half-year insolation analog to the late Holocene, and the 2500-year offset would have little effect on the amplitude of the CO_2 and CH_4 anomalies for that interglaciation.

[81] In addition, the actual trends in the Holocene should be taken into account (Figure 11). The methane concentration fell to ~540 ppb between 11,000 and 5000 years ago before beginning the anomalous rise. With 5000 years still left in the Holocene, and with aridification continuing in north tropical monsoon regions [*COHMAP Members*, 1988], it seems likely that the natural methane value would have fallen well below 540 ppb if it followed a trend at all similar to those in previous interglaciations. Similarly, the CO_2 concentration had dropped from 268 ppm at 10,500 years ago to 261 ppm by 8000 years ago, and it seems likely to have reached a value well below 260 ppm by following a trend similar to previous interglaciations. Even relatively conservative downward projections of the early Holocene CH_4 and CO_2 trends suggest large anomalies compared to the observed rises.

[82] In summary, choosing an insolation analog to the late Holocene (along with corresponding greenhouse gas anomalies) is not an exact science. On the basis of the insolation trends plotted in Figure 10, and the fact that stage 9 is the best summer half-year insolation analog to the present, the natural methane concentration today in the absence of human influences should be ~475 ppb, and the CO_2 concentration should be ~250 ppm. On this basis the preindustrial methane anomaly is 230 ppb, and the CO_2 anomaly is 35 ppm. Future work on gas concentrations in EDC and Fuji ice using an array of tuned timescales should help to refine these estimates.

7. CAN PREINDUSTRIAL AGRICULTURE ACCOUNT FOR THE CH_4 ANOMALY?

[83] The early anthropogenic hypothesis invoked preindustrial farming to explain a methane anomaly that first became detectible near 5000 years ago and grew slowly until the rapid increase that began during the industrial era (Figure 1a). The analysis in sections 4–6 indicated an anomaly of ~230 ppb. The proposal that preindustrial humans could account for an anomaly of this size has been challenged.

[84] *Schmidt et al.* [2004] suggested that the rising Holocene methane trend resulted from an increase in natural methane emissions from expanding circum-Arctic wetlands and low-latitude deltas. In response, *Ruddiman* [2005b] pointed out that an increasing contribution from circum-Arctic wetlands had already been ruled out by *Chappellaz et al.* [1997] on the basis of changes in the interhemispheric CH_4 gradient (the difference between CH_4 concentrations in Greenland and Antarctic ice). Even though wetlands were still slowly expanding in north polar regions during the late Holocene [*Smith et al.*, 2004], the decrease in CH_4 gradient from ~3750 to ~750 years ago requires reduced emissions from circum-Arctic sources. The pervasive summer cooling underway in the Arctic during the late Holocene [*COHMAP Members*, 1988] suppressed boreal methane emissions in summer, as did a trend toward drier kinds of peat bogs [*MacDonald et al.*, 2006].

[85] *Ruddiman* [2005b] also pointed out that late Holocene delta growth in subtropical and tropical regions has not been entirely natural because extensive forest clearing for agriculture caused widespread erosion that increased sediment loads in rivers and greatly enlarged the size of deltas [*Roberts*, 1998; *Vella et al.*, 2005; *Stefani and Vincenzi*,

TABLE 5. Modern (2000) and Preindustrial (1500) CH_4 Emissions[a]

CH_4 Emissions Source	2000 Emissions Baseline	1500 Emissions (Linear Scaling)	Nonlinear Sources in 1500
Human waste	50	4	0
Livestock	93	7	0
Biomass burning	52	4	16
Rice irrigation	60	5	18–27
Climate feedbacks	—		6–15
Total	255	20	49
Atmospheric CH_4 supported, ppb	852	67	164

[a]Values are given in Tg CH_4/year.

2005]. Anthropogenic influences thus account for a substantial part of any late Holocene increase in CH_4 fluxes from deltaic areas. In summary, the Holocene methane trend is anomalous because of anthropogenic interference. This section examines the specific anthropogenic sources of the extra methane.

7.1. Scaling Preindustrial Methane Emissions to Population

[86] In the year 2000 the estimated flux of methane to the atmosphere was 530 Tg/yr, and the atmospheric CH_4 concentration was ~1770 ppb [*Reeburg*, 2003; *Mikaloff Fletcher et al.*, 2004] (1 Tg/yr = 10^{12} g/yr). Because the residence time of CH_4 in the atmosphere is only a decade, the 530 Tg/yr of mean annual CH_4 emissions supported the 1770 ppb concentration. By linear scaling the estimated late Holocene CH_4 anomaly of 230 ppb required annual emissions of ~69 Tg/yr.

[87] One way to estimate past anthropogenic emissions is to assume that the releases were proportional to the number of living humans [e.g., *Chappellaz and Fung*, 1993]. Here the quantitative link between modern population levels and CH_4 emissions is used to estimate preindustrial CH_4 emissions in 1500, the time of the peak CH_4 concentration of 704 ppb [*Etheridge et al.*, 1998].

[88] The year 2000 atmospheric concentration of 1770 ppb [*Reeburg*, 2003] was supported by emissions from a range of natural and anthropogenic sources [*Fletcher et al.*, 2004]. Many of these sources are natural (wetlands and oceans) or are linked to industrial era activities such as fossil fuel extraction. Only a few sources (those listed in Table 5) would have been active in 1500. These "early anthropogenic" sources account for just under half of the methane emissions in 2000 (255 of 530 Tg/yr) and support ~852 ppb of the atmospheric concentration of 1770 ppb.

[89] In 1500 the global population was 465 million, based on data for the Americas from *Denevan* [1992] and for other continents from *McEvedy and Jones* [1978]. This number represents 7.6% of the ~6.1 billion people alive in 2000. Approximately the same percentage applies to southern Asia where the largest populations and major early anthropogenic CH_4 sources are located. Scaled linearly to population, anthropogenic emissions in 1500 would have been ~20 Tg/yr and would have supported an early anthropogenic atmospheric CH_4 concentration of ~67 ppb (Table 5) or just under 30% of the 230 ppb anomaly.

7.2. Disproportionately Large Early Biomass Burning

[90] The remaining CH_4 flux (~49 Tg/yr) must have come from sources that emitted larger per capita amounts of CH_4 than modern populations. Two of the sources in Table 5 seem likely to have been closely coupled to human populations: human waste (for obvious reasons) and gastric emissions and waste from livestock tended to provide food for people. Two potential sources of disproportionately large early CH_4 emissions remain: biomass burning and irrigation for rice.

[91] Linear scaling yields methane emissions of 4 Tg/yr from biomass burning in 1500 (Table 5), close to the 5 Tg/yr estimate of *Chappellaz and Fung* [1993], but recent evidence points to much larger releases. On the basis of a double deconvolution of ice core methane concentrations and $^{13}CH_4$, *Ferretti et al.* [2005] found that the total global contribution from all pyrogenic sources (burned vegetation) between 1000 and 1500 averaged ~25 Tg/yr. If 5 Tg/yr of the 25 Tg/yr pyrogenic total was natural in origin, the other 20 Tg/yr must have come from anthropogenic burning (close to an earlier estimate by *Subak* [1994]). This evidence adds 16 Tg/yr of extra CH_4 emissions to the amount derived from linear scaling (Table 5).

[92] *Ferretti et al.* [2005] also found that the ~40-ppb drop in CH_4 concentration and the large increase in $^{13}CH_4$ after 1500 require a decrease in pyrogenic methane emissions of ~10 Tg/yr and that natural sources were not the primary cause of this decrease. They attributed most of the 10 Tg/yr decrease to the reduction in anthropogenic burning caused by the deaths of tens of millions of indigenous Americans during the pandemic brought on by European contact (see section 10). If indigenous Americans had been contributing methane emissions of ~10 Tg/yr prior to 1500, a global anthropogenic total of 20 Tg/yr at that time seems plausible.

7.3. Feedback Enhancement of the CH_4 Anomaly

[93] The last remaining source of direct anthropogenic emissions is disproportionate releases from early rice irrigation, but these emissions are poorly constrained. Consequently, this section will focus on another (indirect) source of higher methane emissions: positive feedback from a climate system kept warmer by human intervention.

[94] Early anthropogenic emissions of methane and CO_2 exerted a net warming effect on climate by offsetting part of the global mean cooling that would have occurred if climate had cooled naturally (sections 2.3 and 5.2). This imposed warming effect would have produced positive feedbacks that would have enhanced the size of the methane anomaly compared to the natural cooling that occurred during other interglaciations.

[95] Two studies broadly constrain the size of this positive feedback effect. On the basis of a simulation run on the Goddard Institute for Space Studies general circulation

model (GCM), *Shindell et al.* [2004] found that a 3.4°C global mean warming associated with a doubling of CO_2 levels caused an increase in methane emissions from natural wetlands of 78%. In a controlled experiment on a rice paddy, *Allen et al.* [2003] found that CH_4 emissions from the irrigated areas increased by a factor of 4 as a result of the combined effects of a 6°C increase in growing season temperatures and a CO_2 doubling. These studies show that methane releases from natural wetlands and irrigated areas will increase substantially if climate warms and CO_2 fertilization increases. Interpreted conservatively, these results permit a 50% increase in methane releases from wetlands and irrigated areas for a 2.5°C warming and a CO_2 doubling.

[96] In order to assess the possible effect of climate system feedbacks on early methane emissions it is necessary to estimate how much warmer climate was in the year 1500 as a result of anthropogenic emissions of CH_4 and CO_2. The analysis in Table 5 indicates that linear scaling of early anthropogenic CH_4 emissions (20 Tg/yr) and the additional (nonlinear) contribution from biomass burning (16 Tg/yr) would have accounted for a total of 36 Tg/yr of methane emissions in the year 1500. These combined emissions of 36 Tg/yr would have supported an anthropogenic CH_4 concentration in the atmosphere of ~120 ppb. For a global climate sensitivity of 2.5°C a 120-ppb increase in atmospheric CH_4 would warm global mean climate by ~0.06°C (at full climatic equilibrium and including the indirect effects of CH_4 on ozone).

[97] This calculation omits the extra 18–27 Tg/yr of releases from irrigation derived in section 7.4. With these additional emissions included, the total anthropogenic release would amount to 54–63 Tg/yr. For releases of 60 Tg/yr the total effect on the CH_4 content of the atmosphere would increase to ~200 ppb, and the equilibrium temperature effect of all direct methane emissions would be ~0.1°C.

[98] The analysis that follows in section 8 indicates that direct human emissions of CO_2 were responsible for an anomaly of ~9 ppm in 1500. This CO_2 increase would warm global mean climate (at equilibrium) by ~0.11°C. The total anthropogenic CO_2 anomaly is, however, estimated at 35 ppm (sections 4–6). For a 2.5°C global climate sensitivity a 35-ppm CO_2 anomaly would warm global mean climate by ~0.43°C. The combined anthropogenic warming effect from CH_4 and CO_2 emissions could thus range from ~0.21°C (0.10° + 0.11°) to 0.53°C (0.10° + 0.43°).

[99] If the 50% increase in methane emissions for a CO_2 doubling and 2.5°C warming inferred from the results of *Shindell et al.* [2004] and *Allen et al.* [2003] are scaled down linearly to a temperature difference of 0.21° to 0.53°C, the methane releases would have been enhanced by 5 and 9% relative to those that would have occurred during a natural cooling (in the absence of early anthropogenic emissions). If methane emissions from natural wetlands in 1500 were similar to those today (145 Tg/yr [*Fletcher et al.*, 2004]), the 5–9% increase in methane emissions caused by the warm anomaly would have amounted to 6–15 Tg/yr. These additional methane emissions would leave 18–27 Tg/yr that would have to come from the final factor listed in Table 5: disproportionately extensive early rice irrigation (compared to population).

7.4. Disproportionately Extensive Early Rice Irrigation

[100] *Ruddiman and Thomson* [2001] and *Ruddiman* [2003] favored irrigation as the primary explanation for the late Holocene methane anomaly. This rationale arose in part from the fact that the abrupt reversal in the natural downward trend of atmospheric CH_4 near 5000 years ago matched the era in which irrigation was first used to grow wet-adapted strains of rice in Southeast Asia. By 3000 years ago, irrigated rice was grown from China to the Ganges Valley in eastern India [*Grigg*, 1974].

[101] For rice irrigation to be the explanation for the remaining deficit, it would have to account for both the 5 Tg/yr estimated from linear scaling as well as the extra 18–27 Tg/yr needed to close the methane source budget. The total, 23–32 Tg/yr, amounts to ~40% to 50% of the estimated 60 Tg/yr of emissions from modern rice irrigation. If CH_4 emissions are assumed to be proportional to the area irrigated, this means that 40–50% of the area now irrigated would have to have already been in irrigation by 1500.

[102] This estimate contradicts an analysis by *Ramankutty and Foley* [1999], who estimated that the area cultivated for crops in India and China even in 1700 was only 10–30% of that today. Their estimates, however, were based on backward extrapolation of much more recent trends. Accurate land use data do not exist before 1980 in China [*Houghton*, 1999] and before 1880 in India [*Flint and Richards*, 1991]. As a result, *Ramankutty and Foley* [1999] used an algorithm based on population scaling to extrapolate land use prior to 1880 in India and 1980 in China.

[103] *Ruddiman and Thomson* [2001] noted that the approach of scaling land use estimates to population change does not work for recent decades. Between 1950 and 1990, rice yields rose by ~300%, and global and Asian populations increased by ~100%, but the area irrigated for rice grew by only ~41% [*International Rice Research Institute* (*IRRI*), 1991; *Minami and Neue*, 1994]. During this interval, farmers were able to grow much more rice per unit area of land irrigated because of the "green revolution," new types of genetically modified rice and more extensive use of fertilizers. These innovations completely overrode a linear link between population growth and area farmed.

[104] Similar innovations, but of a simpler and slower kind, have occurred throughout agricultural history and have altered the relationship between total area farmed and rice yield. When rice irrigation was introduced in southern China near 5000 years ago [*IRRI*, 1991], the first areas irrigated were largely broad valleys within easy reach of major streams and rivers [*Grigg*, 1974; *Simmons*, 1996]. Such areas could be irrigated with relatively little effort by grading already flat land and constructing canals to deliver water. *Ruddiman and Thomson* [2001] suggested that this early rice agriculture was relatively inefficient, with weeds prominent in the rice fields. Because weedy vegetation

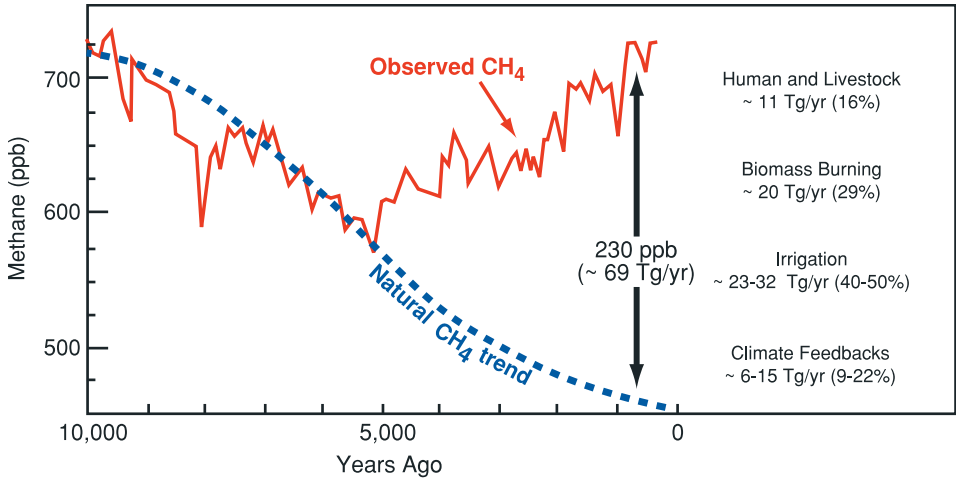

Figure 12. Estimated anthropogenic CH_4 anomaly of 230 ppb in the year 1500 accounted for by contributions from several sources: emissions from livestock and human waste (both linearly tied to human population), disproportionately large emissions from biomass burning and irrigation, and climate system feedbacks.

produces as much CH_4 as rice [*Yamane and Sato*, 1963], early methane releases are likely to have been disproportionately large compared to the size of the populations fed. During subsequent millennia, with enormous population increases in Asia [*McEvedy and Jones*, 1978], far more labor became available to suppress weeds and increase rice yields per acre.

[105] From 2000 to 1000 years ago the technique of terracing hillsides for "padi" farming of rice came into practice and spread across Southeast Asia, yet this labor-intensive engineering added relatively small additional areas of land to the total area in cultivation. Given the large amount of labor required and the small additional rice yields that resulted, people would only have gone to the trouble of irrigating steep hillsides because they needed food and because the flatter areas in the broad river valleys were already in irrigation. This evidence argues that large river valleys in many areas were irrigated long before industrial times. This evidence is consistent with the idea that methane emissions would have been disproportionately large compared to population sizes. During the last 1000 years, innovations in farming technique further increased food yields per acre of land cultivated and decoupled any linear link between food produced and area farmed [*Grubler*, 1994].

[106] In summary, roughly 60–75% of the 230-ppb methane anomaly in the year 1500 (Table 5 and Figure 12) can be accounted for by releases from livestock and human waste in amounts proportional to the human populations of the time; disproportionately large emissions from biomass burning, especially in the Americas; and enhanced CH_4 emissions in a climate kept warmer than natural processes would have produced.

[107] The remaining 25–40% of the methane anomaly must have come from disproportionately large emissions from early rice irrigation. The estimate of irrigation emissions in Table 5 (18–27 Tg/yr) was derived as a residual calculation and requires fluxes 40–50% as large as today in the year 1500, consistent with indirect historical evidence that early irrigation was disproportionately extensive compared to population size. An effort can and should be made to constrain the history of irrigation of the major river valleys of southern Asia in a more quantitative way.

8. CAN PREINDUSTRIAL AGRICULTURE ACCOUNT FOR THE CO_2 ANOMALY?

[108] *Ruddiman* [2003] claimed that a 40-ppm preindustrial CO_2 anomaly was caused by deforestation and other preindustrial burning of fossil fuel. Scaling up from an estimate from *Indermuhle et al.* [1999] based on carbon cycle modeling, he estimated that such an anomaly would require ~320 Gt C of anthropogenic emissions during the last 8000 years.

[109] That claim is no longer tenable. *Joos et al.* [2004] pointed out that the carbon input needed to account for a 40-ppm anomaly had to have been at least 550 Gt. This number was derived by multiplying the 40-ppm anomaly by the 2.13-Gt C weight of each part per million of CO_2 in the atmosphere and by 100/15 to allow for the ~15% of emitted CO_2 that stays in the atmosphere for millennia. The 550-Gt estimate far exceeds any possible emissions from deforestation. The initial attempt by *Ruddiman* [2003] erred mainly in assigning full carbon densities to many areas where steep or rocky slopes and low rainfall actually favor lower-density forest or open woodland.

[110] *Joos et al.* [2004] provided additional evidence against such massive deforestation. They calculated that 550 Gt of terrestrial carbon (averaging −25‰) would shift the $\delta^{13}C$ content of CO_2 by −0.6‰, yet *Indermuhle et al.* [1999] detected only a 0.1–0.2‰ decrease in the

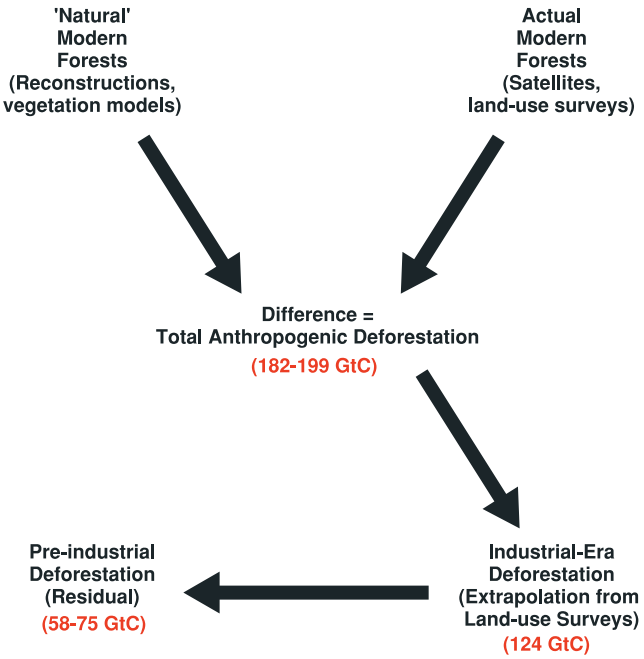

Figure 13. Preindustrial deforestation is estimated as a residual value by estimating the total amount of anthropogenic deforestation (the difference between natural and actual forests) and subtracting the estimated deforestation during the industrial era (post-1850) based on backward extrapolation of recent land use changes, based on the work of *DeFries et al.* [1999], *Houghton* [1999], and *Joos et al.* [2004].

last 7000 years, and *Eyer et al.* [2004] found a negligible decrease over this interval.

[111] *Joos et al.* [2004] concluded that preindustrial (pre-1850) anthropogenic emissions totaled only ~60–80 Gt C on the basis of a method that *DeFries et al.* [1999] had used to produce an estimate of 48–57 Gt C. The method is summarized in Figure 13. First, satellite data (tested against land use data) are used to estimate the extent of modern forests, which are then converted to estimates of global carbon content. These values are then compared to estimates of the "natural" forests that should exist today in the absence of human influence. The difference between the two estimates, the total amount of deforestation by humans, amounts to 182 Gt C for the natural vegetation reconstruction of *Mathews* [1983] and 199 Gt C for that of *Leemans* [1990]. These total amounts are then allocated into the decreases occurring before and after 1850 on the basis of land use data from *Houghton* [1999]. Because Houghton estimated a net land use decrease of ~124 Gt C since 1850, the remaining 58–75 Gt C is the estimated pre-1850 loss shown in Figure 13.

[112] In summary, preindustrial anthropogenic carbon emissions cannot possibly have amounted to 550 Gt, and yet a large (~35 ppm) CO_2 anomaly still exists (section 6 and Figure 11). These incompatible observations pose a major enigma: How can humans be responsible for a CO_2 anomaly of 35 ppm when the amount of carbon directly generated by human activities is so small? This section will address this question first by reevaluating estimates of preindustrial carbon emissions and then by exploring climate system feedbacks that could account for the remainder of the CO_2 anomaly and for the negligible $\delta^{13}CO_2$ changes during the Holocene.

8.1. Uncertainties in Satellite and Land Use Estimates of Deforestation

[113] The method used by *DeFries et al.* [1999] for estimating preindustrial anthropogenic deforestation (Figure 13) has inherent uncertainties. The two estimates of total carbon stored in "natural forests" (182 and 199 Gt) by *DeFries et al.* [1999] differ by less than 10%, despite the fact that the compilation by *Mathews* [1983] was based on land use data and that of *Leemans* [1990] was based on a Holdridge scheme. Estimates for most individual continents in these two reconstructions fell within 15–30%, although the estimate for South America based on the reconstruction of *Mathews* [1983] was 15 Gt C, while that based on the reconstruction of *Leemans* [1990] was 40 Gt C.

[114] The estimate of forest extent at the start of the industrial era (usually defined as 1850) is far more uncertain. *DeFries et al.* [1999, p. 804] noted that "spatially explicit global data that historically account for changes in land cover do not exist." Most nations have kept accurate land use records only since World War II [*Houghton*, 1999]. By the time reliable data first became available from China in 1980 [*Houghton and Hackler*, 2003], deforestation had ended and net reforestation was underway [*Ramankutty and Foley*, 1999]. Consequently, none of the history of deforestation in China is constrained by modern land use data.

[115] Estimates of early industrial (pre-1850) forest extent rely entirely on backward extrapolations based on some form of scaling to past population size. Through time, however, innovations in farming techniques and an ongoing shift of people from farms to cities have caused a steady reduction in the ratio of land farmed to population fed [*Grubler*, 1994] (see also section 7.4). Population-based extrapolations will thus tend to underestimate the extent of preindustrial deforestation because recent per capita land use is much smaller than it was in the past.

[116] Because of the need for large extrapolations back through time, estimates of early deforestation vary considerably. Using data from *Houghton* [1999], *DeFries et al.* [1999] estimated that ~33% of total deforestation by humans had occurred by 1850, but *Ramankutty and Foley* [1999] arrived at an estimate of ~47% for the same interval. At a mean carbon density of 13 Gt per million km^2 [*Houghton*, 1999] these two estimates disagree by ~17 Gt C.

[117] Perhaps the most serious shortcoming of the method shown in Figure 13 is that it fails to include some forms of preindustrial deforestation (and related carbon emissions). The estimate of actual modern forests fails to include regions that were cleared in early industrial or preindustrial times but have subsequently been reforested. Reforestation has mainly occurred in temperate regions as mechanization has led to increasingly productive farming of prairies and steppes. *Ramankutty and Foley* [1999] found that 1.5 million km^2

of global cropland have reverted to forest during the last 150 years, yet this area must have been in a deforested state in late preindustrial time. At a mean carbon density of 13 Gt per million km^2 [*Houghton*, 1999] these 1.5 million acres would have contained ~20 Gt C. This amount should be added to the total preindustrial carbon release estimated in Figure 13.

[118] A similar problem arises from the overly broad definition of "forests" used in land use and satellite studies. For example, *Houghton and Hackler* [2003] estimate that 0.5 million km^2 of the area described as "forest" in China actually consists of tree plantations and shelterbelts. These regions were obviously cut at some time in the past and may not have been immediately put into tree plantations or shelterbelts. The areas that were cut as of the late preindustrial era would then add to the total amount of preindustrial deforestation. At 13 Gt C per million km^2 these areas represent ~6.5 Gt C of early carbon emissions in China. Because China has long accounted for ~30% of the total population of Eurasia [*McEvedy and Jones*, 1978], the total area devoted to these land uses in southern Eurasia might well have amounted to 1 million km^2 or more. At 13 Gt C/km^2 these replanted areas in Eurasia could originally have contained at least ~13 Gt C.

[119] A final problem is the effect of human interference with "natural" climate. Vegetation models that rely on the present-day distribution of temperature and precipitation to define "natural" vegetation encounter the problem that prior forest clearance has altered the current climatic state. This problem is potentially critical in summer monsoon regions of Asia, where deforestation reduces recycling of moisture via evapotranspiration [*Lean and Warrilow*, 1989; *Hoffman and Jackson*, 2000]. Reduced moisture recycling shortens the summer wet season at the expense of the dry season, thereby pushing climate toward conditions that favor dry forest biomes with less carbon. Attempts to estimate carbon in "natural" modern forests across southern Asia could thus underestimate the amounts that would otherwise be present. If the "natural" forests of southern Asia (covering ~7–8 million km^2) contained just 10% more carbon than the estimates of *Mathews* [1983] and *Leemans* [1990], the natural carbon tally in Figure 13 would be higher by ~10 Gt C.

[120] *Olson et al.* [1983] estimated that forests and woodlands 6000 years ago held at least 240 Gt C, with floodplains and wetland forests adding to this total. This estimate exceeds those of *Mathews* [1983] and *Leemans* [1990] by ~40–60 Gt C. Part of this difference probably reflects natural late Holocene losses of forest carbon caused by gradual weakening of the Asian monsoon [*COHMAP Members*, 1988], but human interference during recent millennia may also explain why this estimate of natural forests is much larger than those of *Mathews* [1983] and *Leemans* [1990].

[121] In summary, the estimate of preindustrial deforestation in Figure 13 omits ~20 Gt C in areas that were once cut but are now reforested and perhaps another 13 Gt in areas previously cut but now replanted in tree plantations, shelter breaks, and orchards. Human overprints on estimates of the "natural vegetation" could have added a few tens of gigatons C to this total.

8.2. Deforestation From the Historical-Ecological Perspective

[122] A different view of early deforestation emerges from studies in human ecology, environmental history, archeology, and anthropology [*Taylor*, 1983; *Simmons*, 1996; *Williams*, 2003]. This difference can be summarized by the discrepancy in estimates of the per capita area occupied by early farmers, called here the "forest footprint."

[123] The global mean forest footprint of humans during industrial time can be estimated by dividing the net amount of area deforested between 1850 and 1990 (8×10^6 km^2 [from *Houghton*, 1999]) by the increase in population (~3.8 billion people). This calculation gives an average forest footprint of ~0.2 to 0.3 ha/person [*Williams*, 1990; *Grubler*, 1994].

[124] In contrast, the historical-ecological literature suggests a much larger forest footprint in preindustrial times. *Gregg* [1988] calculated the amount of cleared land required by a village of 30 people in central Europe late in the Neolithic era (~6000 years ago). She estimated the per capita human footprint at 3 ha. More than 40% of this total was in pastures and hay meadows for livestock, and another 40% was accounted for by a woodlot cut on a rotating basis. Only 14% (0.4 ha) was used to raise crops, with an equivalent amount lying fallow each year.

[125] *Ruddiman* [2003] noted that the Domesday survey of England in 1086 found ~90% clearance of lowland regions at a time when the population was 1.5 million people. *Rackham* [1980] used an array of methods (place names, archeological sites, and paleobotanical evidence) to assess the accuracy of the Domesday survey and concluded that 90% may have been an underestimate of the actual extent of clearance. *Rackham* [1980] and *Taylor* [1983] mustered a range of evidence that extensive deforestation occurred in England well before Domesday time.

[126] The average density of the Domesday population on land below 1000 m elevation was 11–12 persons/km^2. Inverting this density gives a per capita footprint of 9 ha/person, 3 times larger than that for late Neolithic Europe. The intervening threefold increase occurred during the discovery of bronze and iron axes and plows, as well as the domestication of horses and other draft animals. Although 9 ha seems surprisingly large, *Williams* [1990] estimated that one person can girdle all of the trees within one hectare in 50 working days, a rate that translates to 2–4 ha per year for a single person working only in the winter months. Evidence cited by *Chao* [1986] from other parts of western Europe indicates similar forest footprints in medieval times.

[127] Both of these estimates of the preindustrial forest footprint exceed the industrial era estimate by an order of magnitude or more. A possible explanation for this striking difference lies in the long-term trajectory of land clearance

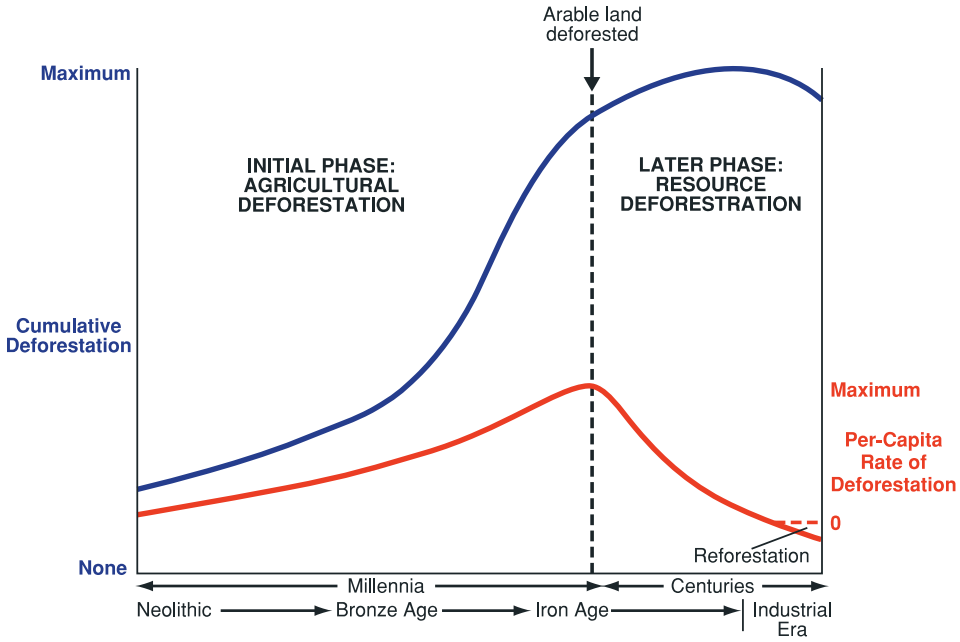

Figure 14. Inferred trajectory of deforestation in England based on historical-ecological data. An early phase of large-scale land clearance for agriculture (“agricultural deforestation”) continued until all arable land was in use (soon after 1089 in England). The later (and final) phase of deforestation of higher, more remote terrain (“resource deforestation”) was smaller in magnitude. Per capita deforestation peaked near the end of the phase of agricultural deforestation and then fell substantially.

in England (Figure 14). Although the trajectory shown is largely hypothetical, it is consistent with the available environmental history.

[128] In the initial phase, called here “agricultural deforestation,” old growth forests were cut to open arable land for crops and pastures. Because wood was abundant and populations were small, per capita deforestation rates at this stage were high, and vast areas of lowland forest were gradually removed [*Williams*, 2003]. This early phase of deforestation received little comment from contemporary observers in part because it achieved desirable goals (food production and reduction of habitat for dangerous predators) and also because much of it preceded the advent of systematic written records. Although forests may have been burned and cleared for summer pastures to elevations exceeding 1000 m, many high-elevation regions remained untouched.

[129] The second phase of deforestation, called here “resource deforestation,” was one in which forested areas remaining on higher and steeper terrain were cut, well after most of the arable land had been cleared. Wood from these regions was used mainly for building homes and ships, for cooking and heating, and for charcoal production for smelting. Each of these uses of wood was, however, much smaller than the early losses to agricultural clearance [*Williams*, 1990, 2003]. The remaining forests often became managed woodlots that were cut repeatedly. This resource deforestation phase was often commented on by contemporary observers because the impending loss of the last forests seemed threatening and because environmental damage was now more obvious [*Bechmann*, 1990; *Elvin*, 1993]. Without forest cover, rainwater tended to erode steep slopes, and rivers received mud-laden debris. These two phases of deforestation obviously overlapped to some extent. In the earlier agricultural deforestation phase some wood was burned for heating and cooking, and some timber was used for home building.

[130] The Domesday survey apparently caught England near the point of transition between the two phases. Not long afterward, access of commoners to the remaining forested areas (mainly hunting and woodlot preserves for use by royalty and nobility) was limited by new laws. By the 1300s, England was beginning to import timber from Germany and Scandinavia [*Rackham*, 1980]. By 1500, when imported food had not yet begun to meet a significant part of the nutritional needs of the English population, nearly 5 million people were being fed from a farmed area that was only slightly larger than it had been in 1089.

[131] During those 400 years, agricultural productivity had been revolutionized by eliminating the long fallow intervals between crop plantings through the use of manure from humans and livestock, ash from fireplaces, nitrogen-fixing legumes, crop rotation, and insect control [*Grubler*, 1994]. As farmers extracted increasing food yields per hectare of land, the per capita forest footprint dropped by a factor of 3. After 1500 the introduction of high-yield crops like corn and potatoes introduced from the Americas further increased yields.

[132] The schematic trajectory in Figure 14 is based on a European culture that used Iron Age tools to derive nutrition

TABLE 6. Times When Populations of Various Regions Reached the Domesday Density Threshold for Complete Deforestation of Arable Land[a]

Country/Region	Domesday Population Threshold, 10^6	Date Threshold Reached
Greece	0.6	before 0
Italy	1.7	before 0
Spain/Portugal	5.3	200
Czechoslovakia	1.1	800
France	6.1	1000
Belgium/Netherlands/Luxembourg	0.7	1000
Austria	0.6	1000
British Isles	2.5	1100
Germany	5.2	1200
Hungary	1.0	1300

[a]See *McEvedy and Jones* [1978] for region information. Domesday density threshold is 11 persons/km^2 [*Rackam*, 1980].

from dry land farming and from tending of livestock. Other regions and other cultures followed similar (but not identical) trajectories because of the different techniques they used to grow different crops. At a global scale, however, the general trend through time has been toward increased yields per hectare farmed and thus a reduction in the per capita forest footprint. In recent decades, productivity has become high enough for many countries to allow marginal agricultural land to revert to forest.

[133] In summary, the per capita forest footprint has fallen from several hectares in preindustrial times to just a few tenths of a hectare in the 1900s (Figure 14). For this reason the modern per capita forest footprint is not a valid basis for estimating past (preindustrial) changes, and scaling past land uses directly to population is not justified.

8.3. Carbon Emissions From Preindustrial Deforestation

[134] As noted in section 8.1, the estimated 58–75 Gt of preindustrial carbon release in Figure 13 did not take into account either ~20 Gt of carbon in once deforested areas that have become reforested or ~13 Gt in once deforested areas that are now planted in shelterbelts, orchards, and tree plantations. This additional carbon would increase the preindustrial emissions resulting from deforestation by several tens of gigatons.

[135] As pointed out by *DeFries et al.* [1999], neither preindustrial nor early industrial changes in land use anywhere in the world are at all constrained by valid surveys. In many countries, even changes prior to 1900 or 1950 are based on backward extrapolation. As a result it is impossible to construct a bottom-up compilation of deforestation for the late preindustrial era. Instead, the approach taken here is to examine regions in which historical ecological evidence indicates that cumulative deforestation late in the preindustrial era could have been considerably higher than the amounts proposed by *DeFries et al.* [1999].

[136] One initial complication is that CO_2 reached the peak preindustrial value of 284 ppm near 1200 (see the Law Dome record in Figure 2) but then fell by ~7–8 ppm during the next 500 years. Part of this decrease during late preindustrial time may have resulted from a cooling driven by solar-volcanic forcing [*Gerber et al.*, 2003], but the analysis in section 10 of this paper suggests that more than half of the CO_2 drop came about because of large-scale reforestation following massive mortality caused by pandemics.

[137] Because of these variations the choice of a single time as representative of "the preindustrial Holocene" is arbitrary. Rather than choosing the smaller 276–277 ppm CO_2 value near 1700, this study uses the earlier peak CO_2 concentration of 284 ppm, which began near the year 1200 and continued for several centuries (Figure 2). The focus here will be on regions where early deforestation (well before the industrial era) could account for the carbon omitted from the calculations shown in Figure 13, as described in section 8.1.

8.3.1. Europe

[138] Environmental historians have concluded that most of Europe was deforested many centuries ago. The Domesday population density of 11/km^2 that produced 90% deforestation of England in 1089 can be used to estimate the time of similar levels of deforestation in other countries that practiced similar agriculture using Iron Age technology (Table 6). By this measure most of the agricultural land in Greece, Italy, and the Iberian Peninsula would have been deforested by the Roman Era, consistent with contemporary observations [*Hughes*, 1975; *Thirgood*, 1981; *Simmons*, 1996]. Populations then decreased during the pandemic of the late Roman Era.

[139] During a subsequent doubling of population between 1000 and 1300, countries as far north as the Baltic Sea and as far east as the border of Poland reached the Domesday density threshold (Table 6), and historical evidence indicates that much of the arable land in that area was cleared [*Jager*, 1951; *Darby*, 1956; *Taylor*, 1983; *Williams*, 2003]. Most of the forest that remained was in nonarable locations: steep mountain terrain, rocky outcrops, and boggy wetlands [*Darby*, 1956]. With the forests reduced to small remnants, countries passed laws restricting access of "commoners" to the remaining preserves [*Williams*, 2003].

[140] The countries of southwestern Europe listed in Table 6 cover just under 3 million km^2, of which 27% (0.8 million km^2) is presently forests and woodlands and just under 2 million km^2 is in agricultural use (crops and meadows). The lesson from the Domesday survey is that England was as deforested in 1089 as it is today (~90%). If this is also true for the other countries in this part of Europe by the year 1300 (as suggested by Table 6), then ~2 million km^2 were already in agricultural use by 1300. At a carbon density of 13 Gt/million km^2, total carbon emissions by that time would have been 26 Gt, or 12.5 Gt higher than the 12.5–13 Gt estimate of *DeFries et al.* [1999] for the year 1850 based on backward extrapolation from land use in recent decades.

[141] In regions with lower population densities (Scandinavia, the easternmost Baltic, and westernmost Russia), deciduous and conifer forests still existed in late preindustrial times. By 1500, well before the revolution caused by mechanized agriculture, the combined population in these regions had reached ~18 million people. If the per capita forest footprint for this region was as small as the 3-ha late Neolithic value of *Gregg* [1988], forest clearance would have amounted to 0.54 million km^2 and would have released ~7 Gt C (assuming 13 Gt C per million km^2). By this time, more technologically advanced (and deforested) countries of western Europe had long been exploiting these regions for lumber for centuries.

[142] In summary, pervasive early deforestation of southern and western Europe and more limited deforestation of northeastern Europe could have released ~33 Gt of carbon by the year 1500. This estimate exceeds the estimate given by *DeFries et al.* [1999] for the year 1850 by ~20 Gt C.

8.3.2. China

[143] *Houghton and Hackler* [2003] estimated that eastern China once had 4.25 million km^2 of natural forest, compared to the current cover of ~1.25 million km^2, of which ~0.85 million km^2 is true natural forest (not in tree plantations or shelterbelts). Net deforestation in China has thus amounted to ~3.4 million km^2. Deciduous forests in the northern part of eastern China account for about half of this total, and tropical moist forests in the south and southeast account for the other half.

[144] Documentary evidence indicates that China had progressed farther along the deforestation trajectory shown in Figure 14 than Europe. Between the Han dynasty (the first two centuries A.D.) and the 1700s the population of China increased by a factor of more than 4 [*McEvedy and Jones*, 1978], while the amount of cultivated land increased by just over 50% [*Chao*, 1986]. As a result the per capita allotment of cultivated land fell by a factor of 3.5 during that interval. Arable land was divided among all male heirs into ever smaller parcels farmed ever more intensively: the labor-intensive "garden-style" agriculture of China. Apparently, even 2 millennia ago, China had passed through most of the early phase of extensive agricultural deforestation shown in Figure 14. By late preindustrial times, cumulative deforestation was extensive. *Houghton and Hackler* [2003, pp. 3–5] noted that "much of China was already deforested by 1700 AD."

[145] Deciduous forests in the northern half of China originally covered some 1.82 million km^2, but they are now reduced to 0.52 million km^2. *Houghton and Hackler* [2003] inferred that ~0.82 million km^2 of deforestation had occurred in the north by 1700, primarily in the heavily populated eastern plain of northeast China and regions to the north. By that time, *McEvedy and Jones* [1978] estimated that the population of China was 150 million, with less than half of that total living in the north. For that population level the amount of deforestation estimated by *Houghton and Hackler* [2003] requires a per capita forest footprint of 1.6 ha in northern China.

[146] This estimated footprint is just over half of that for late Neolithic Europe [*Gregg*, 1988] and less than a fifth of the Domesday value of 9 ha for Iron Age Europe. Yet early agriculture and land use in Europe and northern China were similar: dry land farming (wheat, barley, and millet), Iron Age tools, draught animals, and wood for cooking and heating in cold winters. The assumption used here is that the per capita forest footprint in northern China was at least equal to that of Neolithic Europe (3 ha). In that case, total forest clearance would have been ~1.5 million km^2 out of 1.82 million km^2 or ~0.7 million km^2 more than the estimate of *Houghton and Hackler* [2003]. At 13 Gt C per million km^2 this would be equivalent to an additional 9 Gt C of early deforestation relative to their estimate.

[147] Historical evidence provides some support for this interpretation, because coal had replaced wood as the major fuel source near the northeastern capital city at Kaifeng by the Sung dynasty in the 1200s (section 8.4). *Hartwell* [1962] noted that a commentary from this period indicated that everyone burned coal rather than wood or charcoal. References to ongoing deforestation in northern China persist into the last 2 centuries [*Elvin*, 1993], but these generally refer to remote high-mountain areas or to marshes, consistent with late phase resource deforestation (Figure 14). *Elvin* [1993] summarized laws and moral exhortations extending back more than a millennium that prohibited or restricted cutting of remaining forest preserves in mountains.

[148] In southern China, greatest population growth came somewhat later as rice farming expanded. *Houghton and Hackler* [2003] favored a "reference" scenario in which ~0.17 million km^2 of deforestation had occurred in the southeast and southwest regions by 1700, by which time the population was more than half of the 150 million total for China [*McEvedy and Jones*, 1978]. These estimates yield a per capita forest clearance of ~0.2 ha or just one fifteenth the value estimated for Neolithic Europe and slightly more than one fiftieth of the Iron Age Domesday value. Because rice farming is more productive per acre than dry land farming, the per capita footprint in the south was probably smaller than that in the north. Still, the livestock used for work in the rice paddies needed pastures, and many people in the south practiced dry land (nonirrigated) farming and used wood for cooking. A footprint of 0.2 ha seems far too small for this region.

[149] *Houghton and Hackler* [2003] also published an alternative "early" deforestation scenario in which ~1.07 million km^2 of clearance had occurred by 1700 or 0.9 million km^2 more than in their reference scenario. The per capita forest footprint for this early scenario is a somewhat more plausible 1.2 ha, and it would increase carbon emissions prior to 1700 by ~12 Gt C.

[150] In summary, plausible early deforestation scenarios for China could add more than 20 Gt C to the "reference" scenario of *Houghton and Hackler* [2003]. Total carbon emissions from China by the 1700s would then amount to ~33 Gt C. Most of this "early" deforestation would have occurred by 1200, when the population of China reached

~115 million, almost as large as the 130 million in 1700 [*McEvedy and Jones*, 1978]. By comparison, *DeFries et al.* [1999] estimated that carbon emissions from all of Asia by 1850 totaled only 21 or 28 Gt C.

8.3.3. The Americas

[151] For North and South America combined, *DeFries et al.* [1999] estimated carbon emissions by 1850 at 5.7 Gt C, compared to a total modern-day loss to deforestation of either 42 or 66 Gt C. As noted in section 2.4, however, the peak late Holocene CO_2 value occurred centuries before European contact and pandemic-driven reforestation (Figure 2 and section 10). At that time, indigenous populations in the Americas were very large.

[152] By 1500 an estimated 55 million people lived in the Americas, mostly in naturally forested areas [*Denevan*, 1992]. The per capita amount of land in cultivation or in fallow was 0.4–1.4 ha/person [*Hurt*, 1987; *Krech*, 1999], equivalent to the estimate by *Gregg* [1988] for Neolithic Europeans. Assuming an average footprint of 0.9 ha, the 55 million people would have cleared ~0.5 million km^2 and emitted ~6.5 Gt C (at an average carbon density of 13 Gt/km^2).

[153] This estimate, however, omits an important consideration: fire. In contrast to Neolithic Europeans most indigenous Americans kept no livestock (except for Andean llamas and alpacas). Instead, to supplement their needs for nutrition, they repeatedly burned vegetation to maintain grassland, attract game, and promote growth of berries and other foods. The additional "clearance" by burning, generally thought by paleoecologists to have been extensive, would have added considerably to the footprint based only on land under cultivation.

[154] On the basis of the added clearance by burning the human forest footprint in the Americas is (arbitrarily) assumed to have been 2 ha, compared to 3 ha in Neolithic Europe. For a population of 55 million the total amount of deforestation just before European arrival would have been 1.1 million km^2. *Faust et al.* [2006] arrived at a nearly identical value. At a mean carbon density of 13 Gt C per million km^2 [*Houghton*, 1999], total deforestation by 1500 would have produced ~14 Gt C. This estimate exceeds that of *DeFries et al.* [1999] for pre-1850 deforestation by ~8 Gt C.

[155] In summary, carbon emissions from preindustrial deforestation in three regions by the year 1500 appear to have been considerably higher than the amounts estimated by *DeFries et al.* [1999] for 1850. The differences arise from more extensive early deforestation in Europe (~20 Gt), in China (~20 Gt), and in the Americas (~8 Gt). These estimates would add ~48 Gt of cumulative emissions to the preindustrial total of 48–57 Gt estimated by *DeFries et al.* [1999]. The 48 Gt estimate is larger than the amount of carbon not accounted for by the method shown in Figure 13 (section 8.1). Although these regional estimates are obviously crude, the complete lack of land use data prior to 1850 means that any estimate of this kind based on any method will necessarily be very uncertain.

[156] Future efforts to improve on estimates of early deforestation may prove to be difficult. One obvious avenue to pursue would be to examine ^{14}C-dated pollen spectra in lakes to quantify deforestation. In many regions, however, the composition of forests in low-lying arable regions is not much different from that on nearby slopes that are not suitable for agriculture. The removal of trees for agriculture may thus leave little imprint on pollen spectra in lake sediments.

[157] Changes in pollen accumulation rates could also reflect deforestation but, again, with complications. The loss of trees would diminish the supply of pollen, but the clearing of the landscape would tend to mobilize the movement of pollen-bearing soils from newly eroded areas into lakes. The net effect on mass pollen accumulation rates would be a complicated function of these two factors.

8.4. Other Sources of Anthropogenic Carbon

[158] Two other sources of early anthropogenic carbon added to late Holocene emissions from early deforestation are burning of coal in China, which began about 2 millennia ago, and the loss of deep soil carbon caused by long-term degradation of Eurasian soils.

[159] Since at least the fourth century A.D., coal has been extracted from surface outcrops and shallow pit mines in China and used as a fuel source for heating and cooking [*Hartwell*, 1962; *Freese*, 2003]. By 1000, burning of coal was prevalent in the north, while firewood was rationed and charcoal making was forbidden. As noted earlier, *Hartwell* [1962] quoted historical sources that coal, rather than wood, was burned near twelfth century Kaifeng. By the Sung dynasty in the 1200s, China had become the world's first partly "industrialized" country, with greater iron production than would later occur in Europe even during the early stages of the industrial era.

[160] It is risky to try to convert anecdotal historical information of this kind into estimates of carbon emissions, but as a crude attempt the assumption is made here that 25% of the Chinese population burned coal for cooking and home heating from 0 A.D. until 1200. If each five-person family that used coal burned a total of 10 kg/d (50% carbon by weight), then each family would have emitted ~5 kg of carbon per day or 1.8 t/yr. If the population estimates for China given by *McEvedy and Jones* [1978] are used to integrate the emissions over 1500 years, the estimated total is 9 Gt C.

[161] Severe degradation of landscapes in tropical Asia is a second potential source of additional preindustrial carbon. Traditional estimates of carbon release are based on tabulations of the changes that result from converting forest of various types to either crops or pastures [*Houghton*, 1999]. Living vegetation accounts for 63–87% of the carbon loss, and the rest comes from reductions in litter and highly reactive "labile" carbon in the upper soil profile.

[162] Over thousands of years, however, other considerations come into play. Some areas have been severely degraded by millennia of cumulative erosion and persistent overgrazing [*Hughes*, 1975; *Thirgood*, 1981; *Roberts*, 1998]. In such regions, extreme degradation has left formerly arable land useless, with little if any soil carbon left.

Some steep, once forested hillsides have lost most of their former soil cover. As the deep soil carbon in these regions was slowly "exhumed" toward the surface, it entered an environment richer in oxygen and biologically active microbes. As erosion and degradation continued, some of the deep carbon was oxidized and lost to the atmosphere, and some was carried to lakes and floodplains and buried without oxidizing.

[163] *DeFries et al.* [1999] estimated that 20–33% of the area of Eurasia that was once forested is now in a degraded condition because of unsustainable land use practices. An upper limit on the amount of deep soil carbon lost to the atmosphere can be calculated by assuming that all of the carbon in once forested but now degraded regions has been lost to the atmosphere. In such areas the additional carbon loss could have added an extra 30–60% (45% average) to the amounts calculated using values from *Houghton* [1999]. If 25% of the forested lands of southern Eurasia were degraded in this manner, carbon emissions would have amounted to roughly 11 Gt C (100 Gt $\times$ 0.25 $\times$ 0.45). Because some of this exhumed carbon was quickly reburied in lakes and deltas, the total amount lost to the atmosphere would likely have been smaller, perhaps by half, for a total of $\sim$5 Gt C.

[164] In summary, early burning of coal in China and deep erosion of soils in degraded regions of Eurasia could have contributed more than 14 Gt C of additional preindustrial emissions. Combined with the extra 48 Gt C from early deforestation (sections 8.1–8.3), the estimates in Figure 13 would need to be increased by $\sim$62 Gt C. Total preindustrial carbon emissions would then have amounted to (58–75) + 62 = 120–137 Gt C.

[165] On the basis of the 1-ppm increase in CO_2 for each 14.15 Gt increase in carbon emissions, cumulative emissions of 120–137 Gt C would account for a preindustrial anthropogenic CO_2 increase of $\sim$9 ppm. Although more than twice the amount estimated by *DeFries et al.* [1999], this estimate still falls well short of accounting for the 40-ppm anomaly proposed by *Ruddiman* [2003] or the 35-ppm CO_2 anomaly proposed in section 6.

8.5. Feedback Enhancement of the Anthropogenic CO_2 Anomaly

[166] The conclusion that direct anthropogenic carbon emissions can only explain a late Holocene CO_2 anomaly of $\sim$9 ppm presents a dilemma, because the late Holocene CO_2 trend is still anomalous by $\sim$35 ppm (section 6) and this anomaly is still most parsimoniously explained as being anthropogenic in origin. The only way out of this dilemma is to assume that the remaining $\sim$75% of the CO_2 carbon came from elsewhere in the climate system. One promising source of the extra carbon is from an ocean that was kept anomalously warm by human activities.

[167] In previous interglaciations, natural CO_2 decreases of 35–55 ppm occurred soon after peak interglacial warmth (Figure 11). Accompanying decreases must also have occurred in the amount of carbon in both the surface ocean (because of rapid exchanges with the atmosphere) and in terrestrial vegetation (because tropical monsoons were weakening and because ice sheets had begun to replace tundra and forest). All of this displaced carbon must have ended up in the only remaining carbon reservoir: the deep ocean.

[168] During the middle and late Holocene, as proposed earlier in section 8, human activities (deforestation and preindustrial coal burning) added an estimated 120–137 Gt C to the atmosphere. As millennia passed, the deep ocean would have slowly taken up about 85% of this amount, leaving less than 20 Gt of anthropogenic carbon in the atmosphere.

[169] The fate of the anthropogenic carbon is, however, only one part of the late Holocene carbon budget. Another important issue is whether the Holocene ocean cooled and took up as much carbon as it had during the early parts of previous interglaciations. Evidence from two key areas, the Southern Ocean and the deep Pacific Ocean, suggests that the ocean did not cool but instead remained anomalously warm during the Holocene. This anomalous warmth would have resulted in carbon exchanges unlike those during previous interglaciations.

[170] Estimates of sea surface temperature (SST) based on planktic faunal assemblages shows that the Southern Hemisphere is an "early responder" to orbital forcing [*Hays et al.*, 1976; *Imbrie et al.*, 1989], and SST estimates derived from alkenone and Mg/Ca ratios confirm this conclusion [*Waelbroeck et al.*, 1995; *Brathauer and Abelmann*, 1999]. Southern Ocean surface temperatures cooled well toward glacial maximum values early in previous interglacial stages 5 and 7 but did not decrease during the last 5000 years and instead remained $\sim$3°C warmer (Figure 15a). Ice core deuterium (δD) ratios (Figure 15b), a proxy for temperature [*Jouzel et al.*, 1990], also decreased (cooled) during the first half of the Holocene but then showed little or no net change during the last 5000 years. In contrast, the four previous "natural" interglaciations show continuing δD decreases (cooling) during the times equivalent to the late Holocene. On the basis of this evidence the late Holocene Southern Ocean has remained anomalously warm.

[171] Oxygen-isotopic ratios show similar late Holocene anomalies. The SPECMAP δ^{18}O stack of *Imbrie et al.* [1984] is based on planktic foraminifera from the Southern Ocean and tropical Atlantic Ocean. During the last 5000 years, δ^{18}O values decreased, but they were increasing during similar parts of previous interglaciations (Figure 16a). Some of the δ^{18}O increases during the prior interglaciations resulted from the growth of Northern Hemisphere ice sheets, but early sea surface cooling in the tropical and Southern Ocean also contributed to this trend [*Lea et al.*, 2001].

[172] In the benthic foraminiferal δ^{18}O stack of *Lisiecki and Raymo* [2005], δ^{18}O values remained negative during the late Holocene, but they increased during the comparable parts of previous interglaciations (Figure 16b). Again, ice growth accounted for part of the δ^{18}O increases during the prior interglaciations, but deep ocean temperature also decreased at those times [*Chappell and Shackleton*, 1986;

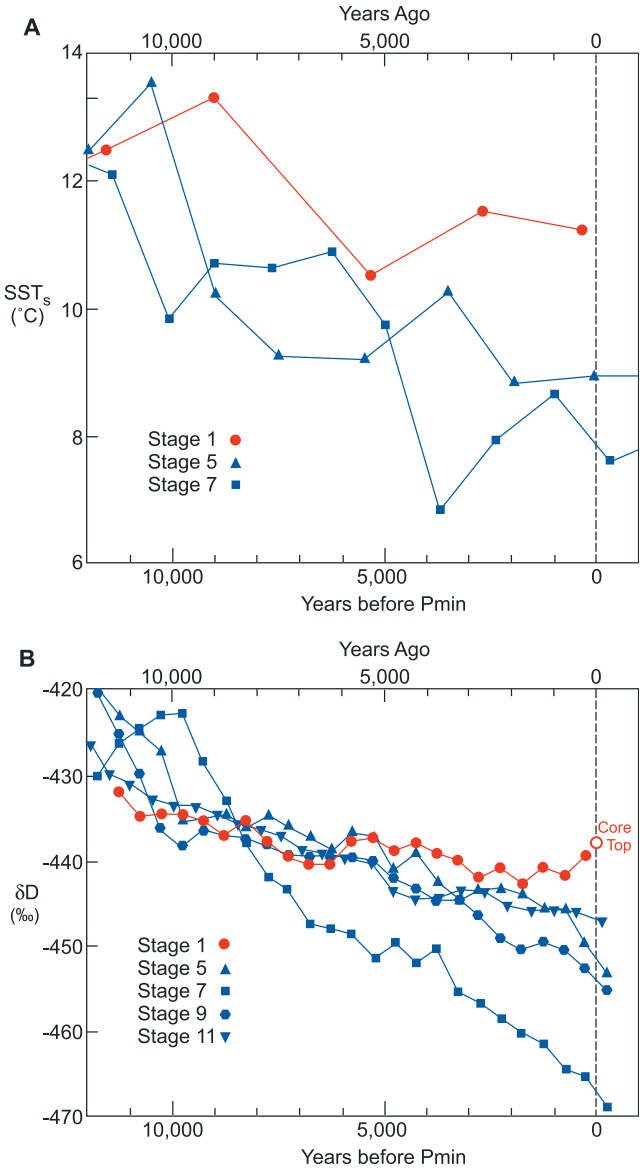

Figure 15. Two climatic indices suggesting that Holocene temperatures in the Antarctic region remained warm during the last 5000 years but fell during similar stages of previous interglaciations: (a) estimated sea surface temperature based on radiolarian assemblages from core RC11-120 [*Hays et al.*, 1976] and (b) deuterium (δD) values in Vostok ice [*Petit et al.*, 1999].

Martin et al., 2002]. In summary, oxygen-isotopic trends indicate that the late Holocene was a time of anomalous deep ocean warmth.

[173] General circulation models provide some insight into the reason for anomalous warmth in the Southern Ocean. *Ruddiman et al.* [2005] ran an experiment with the Global Environmental and Ecological Simulation of Interactive Systems (GENESIS) model with greenhouse gas concentrations reduced to the preindustrial levels proposed in the early anthropogenic hypothesis: 240 ppm for CO_2 and 450 ppb for CH_4. The mean annual SST decrease exceeded 3°C in the Southern Ocean (Figure 17), and the SST decrease in winter near the sea ice boundary was ~5°C. Similar experiments with the community climate system model (CCSM) (S. J. Vavrus et al., Climate model tests of the anthropogenic influence on greenhouse-induced climate change: The role of early human agriculture, industrialization, and vegetation feedbacks, submitted to *Quaternary Science Reviews*, 2007, hereinafter referred to as Vavrus et al., submitted manuscript, 2007) have simulated even larger SST anomalies in the Southern Ocean.

[174] These experiments suggest a large temperature response in the Southern Ocean to the combined anthropogenic effect of the full industrial and preindustrial greenhouse gas anomalies. These results would, however, need to be scaled down to constrain the smaller effect of the direct preindustrial emissions on this region. The analysis in section 7.3 suggested that humans were directly responsible for ~200 ppb of the total CH_4 anomaly of 230 ppb, and the analysis in sections 8.3 and 8.4 suggested that humans were directly responsible for ~9 ppm out of a CO_2 anomaly of 35 ppm. Together these "direct" anthropogenic emissions would have produced an equilibrium global mean temperature response of ~0.21°C (section 7.3).

[175] This value represents ~30% of the ~0.75°C response to the anomalies used in the modeling experiments with the full greenhouse gas reductions (40 ppm CO_2 and 250 ppb CH_4). Assuming linear scaling (which may or may not be valid), the 3°C mean annual SST response near the sea ice margin in the Southern Ocean would have been reduced from ~3°C to ~1°C and the winter SST response reduced from 5°C to ~1.7°C. These results suggest that direct emissions of greenhouse gases by humans could have kept the late Holocene Southern Ocean warmer by 1°–1.7°C than it was during comparable parts of prior interglaciations.

[176] Because of this anomalous warmth, exchanges of carbon with the atmosphere should have been different from those in previous interglaciations. *Stephens and Keeling* [2000] proposed that advances of Antarctic sea ice may drive down atmospheric CO_2 values by reducing carbon exchanges between Southern Ocean surface water and the atmosphere. Increased stratification of Antarctic surface waters during colder climates may also have had the same effect [*Francois et al.*, 1997; *Sigman and Boyle*, 2000]. The implication of these studies is that the failure of the Southern Ocean to cool during the Holocene could have left atmospheric CO_2 levels anomalously high.

[177] Anomalous warmth in the Southern Ocean could also be the reason for anomalous warmth in the deep Pacific Ocean. Because bottom water formed in the Southern Ocean is the volumetrically dominant water mass in the deep Pacific and the world ocean, anomalous warmth in high southern latitudes should have propagated through the deep ocean within the turnover time of ~1000 years. Deep ocean temperature changes, in turn, affect atmospheric CO_2 levels because CO_2 solubility decreases with increasing water temperature. Consequently, an anomalously warm deep ocean in the Holocene would have taken up less

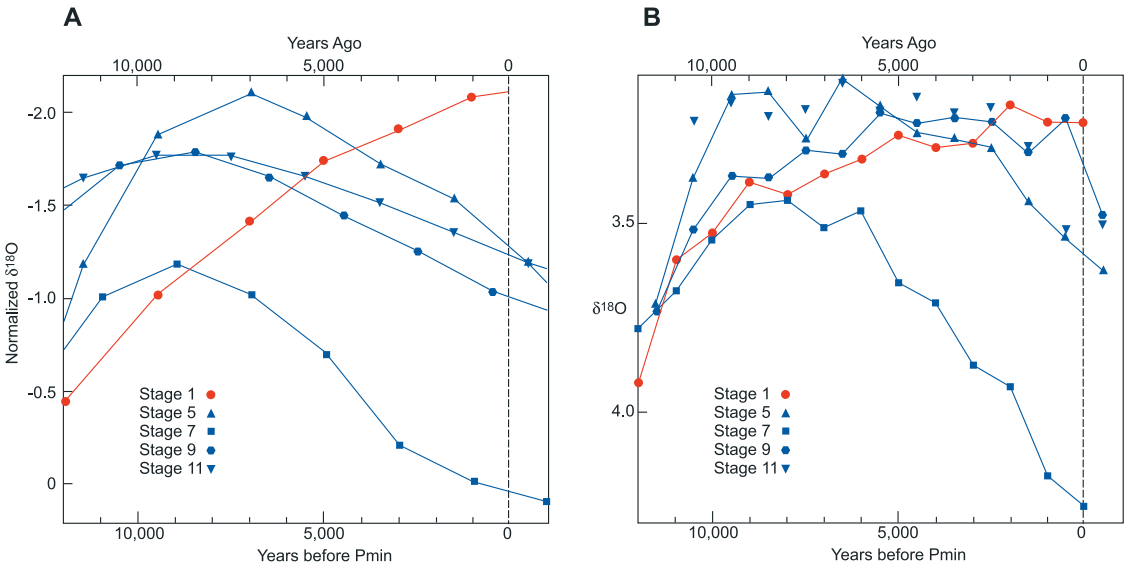

Figure 16. Marine $\delta^{18}O$ values, which remain approximately stable during the Holocene but increase during early parts of interglacial stages 5, 7, 9, and 11. (a) SPECMAP $\delta^{18}O$ stack based on planktic foraminifera [*Imbrie et al.*, 1984], with ages increased by 2000 years to allow for shorter ice sheet response times assumed by *Imbrie et al.* [1992]. (b) Stack of benthic foraminiferal $\delta^{18}O$ values from *Lisiecki and Raymo* [2005].

CO_2 than it did during previous interglaciations, leaving atmospheric CO_2 concentrations anomalously high.

[178] *Ruddiman* [2003] defined the anthropogenic CO_2 anomaly as the difference between the late Holocene value and the concentrations during the most similar times in previous interglaciations. Given this definition, the lack of a Holocene CO_2 decrease because of carbon feedback from a warm ocean is a direct contribution to the size of the CO_2 anomaly. The obvious question now at hand is this: How large could this feedback contribution to the CO_2 anomaly be?

[179] *Martin et al.* [2005] analyzed past relationships between changes in ocean temperature and atmospheric CO_2. They found that CO_2 values were ~12 ppm higher when the deep ocean was warmer by 1°C as a result of the inverse relationship between temperature and CO_2 solubility. Present-day benthic $\delta^{18}O$ values average about 0.4‰ less than comparable intervals in previous interglaciations (Figure 16b). If ice volume and temperature changes each explain half of this anomaly, the late Holocene ocean was anomalously warm by ~0.8°C. On the basis of the calibra-

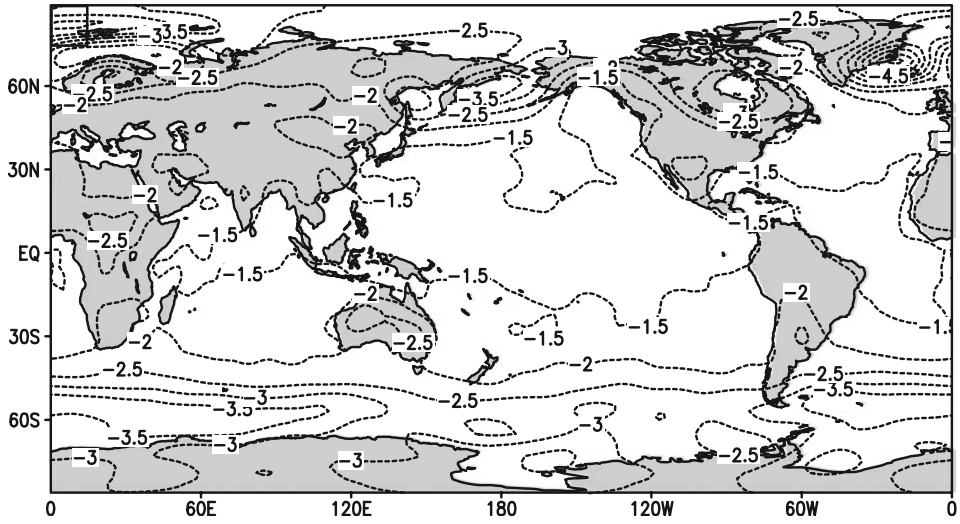

Figure 17. Removing all anthropogenic (industrial and preindustrial) contributions from control case greenhouse gas concentrations in a general circulation model cooling Earth's surface, particularly along the sea ice margin in the Southern Ocean [*Ruddiman et al.*, 2005].

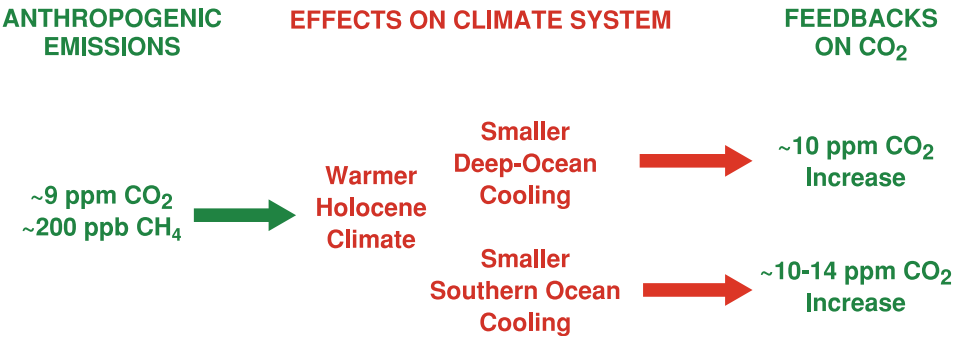

Figure 18. Direct emissions of methane and CO_2 by humans during the late Holocene causing a warming effect that offset much of the natural cooling that occurred early in previous interglaciations. The resulting warm anomaly in the ocean would have added CO_2 to the atmosphere by reducing CO_2 solubility and by capping air-sea exchanges in the Southern Ocean.

tion used by *Martin et al.* [2005], the atmosphere would then contain ~10 ppm more CO_2.

[180] *Martin et al.* [2005] also inferred that a second contribution to CO_2 changes resulted from processes probably centered in the Southern Ocean, such as changes in sea ice extent and upper ocean stratification. They inferred that each 1°C warming of the deep ocean correlated with a 12- to 18-ppm increase in atmospheric CO_2. For a deep ocean warming of 0.08°C, their estimate of this additional (probably Southern Ocean) contribution is an additional 10–14 ppm CO_2 decrease.

[181] On the basis of these CO_2/temperature links inferred by *Martin et al.* [2005], anomalous Holocene warmth in the deep ocean and Southern Ocean could have increased atmospheric CO_2 by 20 to 24 ppm as a positive feedback (Figure 18). The high end of this range would nearly close the gap between the small (9 ppm) CO_2 anomaly directly supported by anthropogenic carbon releases and the full (35 ppm) CO_2 anomaly.

[182] Because the true relationships between ocean temperatures and CO_2 feedbacks are not yet well known, this analysis is obviously somewhat speculative. It does, however, suggest a promising direction to pursue in order to resolve the dilemma about the Holocene CO_2 anomaly.

[183] In addition, carbon feedback from an anomalously warm ocean could also help to explain the negligible change in $\delta^{13}C$ of CO_2 during the late Holocene found by *Indermuhle et al.* [1999] and *Eyer et al.* [2004]. If one quarter of the CO_2 anomaly resulted from the addition of isotopically negative terrestrial carbon ($\delta^{13}C = -25‰$), while the remaining 75% was derived from inorganic ocean carbon with $\delta^{13}C = 0‰$, the larger amount of relatively positive ocean carbon would have diluted much of the negative $\delta^{13}C$ signature of the terrestrial carbon. As a result the combined $\delta^{13}C$ input from the two sources would then have a composition little different from the mean value in the natural atmosphere (−6.5‰). Consequently, humans could have been responsible for the full CO_2 anomaly of 35 ppm without causing large alterations in the mean carbon-isotopic composition of atmospheric CO_2.

[184] Future research on high-resolution ocean cores is needed to verify the size of the anomalous late Holocene temperature responses proposed for the Southern Ocean and the deep ocean. For the deep Pacific Ocean, which is most representative of global mean deep ocean values, these tests may be difficult because of pervasive late Holocene dissolution. Investigations of late Holocene trends in the Southern Ocean, and in long Antarctic ice cores, are more likely to be successful. Future research could also focus on possible terrestrial vegetation feedbacks on the amount of carbon in the atmosphere, such as changes from C3 to C4 vegetation and temperature effects on net primary productivity.

9. HAVE HUMANS PREVENTED THE ONSET OF A NEW GLACIATION?

[185] Another challenge to the early anthropogenic hypothesis questions the claim that a new glaciation is overdue because of greenhouse gas emissions by early farmers during the last few thousand years. Part of the original claim was based on the large increases in $\delta^{18}O$ values that occurred within 10,000 years after the peak interglaciations in interglacial stages 5, 7, and 9. Those increases indicated that substantial volumes of new ice were accumulating by the times most analogous to today. Another line of evidence for an overdue glaciation was the fact that the ice volume model of *Imbrie and Imbrie* [1980] simulated a small ice volume increase during the last few thousand years. The challenges to the "overdue glaciation" claim have focused on the fact that the insolation decreases early in stages 5, 7, and 9 were much larger than those in the Holocene and for that reason cannot be used to predict late Holocene glaciation.

[186] This idea has been tested by using the greenhouse gas trends proposed in the original early anthropogenic hypothesis as input to two types of model simulations along with Holocene insolation trends. Simulations with GCMs provide relatively complete parameterizations of climatic processes but do so at the cost of simulating only a decade or two of climate evolution. These simulations reveal widespread areas where snow cover lasts year-round, a reasonable indication that glacial inception is likely because additional snow accumulates year by year. Models of

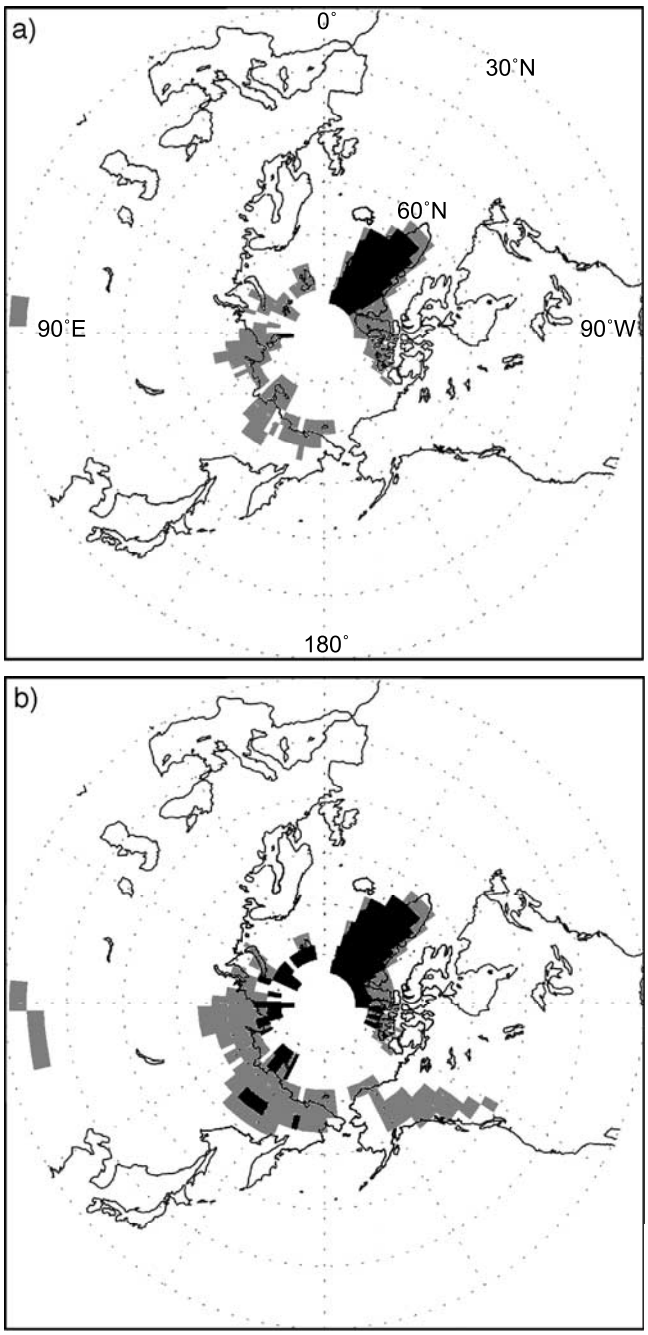

Figure 19. Simulation with the community climate system model (Vavrus et al., submitted manuscript, 2007) showing large increases in permanent snow cover for modern insolation and reduced greenhouse gas concentrations (CO_2 = 240 ppm; CH_4 = 450 ppb): (a) experiment with the basic model and (b) experiment with interactive vegetation added.

intermediate complexity (EMICs) have also been used to test whether or not ice sheets would have grown in the late Holocene. These models can simulate the evolution of climate (and ice sheets) over thousands of years, but they do so at the cost of simplifying many climatic processes.

9.1. Results From Models of Intermediate Complexity

[187] A simulation by *Claussen et al.* [2005] using the climate-biosphere (CLIMBER) model failed to produce new ice during the late Holocene in direct contradiction to the "overdue glaciation" claim. This simulation included the hypothesized 40-ppm lowering of CO_2 concentrations, but it did not use the ~250-ppb lowering of methane trends that were also part of the hypothesis.

[188] *Crucifix et al.* [2005, p. 419] forced the Louvain-la-Neuve model, a zonally averaged model with distinct subsectors, with insolation and reduced CO_2 levels. They concluded that "Holocene glacial inception is plausible but not certain, depending on the exact time evolution of the atmospheric CO_2 concentration." These simulations also omitted the proposed 250-ppb CH_4 decrease.

9.2. Results From General Circulation Models

[189] Several simulations have been run on general circulation models with greenhouse gas concentrations reduced to the levels proposed in the early anthropogenic hypothesis. *Ruddiman et al.* [2005] reported results from the GENESIS AGCM model with T31 resolution and a mixed later ocean model. This simulation produced year-round snow cover in a few grid boxes along the high spine of Baffin Island, thereby providing limited support for the claim that a new glaciation is overdue. Baffin Island has long been regarded as a likely site for glacial inception [*Andrews and Mahaffy*, 1976].

[190] Vavrus et al. (submitted manuscript, 2007) ran two simulations on the community atmosphere model (CAM3) version of the CCSM with T42 resolution and a slab ocean. One experiment that used the basic version of this model produced a large region of year-round snow cover in northern Eurasia as well as small increases in northern Canada (Figure 19a). A second experiment with interactive vegetation produced greater year-round snow cover in northern Eurasia and the Canadian Arctic as well as extensive permanent snow cover in the northern Rocky Mountains (Figure 19b). Evidence from Lake Baikal suggests that parts of Siberia became glaciated in isotopic substage 5.4, soon after the peak interglacial warmth of substage 5.5 [*Karabanov et al.*, 1998].

[191] A third simulation is currently underway with the CCSM linked to a dynamical ocean. This experiment (now approaching equilibrium) is simulating extensive year-round snow cover in northern Eurasia, in northern Canada (including Baffin Island and Quebec/Labrador), and over the Rocky Mountains.

[192] Two simulations with the Canadian Climate Centre modeling and analysis model (a Canadian AGCM) reported by *Vettoretti and Peltier* [2004] also bear on the early anthropogenic hypothesis. In these simulations, insolation was held at the modern level, and CO_2 concentrations were set at 260 and 290 ppm. The experiment with a CO_2 value of 290 ppm did not simulate glaciation, but the one with CO_2 at 260 ppm produced permanent (and steadily increasing) snow cover over Ellesmere Island as well as conditions at or close to glacial inception farther south in the Canadian

Arctic. These results are broadly consistent with the early anthropogenic hypothesis. The methane level in these experiments was not reduced to preindustrial levels.

[193] In summary, two simulations using models of intermediate complexity provide contradictory results about the ''overdue glaciation'' hypothesis, but both simulations omitted the methane forcing proposed in the original hypothesis. In contrast, simulations with general circulation models support the hypothesis that a glaciation of some extent would have begun by now if greenhouse gas levels were now at the reduced levels specified in the hypothesis.

[194] Additional experiments should be run to test the claim that a glaciation is overdue. Future simulations with EMICs should include the methane forcing. Future GCM simulations should use the additional methane forcing and should include the many feedback processes now available in such models. On the basis of the analysis in sections 5 and 6, future tests of the early anthropogenic hypothesis should use a CO_2 concentration of 250 ppm and a methane concentration of 475 ppb, each about 5% higher than the values proposed in the original hypothesis.

10. DID PANDEMICS CONTRIBUTE TO DROPS IN ATMOSPHERIC CO_2?

[195] After rising more or less steadily since 8000 years ago (Figure 1b) the Holocene CO_2 trend began to oscillate near 2000 years ago and then it fell by 7–8 ppm during the last millennium (Figure 2). Several studies have assumed that the CO_2 decrease was a response to temperature variations driven by the frequency of volcanic explosions and small changes in the solar radiative output, but *Ruddiman* [2003] claimed that anthropogenic factors also played a role.

[196] *Gerber et al.* [2003] used a carbon cycle model to quantify CO_2 oscillations and the global temperature change in response to solar-volcanic forcing. The model indicated that forcing sufficient to cause a 1-ppm CO_2 change would have altered surface temperature by 0.08°C. *Gerber et al.* [2003] compiled a composite CO_2 curve by stacking and averaging individual records from four ice cores. Because several large CO_2 oscillations were offset among the individual cores (as in Figure 2), this procedure yielded a smoothed record with a CO_2 drop of ~4 ppm between 1100 and 1700. Across that same interval, *Mann et al.* [1999] and *Crowley* [2000] reconstructed a long-term temperature decrease of ~0.2°C. The relative sizes of these CO_2 and temperature drops appeared to be consistent with the model calibration of *Gerber et al.* [2003].

[197] *Ruddiman* [2003] proposed a different interpretation. He suggested that the large CO_2 changes (Figure 2) were real but that they had been misaligned (offset in age) from record to record because of inadequate dating control. If the CO_2 drops really were as large as 7–8 ppm, solar-volcanic forcing could not have accounted for them without violating the constraint imposed by the relatively small change in reconstructed Northern Hemisphere temperature.

[198] Subsequent work has brought into question the size of the Northern Hemisphere cooling between ~1000–1200 and ~1600–1800. One reconstruction [*Moberg et al.*, 2005] proposed a larger cooling of ~0.5°C during this interval. A cooling of 0.5°C would account for 6.2 ppm of the 7–8 ppm CO_2 drop based on the carbon cycle model used by *Gerber et al.* [2003]. In this case, only a trivially small residual CO_2 drop of 1–2 ppm would remain to be explained by other factors.

[199] The sites chosen by *Moberg et al.* [2005] are, however, biased toward high-latitude and high-altitude regions where temperature responses are known to exceed global mean changes by a factor of 2 or more. Only 2 of the 11 sites lie in the northern tropics (<23.5°N), which encompasses half of the Northern Hemisphere, while 4 of 11 sites lie north of the Arctic Circle (>66.5°N), which encompasses less than 10% of the total area of the Northern Hemisphere.

[200] For those reconstructions that attempt to weight the distribution of proxy records in a more representative way, the estimated cooling between ~1100 and~1700 ranges from 0.15°C to 0.3°C [*Jones and Mann*, 2004]. This range of estimates would require a CO_2 drop of ~2–4 ppm according to the model scaling from *Gerber et al.* [2003]. As a result, ~4–5 ppm of the 7–8 ppm CO_2 drop measured at Law Dome could not be explained by solar-volcanic factors.

[201] Subsequent work on well-dated ice from Dronning Maud Land and the South Pole site has confirmed a CO_2 drop of ~7 ppm from 1100 to 1700 [*Siegenthaler et al.*, 2005b]. Those authors also noted in passing that solar-volcanic forcing is unlikely to account for a decrease this large. If not, additional explanations for the observed CO_2 drop are needed.

[202] *Ruddiman* [2003] reasoned that if human activities were responsible for the rising CO_2 trend through the late Holocene, they might also be part of the explanation for the CO_2 decreases superimposed on that trend. He proposed that major pandemics caused massive mortality that led to reforestation of abandoned land and that carbon sequestered in the growing forests reduced CO_2 concentrations in the atmosphere. The rest of this section, a synthesis of the discussion of *Ruddiman and Carmichael* [2007], revisits this aspect of the early anthropogenic hypothesis.

10.1. Estimating Carbon Sequestration During Pandemics

[203] Three major pandemics occurred in preindustrial times. The first occurred late in the Roman Era and extended over several centuries. From 200 to 600, *McEvedy and Jones* [1978] estimated a cumulative population loss of 10 million people or 40% of the Roman Empire in southern and western Europe, with a lower mortality rate in the more sparsely populated north and east. Broad areas of farmland reverted to waste [*Taylor*, 1983; *Cartwright*, 1991], and populations in most of these regions did not recover to preplague levels until the year 1000.

[204] During the ''Black Death'' pandemic of 1347–1353 in Europe, the Middle East, and North Africa, bubonic plague killed 25–33 million people (one third of the

TABLE 7. Estimated Sequestration of Carbon (in Gt) by Reforestation of Farmland (Crops and Pastures) Abandoned Because of High Pandemic Mortality

Region	Forest	Mortality,[a] millions	Per Capita Footprint, km^2	C Sequestered: Tons per Square Kilometer [b]	C Sequestered: Gigatons
		Late Roman-Era (200–600)			
Scandinavia	conifer	−0.1	0.09	1350	−0.1
North central Europe	deciduous	3.05	0.09	1630	4.5
Southern Europe	Mediterranean	2.05	0.09	1820	3.3
Total					∼7.7
		Black Death (1350–1450)			
Scandinavia	conifer	0.5	0.09	1350	0.6
North central Europe	deciduous	2.6	0.09	1630	7.6
Total					∼8.2
		American (1500–1750)			
North America	deciduous	3.5	0.02	1630	1.1
Mexico	seasonal/dry	15	0.02	800	2.4
Amazon	tropical wet	15	0.02	2190	6.6
Andes	montaine	14	0.02	1300	3.7
Total					∼13.8

[a]Mortality is shown only for regions where deforestation was still underway when the pandemic occurred.
[b]Carbon density values are from *Houghton* [1999].

population), and abandonment of farmland was common in north central Europe [*Darby*, 1956]. Plague recurred for decades after this catastrophe, but populations recovered to preplague levels by 1500.

[205] The arrival of Europeans in the Americas after 1492 introduced a host of diseases from which the indigenous people had no immunity. An estimated 80– 90% of the pre-Columbian population (50 –60 million people) died between 1500 and 1750, with the highest losses probably occurring in the 1500s [*Denevan*, 1992].

[206] The method described in section 8 to estimate terrestrial carbon losses from deforestation can be inverted to estimate carbon sequestration in forests growing on land abandoned as a result of pandemics. Sequestration is the product of the number of people who died, their average forest footprint in square kilometers per person, and the excess carbon density of the regrowing forests in tons of C per square kilometers.

[207] Human forest footprints are specified as in section 8. The Domesday Iron Age footprint of 9 ha is assumed for the two European pandemics, and the Stone Age footprint of 2 ha is assumed for the American pandemic (Table 7). For the long depopulation interval during the late Roman Era each death is assumed to have caused farm abandonment across southern and western Europe except in Greece and Italy [*Taylor*, 1983]. Those regions had surpassed the Domesday population threshold much earlier (Table 6), and a sufficient surplus of people existed to reoccupy the farms of those who died. For these regions, net farm abandonment is assumed.

[208] By the time of the Black Death most of southwestern Europe had passed the Domesday population density threshold, and consequently, most abandoned farms were probably soon reoccupied. In contrast, population densities were still low in northeastern Europe, Scandinavia, and European Russia, and many abandoned farms were not reoccupied for a century or more. Reforestation estimates are based only on those regions. *Jager* [1951] showed that substantial reforestation occurred on the northern German plains after the Black Death pandemic.

[209] The overwhelming impact of the 85–90% mortality rate in the American pandemic rules out any reoccupation of abandoned croplands in most areas. In Mexico, however, the Spanish moved in quickly with livestock and probably prevented major reforestation in lower-lying areas, although not in higher terrain. The reforestation rate for Mexico that is assumed here is 75%.

[210] The product of the total mortality, the human ''footprints,'' and forest-specific carbon densities yields estimates of carbon sequestration for the three pandemics that range from ∼8 to ∼14 Gt (Table 7). *Faust et al.* [2006] derived a similar estimate for the Americas: 1 million km^2 of reforestation (compared to the 1.1 million km^2 estimated here) and 17 Gt of carbon sequestration (compared to the 14 Gt estimated here).

[211] These sequestration totals need to be allocated as time-varying amounts through the duration of the pandemics. Because population data are available with a multidecadal resolution and because ice cores smooth changes in atmospheric CO_2 over decades, changes in carbon sequestration are estimated here in 50-year time steps. A lag of 50 years is added to allow for the time required for abandoned farms to be covered by young forests [*Houghton*, 1999].

[212] *McEvedy and Jones* [1978] estimated that the population of Europe decreased nearly linearly between the Antonine plague in the year 180 and the severe Justinian

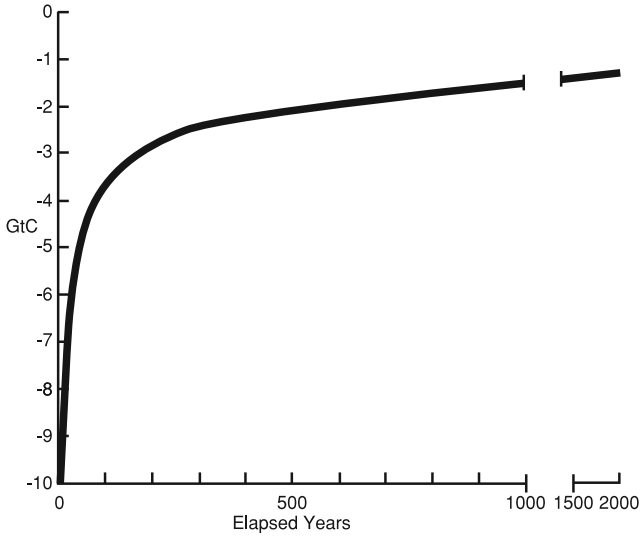

Figure 20. Impulse response function (based on *Joos et al.* [2004]) showing the effect of carbon system exchanges on the amount of carbon in the atmosphere. If 10 Gt C were suddenly sequestered in forests, the initially large perturbation (reduction) in atmospheric CO_2 concentrations would decrease rapidly for several decades and then much more slowly over centuries and millennia.

plague in 540–542. To approximate this loss of population (and ongoing reforestation of abandoned land), the estimated 7.7 Gt of sequestered carbon (Table 7) is distributed evenly across the interval from 200 to 600 at a rate of 0.96 Gt C per half century.

[213] The severe Black Death plague from 1347 to 1353 was followed by smaller recurrences over the next century. Of the 8.2 Gt C estimated to have been sequestered during this pandemic (Table 7), 6 Gt C is allocated to the interval 1350–1400, and the remaining 2.2 Gt C is allocated to the interval 1400–1450.

[214] Historical evidence suggests that the effects of European diseases were most devastating during the early phase of the American pandemic. Very high mortality is recorded during the 1520s and 1530s among the Aztecs, Incas, and populations in southern North America [*Denevan*, 1992]. The estimated 13.8 Gt of total carbon sequestration during this pandemic is distributed as follows: 5 Gt C in each of the half centuries from 1550 to 1600 and 1600 to 1650 and 1.9 Gt C in the intervals from 1650 to 1700 and from 1700 to 1750.

10.2. Simulating the Atmospheric Response to Carbon Sequestration

[215] The second step in assessing the effects of major depopulation episodes is to transform the estimates of carbon sequestration into changes in atmospheric CO_2. If all of the carbon sequestered by forests came from the atmosphere, the exchanges would occur in the ratio 2.13 Gt C/1 ppm CO_2, based on the weight of CO_2. In nature, however, rapid transfers occur between the atmosphere, the surface ocean, and the vegetation and soil reservoirs over years to decades to centuries, while much slower exchanges between these surface reservoirs and the deep ocean occur over centuries to millennia.

[216] If a sudden increase in terrestrial carbon sequestration were to occur, atmospheric CO_2 would abruptly drop, but within 50 years the atmospheric signal would have relaxed nearly halfway back toward the preinput concentration (Figure 20, based on Figure 1 of *Joos et al.* [2004]). The later phase of the CO_2 relaxation is far more gradual because it reflects slow carbon exchanges with the deep ocean and even slower exchanges between deep water and seafloor $CaCO_3$.

[217] To model the changes in atmospheric carbon and CO_2 concentrations that would occur in response to carbon sequestration during pandemics, the filter in Figure 20 is used to redistribute the time-varying estimates of carbon sequestration just discussed (black lines in Figure 21a) among carbon reservoirs during subsequent decades and centuries (solid red line in Figure 21a). The atmospheric carbon perturbations caused by pandemics die off in the same manner as they do in the filter: relatively quickly for a few decades and then much more slowly over centuries to millennia. The filter moves forward in time steps of 50 years, equivalent to the resolution of the historical depopulation estimates.

[218] The model simulation indicates that the atmosphere would have registered a CO_2 decrease of ~1 ppm CO_2 during the interval 600–650 because of reforestation (Figure 21a). This CO_2 deficit then slowly diminished during the following centuries. Between 1400 and 1450 the simulation indicates an abrupt CO_2 decrease of ~2 ppm in response to reforestation during the Black Death pandemic. Concentrations had then barely begun to rebound when the American pandemic caused an additional drop of almost 2 ppm CO_2 between 1600 and 1700 (Figure 21a). Much of the CO_2 anomaly then lingered into the 1700s and 1800s. By that time, Europeans had begun to settle the Americas in large numbers and deforest (or rather "redeforest") many regions that had first been cut prior to the pandemic.

[219] *Ruddiman and Carmichael* [2007] also considered two other anthropogenic factors that might have reduced atmospheric CO_2 during this interval. First, the high mortality rates during the three pandemics would have reduced the global mean rate of deforestation by ending deforestation in the stricken regions for a time. Although deforestation would have continued elsewhere, the reduced rate of deforestation in the pandemic regions would have slowed the supply of CO_2 to the atmosphere.

[220] Second, China experienced massive mortality (an estimated 40 million deaths) between 1250 and 1400 because of civil strife and near collapse of the economic order [*McEvedy and Jones*, 1978; *Livi-Bacci*, 2001; *Deng*, 2003]. Because many people in northern China at this time burned coal instead of wood, these deaths would have reduced releases of carbon to the atmosphere. These two processes (dashed red line in Figure 21a) increased the

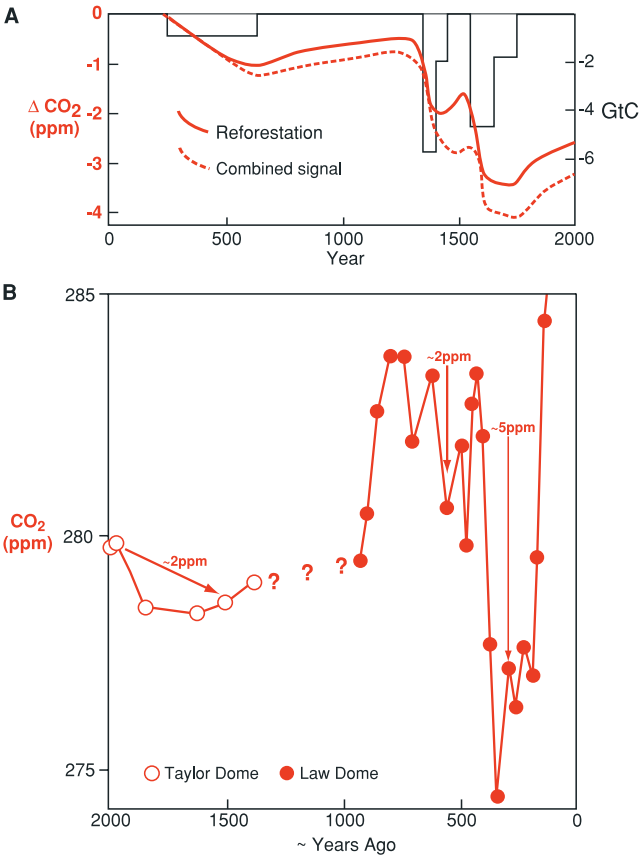

Figure 21. (a) Model simulation of the effects of major depopulation intervals on atmospheric carbon [after *Ruddiman and Carmichael*, 2007]. Solid black lines are estimates of carbon lost from the atmosphere and sequestered in forests, based on historical and ecological data. Solid red line shows the simulated effect of reforestation on atmospheric CO_2 concentration resulting from exchanges with other carbon reservoirs; dashed red line shows additional reductions caused by reductions in deforestation and coal burning. (b) Composite CO_2 target signal compiled from the well-dated Law Dome record [*Etheridge et al.*, 1996] and less securely dated Taylor Dome record [*Indermuhle et al.*, 1999].

simulated net reduction of atmospheric CO_2 to a total of just over 4 ppm by 1600–1700.

[221] The simulation of these anthropogenic effects on atmospheric CO_2 in Figure 21a is compared to a composite signal from a spliced ice core record in Figure 21b. The CO_2 values subsequent to 1000 were taken from Law Dome ice [*Etheridge et al.*, 1996] and were closely constrained by numerous volcanic ash horizons of known age. Prior to that time the composite signal was based on the less securely dated ice core record from Taylor Dome [*Indermuhle et al.*, 1999].

[222] The combined anthropogenic factors can account for about 4 ppm of the 7-ppm CO_2 decrease observed between ~1200 and 1750. This estimate matches the amount that was not explained by the natural cooling. The possibility also remains that positive feedback responses could have amplified the size of the CO_2 response to the pandemics. The most likely feedbacks would be those from fast-response processes in the Southern Ocean. If the Southern Ocean cooled slightly between 1100 and 1700 because of the direct anthropogenic effects on CO_2, feedback from that region might have further reduced the CO_2 concentration in the atmosphere. The deeper ocean would also have had several centuries to register a partial cooling, although it would not have gotten anywhere near a full equilibrium response. These indirect anthropogenic feedbacks could have added to the 4-ppm CO_2 decrease resulting from the direct effects of pandemics and other anthropogenic factors.

[223] If this 4-ppm estimate of the pandemic effect on atmospheric CO_2 concentrations is correct, it would account for a global mean cooling of ~0.05°C between 1200 and 1700. As noted, initial reconstructions of Northern Hemisphere temperature during this interval indicate a cooling of 0.15°C to 0.3°C. Pandemics would then account for ~16% to ~33% of this amount.

[224] Only one reconstruction has attempted a reconstruction of climate during the last millennium in the Southern Hemisphere [*Jones and Mann*, 2004]. This reconstruction did not show a prominent austral cooling between 1200 and 1800, and the global cooling from combining both hemispheres was only about half as large as the estimated Northern Hemisphere cooling. If the global mean cooling is only half of the 0.15° to 0.3°C cooling estimated for the Northern Hemisphere (or just 0.075° to 0.15°C), the estimated pandemic-driven temperature drop of 0.05°C would explain 33% to 66% of the total global cooling.

[225] Recently, proponents of solar forcing have acknowledged that changes in solar irradiance during prior centuries have been smaller than previously thought [*Foukal*, 2003; *Lean*, 2005]. These revised views eliminate much of the solar irradiance forcing previously invoked to explain the century-scale cooling between 1200 and 1700 [e.g., *Crowley*, 2000; *Gerber et al.*, 2003]. This revised view implies that other drivers must have been important in the observed cooling. Anthropogenic forcing is one such possibility.

[226] In summary, pandemic-driven reductions in atmospheric CO_2 can explain half or more of the ~7-ppm drop between 1200 and 1700. Depending on the highly uncertain size of the global mean cooling during this interval, this anthropogenic forcing could account for anywhere between 16% and 66% of the total cooling. In view of the uncertainties in pandemic mortality and in the size of human forest footprints, however, the simulations in Figure 21a should be viewed as a demonstration of the first-order plausibility of the pandemic CO_2 hypothesis rather than as a detailed simulation of actual changes.

[227] Evaluations of the link between the pandemics and the CO_2 trends could be improved by refining the dating of the Taylor Dome record (or new high-resolution ice records) using volcanic ash layers of known age. Two important questions need to be addressed: (1) Does the break in the upward CO_2 trend during the late Holocene correlate with the Roman Era pandemics? (2) Does the age of the rapid CO_2 rebound from these lower values date to ~1000 years

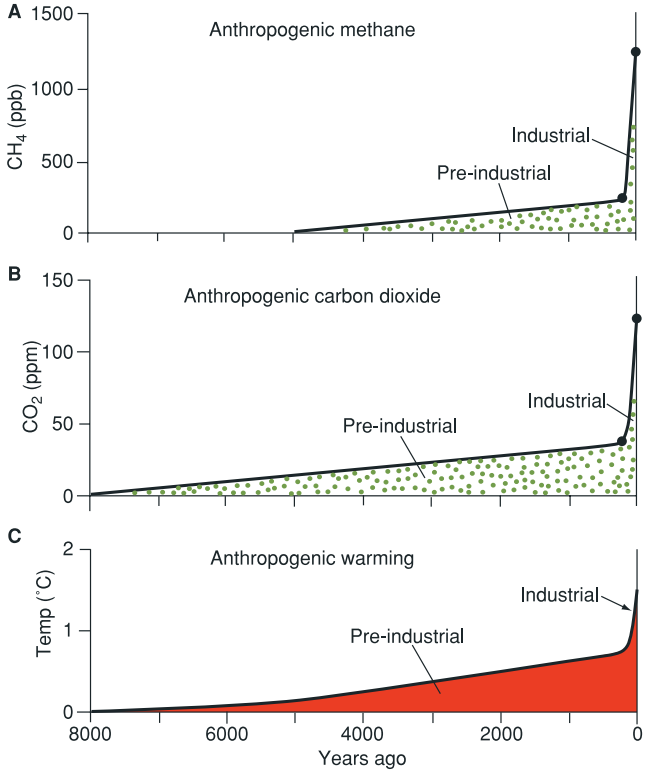

Figure 22. Net anthropogenic contributions during the Holocene to (a) atmospheric CH_4 concentration, (b) CO_2 concentration, and (c) global mean temperature.

ago, a time when global population began a 300-year interval of unusually rapid growth?

11. CONCLUSIONS

[228] This review has addressed major challenges to the anthropogenic explanation for late Holocene CO_2 and CH_4 increases. Sections 4–6 concluded that the CO_2 and CH_4 anomalies are ~35 ppm and ~230 ppb, respectively, or about 90% as large as those initially proposed by *Ruddiman* [2003]. Section 7 concluded that the CH_4 anomaly can reasonably be explained by early human agricultural activities and by climate feedbacks. Section 8 concluded that deforestation and coal burning cannot account for more than ~25% of the ~35-ppm CO_2 anomaly, but the CO_2 trend remains anomalous by that amount and is thus still likely to be of anthropogenic origin. The most likely source of the remaining CO_2 anomaly is carbon from a Holocene ocean that failed to cool as much as it had early in previous interglaciations. The carbon source for the other 75% of the 35-ppm CO_2 anomaly is the largest remaining uncertainty concerning the early anthropogenic hypothesis.

[229] These conclusions should be weighed against the opposite perspective: the validity of natural explanations for the late Holocene gas increases. From the outset, natural explanations encounter the problem that they cannot explain why the gas concentrations fell during similar intervals of the last four interglaciations (stages 5, 7, 9, and 11). An explanation for the Holocene rise cannot explain these earlier drops.

[230] *Broecker et al.* [2001] posed the only natural explanation yet published for the Holocene CO_2 trend: the ocean chemistry hypothesis. They interpreted the Holocene CO_2 rise as a delayed response of the ocean carbonate system to reforestation of the northern continents during the previous deglaciation thousands of years earlier [see also *Joos et al.*, 2004; *Broecker and Stocker*, 2006]. Yet this hypothesis encounters the problem noted above: Why was the Holocene trend entirely different from those during previous interglaciations? Toward the end of the deglaciations leading to interglacial stages 5, 7, 9, and 11, the ice sheets melted and the forests advanced northward, just as they did prior to stage 1. The ocean chemistry hypothesis thus predicts that a CO_2 rise should have occurred early in stages 5, 7, 9, and 11. Yet in each case the CO_2 trend went down not up. The ocean chemistry hypothesis fails all four of these tests.

[231] Both ice cores and marine sediments suggest that interglacial stages 5, 7, 9, and 11 may be the only ones that can serve as definitive tests of the early anthropogenic hypothesis. Peak interglacial intervals in isotopic stages 13 and 15 had lower CO_2 values [*Siegenthaler et al.*, 2005a] and less negative marine $\delta^{18}O$ values [*Imbrie et al.*, 1984; *Lisiecki and Raymo*, 2005] compared to interglacial stage 11 and the subsequent interglaciations. Consequently, natural explanations for the late Holocene greenhouse gas rises fail the only four tests available.

[232] *Crutzen and Stoermer* [2000] defined the "Anthropocene" as the interval in time, the last 2 centuries, when humans caused exponential increases in greenhouse gas concentrations in the atmosphere and accelerating alterations of Earth's surface. The analysis here supports the contention by *Ruddiman* [2003] that human impacts on Earth's surface, on greenhouse gas concentrations, and on global climate began much earlier but at much slower rates (Figure 22).

[233] Although slow in developing, the climatic effect of these early agricultural factors by late in the Holocene rivaled that of the subsequent industrial portion (Figure 22c). Because the climate system had time to come to full equilibrium with the slow greenhouse gas increase over thousands of years, the cumulative effect on global temperature during the time just before the industrial era had risen to ~0.7°C (for a doubled-CO_2 sensitivity of 2.5°C and anomalies of 35 ppm for CO_2 and 230 ppb for CH_4). By the early 2000s the global mean warming of the industrial era had also reached 0.7°C, but the rise in gas concentrations during the past century was so rapid that the climate system has not had time to reach the full equilibrium warming. In addition, part of the greenhouse warming effect has been canceled by cooling from anthropogenic aerosols. As a result the estimated preindustrial anthropogenic warming of ~0.7°C effectively doubles the total net effect of humans on global temperature to ~1.4°C.

[234] A final implication of the early anthropogenic hypothesis is that no natural (preanthropogenic) baseline

existed at any time in the middle or late Holocene. The natural downward trends in CO_2 and CH_4 were overridden by human intervention thousands of years ago, and much of the natural cooling that would have occurred was thereby prevented. Anthropogenic factors also played a role in short-term CO_2 and CH_4 oscillations during the last millennium. A world largely free of human intervention did exist in the early Holocene, when the last of the northern ice sheets were melting and when insolation values were considerably different from those today, but the climate system has been continuously altered by human interference ever since.

[235] **ACKNOWLEDGMENTS.** I thank Bob Smith for help with the graphics, Ann Carmichael for insights into the history of pandemics, Steve Vavrus and John Kutzbach for ongoing modeling efforts, and Michel Crucifix and three anonymous reviewers for helpful comments on the submitted manuscript. This research was funded by NSF grant GA10434.

[236] The Editor responsible for this paper was Ian Fairchild. He thanks Michael Crucifix, two technical reviewers, and one anonymous cross-disciplinary reviewer.

REFERENCES

Allen, L. H., S. L. Albrecht, W. Colon-Guasp, S. A. Covell, J. T. Baker, D. Pan, and K. J. Boote (2003), Methane emissions of rice increased by elevated carbon dioxide and temperature, *J. Environ. Qual.*, *32*, 211–225.

Andrews, J. T., and M. A. W. Mahaffy (1976), Growth rate of the Laurentide ice sheet and sea level lowering (with emphasis on the 115,000 BP sea level lows), *Quat. Res.*, *6*, 167–183.

Bard, E., B. Hamelin, and R. F. Fairbanks (1990), U/Th ages obtained by mass spectrometry in corals from Barbados: Sea level during the past 130,000 years, *Nature*, *346*, 456–458.

Bassinot, F. C., L. D. Labeyrie, E. Vincent, X. Quidelleur, N. J. Shackleton, and Y. Lancelot (1994), The astronomical theory of climate and the age of the Brunhes/Matuyama magnetic reversal, *Earth Planet. Sci. Lett.*, *126*, 91–108.

Bechmann, R. (1990), *Trees and Man: The Forest in the Middle Ages*, translated from French by K. Dunham, Paragon, New York.

Bender, M. L. (2002), Orbital tuning chronology for the Vostok climate record supported by trapped gas comparison, *Earth Planet. Sci. Lett.*, *204*, 275–289.

Bender, M., T. Sowers, and L. Labeyrie (1994), The Dole effect and its variations during the last 130,000 years as measured in the Vostok ice core, *Global Biogeochem. Cycles*, *8*, 363–376.

Berger, A. (1978), Long-term variations of caloric insolation resulting from the Earth's orbital elements, *Quat. Res.*, *9*, 139–167.

Berger, A., and M.-F. Loutre (2003), Climate 400000 years ago, a key to the future?, in *Earth's Climate and Orbital Eccentricity: The Marine Isotopic Stage 11 Question*, *Geophys. Monogr. Ser.*, vol. 137, edited by A. W. Droxler, R. Z. Poore, and L. H. Burckle, pp. 17–26, AGU, Washington, D. C.

Blunier, T., J. Chappellaz, J. Schwander, J. Stauffer, and D. Raynaud (1995), Variations in atmospheric methane concentrations during the Holocene epoch, *Nature*, *374*, 46–49.

Brathauer, U., and A. Abelmann (1999), Late Quaternary variations in sea surface temperatures and their relationship to orbital forcing recorded in the Southern Ocean (Atlantic sector), *Paleoceanography*, *14*, 135–148.

Broecker, W. S., and T. L. Stocker (2006), The Holocene CO_2 rise: Anthropogenic or natural?, *Eos Trans. AGU*, *87*, 27.

Broecker, W. S., J. Lynch-Stieglitz, E. Clark, I. Hajdas, and G. Bonani (2001), What caused the atmosphere's CO_2 content to rise during the last 8000 years?, *Geochem. Geophys. Geosyst.*, *2*(10), doi:10.1029/2001GC000177.

Carcaillet, C., et al. (2002), Holocene biomass burning and global dynamics of the carbon cycle, *Chemosphere*, *49*, 845–863.

Cartwright, F. E. (1991), *Disease and History*, Dorset, N. Y.

Chao, K. (1986), *Man and Land in Chinese History: An Economic Analysis*, Stanford Univ. Press, Stanford, Calif.

Chappell, J., and N. J. Shackleton (1986), Oxygen isotopes and sea level, *Nature*, *324*, 137–140.

Chappellaz, J., and I. Fung (1993), The atmospheric CH_4 increase since the last glacial maximum, *Tellus, Ser. B*, *45*, 228–241.

Chappellaz, J., J.-M. Barnola, D. Raynaud, Y. S. Korotkevitch, and C. Lorius (1990), Atmospheric CH_4 record over the last climatic cycle revealed by the Vostok ice core, *Nature*, *345*, 127–131.

Chappellaz, J., T. Blunier, S. Kints, A. Dallenbach, J.-M. Barnola, J. Schwander, D. Raynaud, and B. Stauffer (1997), Changes in the atmospheric CH_4 gradient between Greenland and Antarctica during the Holocene, *J. Geophys. Res.*, *102*, 15,987–15,997.

Claussen, M., V. Brovkin, R. Calov, A. Ganapolski, and C. Kubatzki (2005), Did humankind prevent a Holocene glaciation?, *Clim. Change*, *69*, 409–417.

COHMAP Members (1988), Climatic changes of the last 18,000 years: Observations and model simulations, *Science*, *241*, 1043–1052.

Crowley, T. J. (2000), Causes of climate change over the past 1000 years, *Science*, *289*, 270–277.

Crucifix, M., M.-F. Loutre, and A. L. Berger (2005), Commentary on "The anthropogenic greenhouse era began thousands of years ago," *Clim. Change*, *69*, 419–426.

Crutzen, P. J., and E. F. Stoermer (2000), The "Anthropocene," *IGBP Newsl.*, *41*, 12–14.

Darby, H. C. (1956), The clearing of the woodland in Europe, in *Man's Role in Changing the Face of the Earth*, edited by W. L. Thomas, pp. 183–216, Univ. of Chicago Press, Chicago, Ill.

DeFries, R. S., C. B. Field, I. Fung, G. J. Collatz, and L. Bounana (1999), Combining satellite data and biogeochemical models to estimate global effects of human-induced land cover change on carbon emissions and primary productivity, *Global Biogeochem. Cycles*, *13*, 803–815.

Denevan, W. M. (1992), *The Native Population of the Americas in 1492*, Univ. of Wis. Press, Madison.

Deng, K. G. (2003), China: Tang, Song and Yuan Dynasties, in *The Oxford Encyclopedia of Economic History*, vol. 2, edited by J. Mokyr, pp. 423–428, Oxford Univ. Press, Oxford, U. K.

Duplessy, J.-C., L. Labeyrie, and C. Waelbrock (2002), Constraints on the ocean oxygen isotopic enrichment between the Last Glacial Maximum and the Holocene: Paleoceanographic implications, *Quat. Sci. Rev.*, *21*, 315–330.

Edwards, R. L., J. H. Chen, T. L. Ku, and G. J. Wasserburg (1987), Precise timing of the last interglacial period from mass-spectrometric determination of thorium-230 in corals, *Science*, *236*, 1547–1553.

Elvin, M. (1993), Three thousand years of unsustainable growth: China's environment from archaic times to the present, *East Asian Hist.*, *6*, 7–46.

EPICA Community Members (2004), Eight glacial cycles from an Antarctic ice core, *Nature*, *429*, 623–628.

Etheridge, D. M., L. P. Steele, R. L. Langenfields, R. J. Francey, J.-M. Barnola, and V. I. Morgan (1996), Natural and anthropogenic changes in atmospheric CO_2 over the last 1000 years from air in Antarctic ice and firn, *J. Geophys. Res.*, *101*, 4115–4128.

Etheridge, D. M., L. P. Steele, R. J. Francey, and R. L. Langenfields (1998), Atmospheric methane between 1000 A. D. and present: Evidence of anthropogenic emissions and climatic variability, *J. Geophys. Res.*, *103*, 15,979–15,993.

Eyer, M., et al. (2004), Comparison of two $^{13}CO_2$ records measured on air from the EPICA Dome C and Kohnen Station ice

cores, paper presented at First General Assembly, Eur. Geosci. Union, Nice, France.
Faust, F. X., C. Gnecco, H. Mannstein, and J. Stamm (2006), Evidence for the postconquest demographic collapse of the Americas in CO_2 levels, *Earth Interact.*, *10*, pap. 11, doi:10.1175/EI157.1.
Ferretti, D. F., J. B. Miller, J. W. C. White, D. M. Etheridge, K. R. Lassey, D. C. Lowe, C. M. MacFarling, M. F. Dreir, C. M. Trudinger, and T. D. van Ommen (2005), Unexpected changes to the global methane budget over the last 2,000 years, *Science*, *309*, 1714–1717.
Fleitmann, D., S. Burns, M. Mudelsee, U. Neff, J. Kramers, A. Mangini, and A. Matter (2003), Holocene forcing of the Indian monsoon recorded in a stalagmite from southern Oman, *Science*, *300*, 1737–1739.
Fletcher, S. E. M., P. Tans, L. M. Bruhwiler, J. B. Miller, and M. Heimann (2004), CH_4 sources estimated from atmospheric observations of CH_4 and its $^{13}C/^{12}C$ ratios: 2. Inverse modeling of fluxes from geographical regions, *Global Biogeochem. Cycles*, *18*, GB4005, doi:10.1029/2004GB002224.
Flint, E. P., and J. F. Richards (1991), Historical analysis of changes in land use and carbon stock of vegetation in south and Southeast Asia, *Can. J. For. Res.*, *21*, 91–110.
Foukal, P. V. (2003), Can slow variations in solar luminosity provide the missing link between the Sun and climate?, *Eos Trans. AGU*, *84*, 205.
Francois, R., M. A. Altabet, E.-I. Yu, D. M. Sigman, M. Bacon, M. Frank, G. Bohrmann, G. Bareille, and L. D. Labeyrie (1997), Contribution of Southern Ocean surface-water stratification to low atmospheric CO_2 concentrations during the last glacial period, *Nature*, *389*, 929–935.
Freese, B. (2003), *Coal: A Human History*, Penguin USA, New York.
Gerber, S., F. Joos, P. Brugger, T. F. Stocker, M. E. Mann, S. Sitch, and M. Scholtze (2003), Constraining temperature variations over the last millennium by comparing simulated and observed atmospheric CO_2, *Clim. Dyn.*, *20*, 281–299.
Gregg, S. A. (1988), *Foragers and Farmers: Population Interaction and Agricultural Expansion in Pre-historic Europe*, Univ. of Chicago Press, Chicago, Ill.
Grigg, D. B. (1974), *The Agricultural Systems of the World*, Cambridge Univ. Press, Cambridge, U. K.
Grubler, A. (1994), Technology, in *Changes in Land Use and Land Cover*, edited by W. B. Meyer and B. L. Turner II, pp. 287–328, Cambridge Univ. Press, Cambridge, U. K.
Hartwell, R. (1962), A revolution in the Chinese iron and coal industries during the northern Sung, 960–1126 AD, *J. Asia Stud.*, *21*, 153–162.
Hays, J. D., J. Imbrie, and N. J. Shackleton (1976), Variations in the Earth's orbit: Pacemaker of the ice ages, *Science*, *194*, 1121–1132.
Hoffman, W. A., and R. B. Jackson (2000), Vegetation-climate feedbacks in the conversion of tropical savanna to grassland, *J. Clim.*, *13*, 1593–1602.
Houghton, R. A. (1999), The annual net flux of carbon to the atmosphere from changes in land use 1850–1990, *Tellus, Ser. B*, *51*, 298–313.
Houghton, R. A., and J. L. Hackler (2003), Sources and sinks of carbon from land-use change in China, *Global Biogeochem. Cycles*, *17*(2), 1034, doi:10.1029/2002GB001970.
Hughes, J. D. (1975), *Ecology in Ancient Civilizations*, Univ. of New Mexico Press, Albuquerque.
Hurt, R. D. (1987), *Indian Agriculture in America: Prehistory to the Present*, Univ. Press of Kan., Lawrence.
Huybers, P. (2006), Early Pleistocene glacial cycles and the integrated summer insolation forcing, *Science*, *313*, 508–511.
Imbrie, J., and J. Z. Imbrie (1980), Modeling the climatic response to orbital variations, *Science*, *207*, 943–953.
Imbrie, J., J. D. Hays, D. G. Martinson, A. McIntyre, A. C. Mix, J. J. Morley, N. G. Pisias, W. L. Prell, and N. J. Shackleton (1984), The orbital theory of Pleistocene climate: Support from a revised chronology of the marine $\delta^{18}O$ record, in *Milankovitch and Climate*, *Part I*, edited by A. L. Berger et al., pp. 269–305, D. Reidel, Dordrecht, Netherlands.
Imbrie, J., A. McIntyre, and A. Mix (1989), Oceanic response to orbital forcing in the late Quaternary: Observational and experimental strategies, in *Climate and Geo-Sciences*, edited by A. L. Berger et al., pp. 121–164, Kluwer Acad., Boston, Mass.
Imbrie, J., et al. (1992), On the structure and origin of major glaciation cycles: 1. Linear responses to Milankovitch forcing, *Paleoceanography*, *7*, 701–738.
Indermuhle, A., et al. (1999), Holocene carbon-cycle dynamics based on CO_2 trapped in ice at Taylor Dome, Antarctica, *Nature*, *398*, 121–126.
International Rice Research Institute (IRRI) (1991), *World Rice Statistics 1990*, Manila.
Jager, H. (1951), Die Entwicklung der Kulturlandschaft in Kriese Hofgeismar, *Gottinger Geogr. Abh. 8*, Dep. of Geogr., Univ. of Gottingen, Gottingen, Germany.
Jones, P. D., and M. E. Mann (2004), Climate over past millennia, *Rev. Geophys.*, *42*, RG2002, doi:10.1029/2003RG000143.
Joos, F., S. Gerber, I. C. Prentice, B. L. Otto-Bleisner, and P. Valdes (2004), Transient simulations of Holocene atmospheric carbon dioxide and terrestrial carbon since the Last Glacial Maximum, *Global Biogeochem. Cycles*, *18*, GB2002, doi:10.1029/2003GB002156.
Jouzel, J., C. Lorius, J. R. Petit, C. Genthon, N. J. Barkov, V. M. Kotlyakov, and V. N. Petrov (1990), Vostok ice core: A continuous isotope temperature record over the last climatic cycle (160,000 years), *Nature*, *329*, 403–409.
Karabanov, E. B., A. A. Prokopenko, D. F. Williams, and S. M. Colman (1998), Evidence from Lake Baikal for Siberian glaciation during oxygen isotope substage 5d, *Quat Res.*, *50*, 46–55.
Krech, S., III (1999), *The Ecological Indian*, W. W. Norton, New York.
Kutzbach, J. E. (1981), Monsoon climate of the early Holocene: Climate experiment with Earth's orbital parameters for 9000 years ago, *Science*, *214*, 59–61.
Labeyrie, L., J.-C. Duplessy, and P. L. Blanc (1987), Variations in mode of formation and temperature of oceanic waters over the past 125,000 years, *Nature*, *327*, 477–482.
Lea, D. W., D. Pak, and H. J. Spero (2001), Climatic impact of late Quaternary equatorial Pacific sea-surface temperature variations, *Science*, *289*, 1719–1724.
Lean, J. (2005), Living with a variable Sun, *Phys. Today*, *58*, 32–38.
Lean, J., and D. A. Warrilow (1989), Simulation of the regional impact of Amazon deforestation, *Nature*, *342*, 411–413.
Leemans, R. (1990), Global data sets collected and compiled by the Biosphere project, working paper, Inst. for Appl. Syst. Anal., Laxenburg, Austria.
Lisiecki, L. E., and M. E. Raymo (2005), A Plio-Pleistocene stack of 57 globally distributed benthic $\delta^{18}O$ records, *Paleoceanography*, *20*, PA1003, doi:10.1029/2004PA001071.
Livi-Bacci, M. (2001), *A Concise History of World Population*, Blackwell, Oxford, U. K.
Loutre, M.-F., and A. Berger (2000), Future climatic changes: Are we entering an exceptionally long interglacial?, *Clim. Change*, *46*, 61–90.
MacDonald, G. M., et al. (2006), Rapid early development of circumarctic peatlands and atmospheric CH_4 and CO_2 variations, *Science*, *314*, 285–288.
Mann, M. E., R. S. Bradley, and M. K. Hughes (1999), Northern Hemisphere temperatures during the past millennium, *Geophys. Res. Lett.*, *26*, 759–762.
Martin, P. A., D. W. Lea, Y. Rosenthal, N. J. Shackleton, M. Sarnthein, and T. Papenfuss (2002), Quaternary deep sea temperature histories derived from benthic foraminiferal Mg/Ca, *Earth Planet. Sci. Lett.*, *198*, 193–209.

Martin, P., D. Archer, and D. W. Lea (2005), Role of deep sea temperatures in the carbon cycle during the last glacial, *Paleoceanography*, *20*, PA2015, doi:10.1029/2003PA000914.

Masson-Delmotte, V., et al. (2006), Past temperature reconstructions from deep ice cores: Relevance for future climate change, *Clim. Past Discuss.*, *2*, 399–448.

Mathews, E. (1983), Global vegetation and land use: New high resolution databases for climate studies, *J. Clim. Appl. Meteorol.*, *22*, 474–487.

McEvedy, C., and R. Jones (1978), *Atlas of World Population History*, Penguin, New York.

McManus, J., D. Oppo, J. Cullen, and S. Healey (2003), Marine isotope stage 11 (MIS 11): Analog for Holocene and future climate?, in *Earth's Climate and Orbital Eccentricity: The Marine Isotopic Stage 11 Question*, *Geophys. Monogr. Ser.*, vol. 137, edited by A. W. Droxler, R. Z. Poore, and L. H. Burckle, pp. 69–85, AGU, Washington, D. C.

Mikaloff Fletcher, S. E., P. Tans, L. M. Bruhwiler, J. B. Miller, and M. Heimann (2004), CH_4 sources estimated from atmospheric observations of CH_4 and its $^{13}C/^{12}C$ ratios: 1. Inverse modeling of source processes, *Global Biogeochem. Cycles*, *18*, GB4004, doi:10.1029/2004GB002223.

Milankovitch, M. M. (1941), *Canon of Insolation and the Ice-Age Problem* (in German), K. Serb. Akad., Beograd. (English translation, Isr. Program for Sci. Transl., Jerusalem, 1969.)

Minami, K., and H.-U. Neue (1994), Rice paddies as a methane source, *Clim. Change*, *27*, 13–26.

Mix, A. C., J. Le, and N. J. Shackleton (1995a), Benthic foraminiferal stable isotope stratigraphy of site 846: 0–1.8 Ma, *Proc. Ocean Drill. Program Sci. Results*, *138*, 839–854.

Mix, A. C., N. G. Pisias, W. Rugh, J. Wilson, A. Morey, and T. K. Hagelberg (1995b), Benthic foraminifer stable isotope record from Site 849 (0–5 Ma): Local and global climate changes, *Proc. Ocean Drill. Program Sci. Results*, *138*, 371–412.

Moberg, A., D. M. Sonechkin, K. Holmgren, N. Datsenko, and W. Karlen (2005), Highly variable Northern Hemisphere temperatures reconstructed from low- and high-resolution proxy data, *Nature*, *433*, 613–617.

Olson, J. S., J. A. Watts, and J. Allison (1983), Carbon in live vegetation of major world ecosystems, *Tech. Rep. TR004*, U.S. Dep. of Energy, Washington, D. C.

Parrenin, F., F. Rémy, C. Ritz, M. J. Siegert, and J. Jouzel (2004), New modeling of the Vostok ice flow line and implication for the glaciological chronology of the Vostok ice core, *J. Geophys. Res.*, *109*, D20102, doi:10.1029/2004JD004561.

Petit, J. R., et al. (1999), Climate and atmospheric history of the last 420,000 years from the Vostok ice core, Antarctica, *Nature*, *399*, 429–436.

Pisias, N. G., A. C. Mix, and R. Zahn (1990), Nonlinear response in the global climate system: Evidence from benthic oxygen isotopic record in core RC13–110, *Paleoceanography*, *5*, 147–160.

Rackham, O. (1980), *Ancient Woodland: Its History, Vegetation, and Uses in England*, Edward Arnold, London.

Ramankutty, N., and J. A. Foley (1999), Estimating historical changes in global land cover: Croplands from 1700 to 1992, *Global Biogeochem. Cycles*, *13*, 997–1027.

Reeburg, W. S. (2003), Global methane biogeochemistry, in *Treatise on Geochemistry*, vol. 2, edited by K. Turekian, pp. 65–94, Elsevier, Amsterdam.

Roberts, N. (1998), *The Holocene*, Blackwell, Oxford, U. K.

Ruddiman, W. F. (2003), The anthropogenic greenhouse era began thousands of years ago, *Clim. Change*, *61*, 261–293.

Ruddiman, W. F. (2005a), Cold climate during the closest stage 11 analog to recent millennia, *Quat. Sci. Rev.*, *24*, 1111–1121.

Ruddiman, W. F. (2005b), Comment on "A note on the relationship between ice core methane concentrations and insolation" by G. A. Schmidt et al., *Geophys. Res. Lett.*, *32*, L15703, doi:10.1029/2005GL022599.

Ruddiman, W. F., and A. G. Carmichael (2007), Pre-industrial depopulation, atmospheric CO_2, and climate, in *Global Environmental Change and Human Health*, edited by M. O. Andeae, U. Confalonieri, and A. J. McMichael, Pontif. Acad. Sci., Rome, in press.

Ruddiman, W. F., and A. McIntyre (1979), Warmth of the subpolar North Atlantic ocean during Northern Hemisphere ice-sheet growth, *Science*, *204*, 173–175.

Ruddiman, W. F., and M. E. Raymo (2003), A methane-based time scale for Vostok ice, *Quat. Sci. Rev.*, *22*, 141–153.

Ruddiman, W. F., and J. S. Thomson (2001), The case for human causes of increased atmospheric CH_4 over the last 5000 years, *Quat. Sci. Rev.*, *20*, 1769–1777.

Ruddiman, W. F., S. J. Vavrus, and J. E. Kutzbach (2005), A test of the overdue-glaciation hypothesis, *Quat. Sci. Rev.*, *25*, 1–10.

Sancetta, C., J. Imbrie, N. G. Kipp, A. McIntyre, and W. F. Ruddiman (1973), Climatic record in North Atlantic deep-sea core V23–82: Comparison of the last and present in interglacials based on quantitative time series, *Quat. Res.*, *2*, 363–367.

Schmidt, G. A., D. T. Shindell, and S. Harder (2004), A note on the relationship between ice core methane concentrations and insolation, *Geophys. Res. Lett.*, *31*, L23206, doi:10.1029/2004GL021083.

Schrag, D., G. Hampt, and D. Murray (1996), Pore fluid constraints on the temperature and oxygen isotopic composition of the glacial ocean, *Science*, *272*, 1930–1931.

Shackleton, N. J. (2000), The 100,000-year ice-age cycle identified and found to lag temperature, carbon dioxide and orbital eccentricity, *Science*, *289*, 1897–1902.

Shindell, D., B. P. Walter, and G. Faluvegi (2004), Impacts of climate change on methane emissions, *Geophys. Res. Lett.*, *31*, L21202, doi:10.1029/2004GL021009.

Siegenthaler, U., et al. (2005a), Stable carbon cycle–climate relationship during the late Pleistocene, *Nature*, *310*, 1313–1317.

Siegenthaler, U., E. Monnin, K. Kawamura, R. Spahni, J. Schwander, B. Stauffer, T. F. Stocker, J.-M. Barnola, and H. Fischer (2005b), Supporting evidence from the EPICA Dronning Maud Land ice core for atmospheric CO_2 changes during the past millennium, *Tellus, Ser. B*, *57*, 51–57.

Sigman, D. M., and E. A. Boyle (2000), Glacial/interglacial variations in atmospheric carbon dioxide, *Nature*, *407*, 859–869.

Simmons, I. G. (1996), *Changing the Face of the Earth*, Blackwell, Oxford, U. K.

Smith, L. C., G. M. MacDonald, A. A. Velichko, D. W. Beilman, O. K. Borisova, K. E. Frey, K. V. Kremenetski, and Y. Sheng (2004), Siberian peatlands: A net carbon source and global methane sink since the early Holocene, *Science*, *303*, 353–356.

Sowers, T., M. Bender, L. Labeyrie, D. Martinson, J. Jouzel, D. Raynaud, J. J. Pichon, and Y. S. Korotkevich (1993), A 135,000-year Vostok-SPECMAP common temporal framework, *Paleoceanography*, *8*, 737–766.

Stefani, M., and S. Vincenzi (2005), The interplay of eustasy, climate and human activity in the late Quaternary depositional environment and sedimentary architecture of the Po delta system, *Mar. Geol.*, *222/223*, 19–48.

Stephens, B. B., and R. F. Keeling (2000), The influence of Antarctic sea ice on glacial/interglacial CO_2 variations, *Nature*, *404*, 171–174.

Subak, S. (1994), Methane from the House of Tudor and the Ming Dynasty: Anthropogenic emissions in the sixteenth century, *Chemosphere*, *29*, 843–854.

Taylor, C. (1983), *Village and Farmstead: A History of Rural Settlement in England*, George Philip, London.

Thirgood, J. V. (1981), *Man and the Mediterranean Forest*, Academic, London.

Vella, C., T.-J. Fleury, G. Raccasi, M. Provansal, F. Sabtier, and M. Bourcier (2005), Evolution of the Rhone delta plain in the Holocene, *Mar. Geol.*, *222/223*, 235–265.

Vettoretti, G., and W. R. Peltier (2004), Sensitivity of glacial inception to orbital and greenhouse gas climate forcing, *Quat. Sci. Rev.*, *23*, 499–519.

Waelbroeck, C., J. Jouzel, L. Labeyrie, C. Lorius, M. Labracherie, M. Stievenard, and N. I. Barkov (1995), A comparison of the Vostok ice deuterium record and series from Southern Ocean core MD 88-770 over the last two glacial-interglacial cycles, *Clim. Dyn.*, *12*, 113–123.

Williams, L. D. (1978), The little ice age glaciation level on Baffin Island, Canada, *Palaeogeogr. Palaeoclimatol. Palaeoecol.*, *25*, 199–207.

Williams, M. (1990), Forests, in *The Earth as Transformed by Human Action*, edited by B. L. Turner, pp. 179–201, Cambridge Univ. Press, Cambridge, U. K.

Williams, M. (2003), *Deforesting the Earth*, Univ. of Chicago Press, Chicago, Ill.

Yamane, I., and K. Sato (1963), Decomposition of plant nutrients and gas formation in flooded soil, *Soil Sci. Plant Nutr.*, *29*, 28–31.

Yuan, D. H., et al. (2004), Timing, duration, and transitions of the last interglacial monsoon, *Science*, *304*, 575–578.

Zohary, D., and M. Hopf (1993), *Domestication of Plants in the Old World*, Oxford Univ. Press, Oxford, U. K.

W. F. Ruddiman, Department of Environmental Sciences, University of Virginia, Clark Hall, Charlottesville, VA 22903, USA. (rudds2@ntelos.net)